Spatiotemporal variabilities in phytoplankton and benthic communities in the Pacific Arctic

(太平洋側北極海における植物プランクトンおよびベントス群集の時空間変動)

北海道大学大学院水産科学院

海洋生物資源科学専攻

Graduate School of Fisheries Sciences

Division of Marine Bioresource and Environmental Science

和賀　久朋

Hisatomo Waga

2018 (平成 30 年)

Table of contents

Chapter 1
General introduction

1.1. Basic concepts of marine ecosystem conservation

The terrestrial and marine ecosystems provide food, shelter, recycling, and other support mechanisms that are valuable for human communities (Field et al., 2014). The ecosystem services, which are defined as benefits that human can obtain from such ecosystems, have currently been attracted a great deal of attention (Fisher et al., 2009). This is an important trend for ecosystem conservation where values are often difficult to describe in economic terms and rarely well-explained in natural resource decisions (Wallace, 2007). Although long term and continuous utilization of the ecosystems services is critical to human survival and well-being (Palmer et al., 2004), Millennium Ecosystem Assessment (MEA, 2005) reported that approximately 60% of the ecosystem services are degraded or used unsustainably. Therefore, managing an ecosystem for sustainable ecosystem services is one of the biggest challenges of current ecosystem science (Palumbi et al., 2009). However, the concept of ecosystem services has yet to gain full traction in the decisions and policies of environmental agencies (Munns et al., 2017), due to not only the lack of appropriate methods but also the spatial and temporal variability of ecosystems (Deininger et al., 2016), especially in the case of marine domain (Barbier, 2012).

Ministry of the Environment (MOE), Government of Japan, has reported that there are several factors that affect or may affect on marine ecosystem: physical alterations that reduce habitats for organisms, pollution of marine environment that deteriorates the quality of ecosystems, excessive harvests that not only reduce the population size of fisheries resources but also change the species composition and even balance in the whole food web, intrusion of alien species that may disturb ecosystems, and impacts of the climate change that may affect the physicochemical environment or system of the ocean (MOE, 2011). The International Panel on Climate Change (IPCC) reported that climate change is projected to amplify existing risks and create new risks for marine systems (IPCC, 2014), and thus the concern about impacts of climate change on marine ecosystem recently became prominent (Gutiérrez et al., 2016; Hernández-Delgado, 2015). As the ecosystem services provided by marine ecosystem have been playing crucial roles in human-well being, such services must be sustained and handed down to the next generation. Hence, addressing our knowledge of marine ecosystem variations in response to climate change is garnering considerable attention for continuous sustainable usage of the blessing from marine ecosystems, and is now one of the most active research subjects not only in Japan but also around the world (MOE, 2011).

1.2. General fingerprints of climate change on marine environment

Climate change has significantly affected marine environment. Ocean heat content has grown substantially since the 1950s, resulting in the increased heat content of the upper 700 m of the global ocean by 14×10^{22} J since 1975 (Levitus et al., 2009). In addition, sea surface temperature (SST) increasing by approximately 0.2°C per decade (Hansen et al., 2006), and these trends in SST are driving elevated evaporation and precipitation rates, which cause fresher and saltier upper-ocean salinity in low-salinity regions and in high-salinity regions, respectively (Hoegh-Guldberg and Bruno, 2010). However, ocean warming is not spatially uniform owing to nonlinear interaction with natural modes of climate variability such as El Ninõ/Southern Oscillation (ENSO) and the North Atlantic Oscillation (Ishii et al., 2006), and affects regional wind patterns and thus ocean circulation (Auad et al., 2006; Roemmich et al., 2007). Furthermore, rising atmospheric carbon dioxide (CO_2) and resulting increased oceanic CO_2 uptake are the predominant factors driving ocean acidification (Dore et al., 2009), with a steady decrease of 0.02 pH units per decade over the past 30 years and an overall decrease since the pre-industrial period of 0.1 pH units (Doney et al., 2009). Other than these factors, variations in a wide range of ocean proxies such as sea level rise, declining oxygen concentration and sea ice have also been reported (Hoegh-Guldberg and Bruno, 2010). Since these physical and chemical changes in marine environment likely have strong effects on marine ecosystems (Poloczanska et al., 2016), it is imperative to understand how variation in ocean condition driven by climate change affects marine ecosystem (Birchenough et al., 2015).

1.3. Drastic changes in marine ecosystem in the Pacific Arctic

The marine environment in the Arctic is particularly sensitive to climate forcing. Actually, the Arctic is experiencing significant ocean warming of approximately three times the global average (Steele et al., 2008). The most conspicuous sign of the warming is dramatic loss of sea ice, and the Arctic is expected to be ice-free during summer starting in the mid- to late twenty-first century (Polyakov et al., 2010). Reductions in sea-ice cover are being further amplified by increased volume fluxes of Pacific water into the Arctic through the Bering Strait (Woodgate et al., 2006, 2015, 2010; Woodgate and Weingartner, 2012) in addition to warming of North Atlantic water that is transported to the Arctic through the Fram Strait (Comiso, 2012), resulting in early sea ice retreat in spring and late sea ice growth in fall (Steele et al., 2008). Since these patterns indicate a shift towards an earlier spring transition between sea-ice-covered and sea-ice-free condition (Grebmeier et al., 2006), recent changes in the sea ice dynamics are driving variations in marine organisms that may signal marine ecosystem reorganization (Grebmeier, 2012). Notably, reduction of sea ice cover have been particularly significant in the

marginal seas of the Alaskan and Russian continental shelves (Steele et al., 2008), including the northern Bering and Chukchi Seas, and hence monitoring of ecosystem changes in response to climate change is a crucial issue in this region.

A large continental shelf in the Pacific Arctic extending from the northern Bering Sea to the southeastern Chukchi Sea (hereafter, the Pacific Arctic) is one of the most biologically productive regions in the world's oceans (Springer et al., 1989). The seasonal cycle of sea ice growth and melt provides suitable conditions for phytoplankton growth (Stabeno et al., 2010); hence, large spring blooms occur at the marginal ice edge and under the ice (Laney and Sosik, 2014). This region has a unique food web structure where a large proportion of primary productivity generated in the surface layer falls directly to the sea floor with little or no zooplankton grazing (Campbell et al., 2009), and the strong pelagic–benthic coupling has maintained large areas of high benthic biomass in the Pacific Arctic. In particular, the patchy areas of remarkably high benthic biomass are called benthic hotspots (Grebmeier et al., 2015b), and these benthic hotspots are known as important foraging area for upper trophic level benthivores (Grebmeier et al., 2006). However, recent increased research activity in the Pacific Arctic is improving our knowledge about variations in benthivores. For instance, gray whales (*Eschrichtius robustus*) primarily used the Chirikov Basin in the northern Bering Sea with dense aggregations of amphipods in the 1980s (Highsmith and Coyle, 1992), whereas aerial surveys conducted in 2002 revealed a 3- to 17-fold decline in their population due to the reduction in prey biomass as much as 50% relative to the 1980s, resulting in an extension of their foraging area to the southern Chukchi Sea (Moore et al., 2003). In addition, spectacled eiders (*Somateria fischeri*), which overwinter in the open-water leads in pack ice south of St. Lawrence Island in the northern Bering Sea to feed on productive bivalve populations (Lovvorn et al., 2003), have drastically decreased their population size coincident with declines in prey density during the last few decades (Lovvorn et al., 2014). Overall, major benthivores in the Pacific Arctic have changed their abundance and distribution in this region, and these changes were strongly linked with variations in their prey availabilities (Moore et al., 2003; Lovvorn et al., 2003, 2014).

1.4. Urgent issue for understanding ecosystem changes in the Pacific Arctic

In the Pacific Arctic food web, even small changes in the lower trophic levels would have cascading effects on the higher trophic levels as a consequence of the short and efficient energy transfer pathways (Grebmeier et al., 2010), and thus the bottom-up control on higher trophic levels is crucial (Schonberg et al., 2014). Indeed, as mentioned above, there is growing evidence of the corresponded changes in benthivores and their prey. However, little is known about a detailed process of spatiotemporal variation in prey of benthivores, namely, benthic

macrofauna, although benthic macrofauna must be a key factor for better understanding about the changing ecosystem in the Pacific Arctic. This poor understanding of the process of macrofuanal variation likely to come from the reason that most of research has been focused on specific macrofaunal components (e.g., single species or life stages) or at assemblage levels, yet such assessments in isolation will have limited validity due to the trophic interaction through the entire food web, including pelagic components (Birchenough et al., 2015).

Historically, bivalves, amphipods and polychaetes are major macrofaunal taxa in the Pacific Arctic, and average macrofaunal biomass in the region persistently exceeded 20 gC m^{-2} for decades (Grebmeier et al., 2015c). Over the several decades, persistent seasonal *in situ* production and advected carbon from upstream sources, coincident with strong pelagic–benthic coupling processes, have maintained four major patches of relatively high macrobenthic community biomass in the Pacific Arctic, which refer to as benthic hotspots. These benthic hotspots occur on the continental shelf in the northern Bering Sea near the St. Lawrence Island Polynya, in the Chirikov Basin south of Bering Strait, in the southeastern Chukchi Sea, and in the northeastern portion of the Chukchi Sea (Grebmeier et al., 2006, 2015a; Grebmeier, 2012). However, time series observation in the regions indicates a latitudinal change in both biomass and composition of macrofaunal community. For example, some of macrofauna are showing significant declines in biomass from 2004 to 2012, both for the composite time-series sites and at select sites located within Anadyr Water (Grebmeier et al., 2015a). In addition, a shift in dominant species from larger bivalve *Nuculana radiata* to smaller bivalve *Ennucula tenuis* has occurred in south of St. Lawrence Island (Grebmeier, 2012; Lovvorn et al., 2009), although further large bivalve *Macoma calcarea* was dominant before 1980s (Lovvorn et al., 2003). Consequently, macrofaunal community in the Pacific Arctic has exhibited drastic changes, yet a large part of those processes still remain unknown. Thus, a process study that investigates links between macrofaunal community and its potential drivers, such as sediment and water column contexts (Cooper et al., 2015; Grebmeier et al., 2015a), would improve our understanding of ecosystem changes in the Pacific Arctic.

1.5. Satellite-based approach for current issue in the Pacific Arctic

Benthic macrofauna are normally stationary in marine sediments, and thus their community patterns are strongly impacted by organic carbon transport from the overlying water column as well as lateral advection (e.g., Lovvorn et al., 2013; Mathis et al., 2014; Grebmeier et al., 2015a). As the Pacific Arctic ecosystem has been characterized as tight pelagic–benthic coupling, variations in the amount of organic carbon transported to the seafloor could be linked strongly with surface phytoplankton production and/or community structure. However, the

spatiotemporal variations in phytoplankton and detailed processes of those influence on benthic organisms via benthic–pelagic coupling have not been well investigated yet and thus have remained as a missing link that is necessary for better understanding of changing Pacific Arctic ecosystems.

Classical methods relying on ship-based observations have been very successful to date in understanding local and snapshot of ocean (Joint and Groom, 2000), although these have difficulty in assessing the fine-scale spatiotemporal variations. A single cell of phytoplankton only lives for a few days and thus population and composition of phytoplankton community fluctuate strongly in a matter of days to weeks (d'Ovidio et al., 2010), while many high latitude benthic macrofauna, especially bivalves, have life spans of years to decades (Ambrose et al., 2006; Mullerlupp and Bauch, 2005). Hence, more adequate methods are required for optimal observation of spatiotemporal dynamics of phytoplankton assemblage. One of the solutions for this problem is to use satellite, which enables us to derive long-term variations of phytoplankton assemblage with fine-scale resolution in terms of both in space and in time. The chlorophyll-*a* (chl*a*) concentration, which is an index of phytoplankton biomass, has been recognized as the most successful satellite product related to phytoplankton assemblage. While chl*a* is still the major satellite product that is utilized by many scientists at various research fields (McClain, 2009), recent efforts have further enabled to estimate not only chl*a* but also taxonomic and size structure of phytoplankton community (Kostadinov et al., 2009; Mouw and Yoder, 2010; Brewin et al., 2011; Devred et al., 2011; Hirata et al., 2011; Roy et al., 2013; Wang et al., 2015) in addition to dominant taxa and size class (Sathyendranath et al., 2004; Alvain et al., 2005). Although satellite-based approaches are generally restricted themselves to only surface information owing to the characteristics, satellite products such as biomass and size structure of surface phytoplankton community could facilitate to understand the linkage between phytoplankton and benthic organisms via benthic–pelagic coupling.

1.6. Objectives and organization of this dissertation

As mentioned above, recent environmental variations are predicted to lead the loss of ecosystem services through the changes in ocean components. This study primarily utilized satellite products in addition to other adequate approaches such as *in situ* observations and laboratory experiments for understanding the process of ecosystem variation in the Pacific Arctic. The main goals of this study are to:

[1] Understand variations in phytoplankton and benthic macrofaunal communities in the Pacific Arctic

[2] Examine detailed process of variation in benthic macrofaunal community based on tight

pelagic–benthic coupling in the region

[3] Forecast future changes in the Pacific Arctic ecosystem in response to ongoing climate forcing

To achieve these objectives, in chapter 2, an approach for monitoring spatiotemporal variation in phytoplankton size structure based on satellite remote sensing was developed, and was used to demonstrate an example of application that has a potential for more adequate prediction of distribution shift in marine organisms. Chapter 3 investigated spatiotemporal variation in satellite-derived phytoplankton size structure and its impact on benthic macrofaunal community in the Pacific Arctic. Chapter 4 provides results that would explain the process of distributional shift in benthic macrofauna in the Pacific Arctic, which found in chapter 3, by conducting a factorial laboratory experiment in addition to *in situ* and satellite observations. Moreover, spatiotemporal variations in species invasion and diversity of benthic macrofaunal community in the Pacific Arctic were investigated in chapter 5. This chapter further examined those causes in terms of northward volume transports from the Pacific to the Arctic seas. Based on these results, overall conclusion in terms of past, current and future perspectives of the Pacific Arctic ecosystem were discussed in chapter 6.

Table 1.1. Summary of abbreviations used in this dissertation.

Abbreviation	Definition
AFDW	Ash-free dry weight
AMP	Arctic Marine Pulses
ArCS	Arctic Challenge for Sustainability
AVISO	Archiving, Validation and Interpretation of Satellite Oceanographic data
AW	Ash weight
CAFF	Conservation of Arctic Flora and Fauna
CCGS	Canadian Coast Guard Ship
CDOM	Colored dissolved organic matter
Chirikov	Chirikov Basin
Chl*a*	Chlorophyll-*a*
Chukchi	Chukchi Sea
CNES	Centre National d'Etudes Spatiales
CO_2	Carbon dioxide
CSD	Chlorphyll-*a* Size Distribution
CTD	Conductivity–temperature–depth
DAAC	Distributed Active Archive Center
DBO	Distributed Biological Observatory
DHA	Docosahexaenoic acid
DMSP	Defense Meteorological Satellite Program
DPA	Diagnostic pigment analysys
DW	Dry weight
EPA	Eicosapentaenoic acid
FA	Fatty acid
GCOM-C	Global Change Observation Mission–Climate
GRENE	Green Network of Excellence
GSFC	Goddard Space Flight Center
GSM	Garver-Siegel-Maritorena
IOP	Inherent optical property
IPCC	International Panel on Climate Chamge
JAXA	Japan Aerospace Exploration Agency
LRM	Low Resolution Mode
MEA	Millennium Ecosystem Assessment
MEXT	Ministry of Education, Culture, Sports, Science and Technology of Japan
MODIS	Moderate Resolution Imaging Spectroradiometer
NAP	Non-algal particle
NARR	North American Regional Reanalysis
NASA	National Aeronautics and Space Administration
NSF	National Science Foundation
NSIDC	National Snow and Ice Data Center
OBPG	Ocean Biology Processing Group
OC3M	Chl*a* 3-band ocean color algorithm for MODIS
OC4L	Chl*a* 4-band linear ocean color algorithm
PacMARS	Pacific Marine Arctic Regional Synthesis
PC	Principal component
PCA	Principal component analysis
PSD	Particle Size Distribution
PUFA	Polyunsaturated fatty acid
QAA	Quasi-analytical algorithm
RRMSE	Relative root mean square error

Table 1.1. Continued.

Abbreviation	Definition
SAR	Synthetic Aperture Rader
SBE	Sea-Bird Electronics, Inc.
SeaWiFS	Sea-Viewing Wide Field-of-View
SIC	Sea ice concentration
SLI	St. Lawrence Island
SOAR	Synthesis of Arctic Research
SWI	Shannon-Weaver Index
SWL	Sir Wilfrid Laurier

Table 1.2. List of symbols and units.

Symbol	Description	Unit
λ	Wavelength	nm
z	Depth	m
$R_{\mathrm{rs}}(\lambda)$	Remote sensing reflectance at λ	sr^{-1}
$L_{\mathrm{w}}(\lambda)$	Water-leaving radiance at λ	W m^{-2} sr^{-1} $\mu\mathrm{m}^{-1}$
$L_{\mathrm{u}}(\lambda, z)$	Upward spectral radiance at λ at z	W m^{-2} sr^{-1} $\mu\mathrm{m}^{-1}$
$E_{\mathrm{d}}(\lambda, z)$	Downward spectral irradiance at λ at z	W m^{-2} $\mu\mathrm{m}^{-1}$
$E_{\mathrm{ds}}(\lambda)$	Above-water downward spectral irradiance at λ	W m^{-2} $\mu\mathrm{m}^{-1}$
$K_{\mathrm{u}}(\lambda)$	Diffuse attenuation coefficient of upward radiance at λ	m^{-1}
$a_{\mathrm{ph}}(\lambda)$	Phytoplankton absorption coefficient at λ	m^{-1}
$a_{\mathrm{ph}}^{\mathrm{std}}(\lambda)$	Normalized phytoplankton absorption coefficient at λ	Dimensionless
$a_{\mathrm{CDOM}}(\lambda)$	CDOM absorption coefficient at λ	m^{-1}
$b_{\mathrm{bp}}(\lambda)$	Particle backscattering coefficient at λ	m^{-1}
D	Diameter	m
D_0	Reference diameter	m
$D_{\max}$	Maximum diameter	m
$D_{\min}$	Minimum diameter	m
D_1, D_2	Arbitrary defined diameter ($D_1 > D_2$)	m
N	Number of particles within given size range	Dimensionless
$N(D)$	Number of particles normalized by size bin width D	m^{-4}
N_0	Reference N at D_0	Dimensionless
ξ	Junge slope of the PSD	Dimensionless
$\mathrm{Chl}a_{\mathrm{total}}$	Total chl*a* from $D_{\min}$ to $D_{\max}$	mg m^{-3}
$\mathrm{Chl}a_{\mathrm{size}}$	Size fractionated chla within given size range	mg m^{-3}
$\mathrm{Chl}a_0$	Reference chl*a* at D_0	mg m^{-3}
η	Junge slope of the CSD	Dimensionless
β_0, β_i	Regression coefficients	Dimensionless
S_i	*i*-th PC score	Dimensionless
v_j	*j*-th variable	Dimensionless
$w_{i,j}$	Loading factors for S_i	Dimensionless
C_j	Model coefficient for v_j	Dimensionless
F_{size}	Fraction of $\mathrm{chl}a_{\mathrm{size}}$ within given range to $\mathrm{chl}a_{\mathrm{total}}$	%
θ	Angle	°
V_θ	Velocity of shift along θ; Wind velocity along θ	km decade^{-1}; m s^{-1}
S_{NS}	North–South spatial gradient	km^{-1}
S_{EW}	East–West spatial gradient	km^{-1}
lat_c	Centroid of biomass-weighted latitude	°
lat	Latitude at a sampling station	°
$biom$	Macrofaunal biomass at a sampling station	gC m^{-1}
$Meas$	*In situ* measured CSD slope	Dimensionless
Sat	Satellite-estimated CSD slope	Dimensionless

Chapter 2

Differences in rate and direction of shifts between phytoplankton size structure and sea surface temperature

2.1. Introduction

Improved understanding of how species shift their distributions is crucial for effective conservation under conditions of climate change (Dawson et al., 2011). Climate velocity representing horizontal velocity of temperature change is derived as the ratio of the long-term temperature trend to the two-dimensional spatial gradient in temperature, and it enables predictions regarding species migration and persistence as an expectation of how species track the location of their thermal niches (Loarie et al., 2009). In marine ecosystem research, climate velocity is calculated from sea surface temperature (SST); hence, I refer here to climate velocity in terms of SST. Some recent studies have exposed a complex mosaic of velocity of SST, suggesting non-uniform shifts in the global oceans with a wide range of rates and directions that deviate from simple poleward migration (Burrows et al., 2011). Therefore, the velocity of SST is expected to describe observed species shifts (Philippart et al., 2011; VanDerWal et al., 2012); however, unexpected shifts that are inconsistent with predictions generated by the velocity of SST have been reported for some species and in certain regions (Pinsky et al., 2013; Poloczanska et al., 2013).

Phytoplankton plays numerous fundamental roles as primary producer in marine ecosystem. For instance, nitrogen fixation by cyanobacteria is an important process in the marine nitrogen cycle especially oligotrophic regions (Zehr et al., 2000). In addition, large species such as diatoms dominate in nutrient rich water, and their presence increases the efficiency of biological pump (Le Quéré et al., 2005). One of the most important functions of phytoplankton is to determine the energy transfer efficiency through the food web, which depends strongly on its size structure (Lalli and Parsons, 1997), and thus the size composition of phytoplankton community is expected to affect species distribution through changes in the food web structure. In addition, compared to ship-based *in situ* observations, satellite-based monitoring has advantage to make continuous, fine-scale measurements that allow the synoptic exploration of vast areas of the world ocean (Marchese et al., 2017). Since recent efforts enabled to derive size structure of phytoplankton community from ocean color data, satellite-based monitoring of phytoplankton size structure is likely to contribute better predictions of species shifts and ecosystem conservations.

In the past decade, various methods have been developed for global estimation of phytoplankton size structure using satellite remote sensing based on optical properties such as

the phytoplankton absorption coefficient ($a_{\mathrm{ph}}(\lambda)$) and the particle backscattering coefficient ($b_{\mathrm{bp}}(\lambda)$) (Fujiwara et al., 2011; Kostadinov et al., 2009; Roy et al., 2013). Kostadinov et al. (2009) proposed a novel method to estimate phytoplankton size structure based on the particle size distribution (PSD) using the slope of $b_{\mathrm{bp}}(\lambda)$. As phytoplankton is the main particle component in the pelagic ocean (Bricaud and Morel, 1986), PSD can in turn be related to phytoplankton size distribution. The principle advantage of this approach is the arbitrariness of the arrangement of the size range, where other methods generally adopt a fixed target group or size class. However, $b_{\mathrm{bp}}(\lambda)$ is affected not only by phytoplankton but also by non-algal particles (NAPs) (Stramski et al., 2004). To overcome this problem, Roy et al. (2013) reconstructed the PSD model using a chlorophyll-*a* (chl*a*)-specific absorption coefficient ($a^*_{\mathrm{ph}}(\lambda)$) at the wavelength of 676 nm. They successfully estimated the phytoplankton size structure; however, the retrieval of inherent optical properties (IOPs) at longer wavelength (such as 676 nm) is quite difficult because of the strong absorption by the water itself (Lee et al., 2002). Some recent studies have demonstrated the utility of the principal component analysis (PCA) approach in deriving information on phytoplankton community structure (Bracher et al., 2015; Craig et al., 2012; Wang et al., 2015). For example, Wang et al. (2015) developed a method to estimate phytoplankton size structure using the spectral features of normalized $a_{\mathrm{ph}}(\lambda)$ captured by PCA. Thus, a PCA approach based on PSD could constitute a powerful tool for the global estimation of the synoptic size structure of the phytoplankton community.

The goal of this chapter is to clarify the similarities and differences between the changes in phytoplankton size structure and SST. To achieve this objective, a model for retrieving phytoplankton size structure was developed by quantifying the phytoplankton size distribution using spectral features of $a_{\mathrm{ph}}(\lambda)$. The developed model was applied to satellite remote sensing data to estimate the phytoplankton size distribution, and then velocity of the phytoplankton size distribution was compared with that of SST owing to demonstrate a potential of satellite-derived phytoplankton size structure regarding to better predictions of species distributional shifts occurring now and in the future.

2.2. Materials and methods

2.2.1. *In situ* data

The dataset used in this chapter was obtained from a wide area following 23 cruises over a 16-year period (Figure 2.1, Table 2.1). At each station, size fractionated chl*a* ($\mathrm{chl}a_{\mathrm{size}}$), light absorption coefficient, and spectral radiation were measured, the detailed procedures of which are described below. Note that the spectral radiation was not observed at some stations. Seawater samples were collected from the sea surface (0 m) using a clean plastic bucket.

Various filters were used to obtain $\mathrm{chl}a_{\mathrm{size}}$ during each cruise (Table 2.2). Seawater samples were filtered onto polycarbonate membrane or nylon mesh filters and GF/F filters under low vacuum pressure. After filtration, the filter was immediately soaked in *N*,*N*-dimethylformamide, and pigments were extracted for 24 h in the dark at −20°C (Suzuki and Ishimaru, 1990). The chl*a* concentrations were determined by the fluorescence acidification technique (Holm-Hansen et al., 1965) during JARE-42, JARE-43, UM0203, 44Tangaroa and UM0405 and the non-acidification technique (Welshmeyer, 1994) during other cruises using a 10-AU fluorometer (Turner Designs Inc., USA).

To measure phytoplankton absorption spectra, particles in water samples were collected onto a GF/F filter. The optical density (*OD*) of particles on the filter was measured immediately after sampling using a MPS-2400 or a MPS-2450 spectrophotometer (Shimadzu, Japan) at wavelengths of 350–750 nm, and the absorption coefficient of the total suspended particles ($a_{\mathrm{p}}(\lambda)$) was determined from the *OD* according to the quantitative filter technique (Mitchell, 1990). The *OD* of the NAPs was then measured after soaking in methanol (Kishino et al., 1985) or sodium hypochlorite (Tassan and Ferrari, 1995), and the absorption coefficient of the NAPs ($a_{\mathrm{d}}(\lambda)$) was quantified as well as $a_{\mathrm{p}}(\lambda)$. Finally, $a_{\mathrm{ph}}(\lambda)$ was obtained by subtracting $a_{\mathrm{d}}(\lambda)$ from $a_{\mathrm{p}}(\lambda)$.

In situ spectral distributions of the underwater radiation were acquired using a SMPR (Satlantic Inc., Canada), a HyperPro (Satlantic Inc., Canada) or a PRR-800/810 (Biospherical Instruments Inc., USA). The HyperPro measures underwater downward spectral irradiance ($E_{\mathrm{d}}(\lambda, z)$) and upward spectral radiance ($L_{\mathrm{u}}(\lambda, z)$) at 136 wavelengths between 350 and 800 nm. The SPMR and PRR800/810 measure those radiations at 13 and 17 wavelengths between 400 and 705 nm and between 380 and 765 nm, respectively. These measurements were acquired at the same time as above-water measurements of downward spectral irradiance ($E_{\mathrm{ds}}(\lambda)$), which were taken using a sensor mounted on the ship deck.

Remote sensing reflectance ($R_{\mathrm{rs}}(\lambda)$) was calculated as the ratio of the water-leaving radiance $L_{\mathrm{w}}(\lambda)$ to $E_{\mathrm{ds}}(\lambda)$:

$$R_{\mathrm{rs}}(\lambda) = L_{\mathrm{w}}(\lambda)/E_{\mathrm{ds}}(\lambda). \tag{2.1}$$

The $L_{\mathrm{w}}(\lambda)$ was obtained from $L_{\mathrm{u}}(\lambda, z)$ just beneath the water surface ($L_{\mathrm{u}}(\lambda, 0-)$), which was determined as the fitting coefficient of near-surface $L_{\mathrm{u}}(\lambda, z)$ and the water-air interface propagation factor of 0.544 (Darecki and Stramski, 2004) as follows:

$$L_{\mathrm{w}}(\lambda) = 0.544 \times L_{\mathrm{u}}(\lambda, 0-), \tag{2.2}$$

$$L_u(\lambda, z) = L_u(\lambda, 0-) \times \exp[-K_{\mathrm{u}}(\lambda) \times z], \tag{2.3}$$

where z and $K_u(\lambda)$ are the depth and diffuse attenuation coefficient of upward radiance, respectively. Then, $R_{rs}(\lambda)$ was resampled at 10 MODIS bands (412, 443, 469, 488, 531, 547, 555, 645, 667, and 678 nm) from the original wavelength of the spectroradiometers using spline interpolation (Wang et al., 2015). To estimate $a_{ph}(\lambda)$ from *in situ* $R_{rs}(\lambda)$, the latest version of the quasi-analytical algorithm version 6 (QAA-v6) (Lee et al., 2002, http://www.ioccg.org/groups/software.html) was applied to the observed $R_{rs}(\lambda)$.

2.2.2. Satellite remote sensing data

The latest (R2014.0) level-3 standard mapped daily images of $R_{rs}(\lambda)$ derived by Moderate Resolution Imaging Spectroradiometer (MODIS)-Aqua were downloaded from the National Aeronautics and Space Administration (NASA) Ocean Biology Processing Group (OBPG) with 9 km spatial resolution. $R_{rs}(\lambda)$ at 10 bands (λ = 412, 443, 469, 488, 531, 547, 555, 645, 667 and 678 nm) were obtained for 2002–2017. $a_{ph}(\lambda)$ at MODIS bands were derived from $R_{rs}(\lambda)$ using QAA-v6. Chl*a* concentration was computed from $R_{rs}(\lambda)$ using the OC3M algorithm (O'Reilly et al., 2000). Furthermore, monthly averaged SST data derived by MODIS-Aqua with 9 km spatial resolution were obtained for 2002–2017. These satellite data were resampled on a 1° × 1° grid and composited as monthly averages to minimize local and transient variabilities.

2.2.3. Model description

Assuming that the PSD follows the Junge-type power law size distribution (Barder, 1970), the number of particles per unit volume of seawater normalized by the size bin diameter (D), $N(D)$, can be expressed as follows:

$$N(D) = N_0(D/D_0)^{-\xi}, \tag{2.4}$$

where ξ is the Junge slope of the PSD, and D_0 is a reference diameter at which $N_0 = N(D)$. Therefore, the total number of particles in a given size range can be derived by integrating Eq. (2.4) from the minimum diameter (D_{min}) to the maximum diameter (D_{max}); thus, enabling the PSD to be partitioned into distinct classes described by

$$N = \int_{D_{min}}^{D_{max}} N_0(D/D_0)^{-\xi} dD. \tag{2.5}$$

Given that the chl*a* is particulate, and thus the chl*a* size distribution (CSD) also follows the Junge-type power law distribution, the total chl*a* ($chla_{total}$) and $chla_{size}$ in a given size rage from D_1 to D_2 can be expressed using Eqs. (2.6) and (2.7) as follows:

$$\mathrm{chl}a_{\mathrm{total}} = \int_{D_{\mathrm{min}}}^{D_{\mathrm{max}}} \mathrm{chl}a_0 (D/D_0)^{-\eta} dD, \tag{2.6}$$

$$\mathrm{chl}a_{\mathrm{size}} = \int_{D_1}^{D_2} \mathrm{chl}a_0 (D/D_0)^{-\eta} dD\,, \tag{2.7}$$

where $\mathrm{chl}a_0$ is the reference chl*a* at D_0 (here, 0.7 μm), and η is the exponent of the chl*a* size spectrum (hereafter, CSD slope). Larger magnitudes of the CSD slope indicate a large proportion of smaller phytoplankton, whereas smaller magnitudes suggest predominance of larger phytoplankton. In this chapter, D_{min} and D_{max} were assumed as the pore size of GF/F filter (i.e., nominal 0.7 μm) and 200 μm (Dussart, 1965), respectively. The CSD slope is derived as the slope of the liner regression in log-space between the inverse log-transformed median diameters from log-transformed D_1 to D_2 and $\mathrm{chl}a_{\mathrm{size}}$ normalized by the size bin width. Note that the intercept of the liner regression showed significant ($p < 0.05$) negative relationship with the slope, suggesting the intercept and slope covary in response to the size structure of phytoplankton community.

The chl*a* fraction of an arbitrarily defined size rage (F_{size}) can be derived using the CSD slope as follows:

$$F_{\mathrm{size}} = \frac{\mathrm{chl}a_{\mathrm{size}}}{\mathrm{chl}a_{\mathrm{total}}} = \frac{\int_{D_1}^{D_2} \mathrm{chl}a_0 (D/D_0)^{-\eta} dD}{\int_{D_{0.7}}^{D_{200}} \mathrm{chl}a_0 (D/D_0)^{-\eta} dD} = \frac{D_2^{1-\eta} - D_1^{1-\eta}}{200^{1-\eta} - 0.7^{1-\eta}}, \tag{2.8}$$

where the constants $\mathrm{chl}a_0$ and D_0 no longer exist in Eq. (8), such that only the CSD slope and diameter range are required for estimating each fraction of the phytoplankton size classes. Figure 2.2 is an example of the relationship between the CSD slope and F_{size}. Here, phytoplankton was partitioned into three size classes: picoplankton (0.7–2.0 μm), nanoplankton (2.0–20.0 μm), and microplankton (20.0–200.0 μm). The microplankton dominate when the CSD slope is smaller than 1.0, nanoplankton dominate when the CSD slope value is 1.0–1.5, and picoplankton begin to dominate when the CSD slope extends beyond 1.5.

2.2.4. Quantification of the CSD slope

To quantify the CSD slope, I focused on the spectral shape of normalized $a_{\mathrm{ph}}(\lambda)$ ($a_{\mathrm{ph}}^{\mathrm{std}}(\lambda)$). The $a_{\mathrm{ph}}^{\mathrm{std}}(\lambda)$ was derived from the wavelength mean and standard deviation of $a_{\mathrm{ph}}(\lambda)$ at 10 MODIS bands. The formula for $a_{\mathrm{ph}}^{\mathrm{std}}(\lambda)$ is shown below:

$$a_{\mathrm{ph}}^{\mathrm{std}}(\lambda) = \left[a_{\mathrm{ph}}(\lambda) - \mathrm{mean}\left[a_{\mathrm{ph}}(\lambda)\right]\right] / \mathrm{std}\left[a_{\mathrm{ph}}(\lambda)\right], \tag{2.9}$$

where $\mathrm{mean}\left[a_{\mathrm{ph}}(\lambda)\right]$ and $\mathrm{std}\left[a_{\mathrm{ph}}(\lambda)\right]$ are the wavelength mean and standard deviation of

$a_{\mathrm{ph}}(\lambda)$, respectively. Although the spectral shape of $a_{\mathrm{ph}}^{\mathrm{std}}(\lambda)$ vary with the phytoplankton size structure, the accuracy of satellite-derived $a_{\mathrm{ph}}(\lambda)$ is generally pore in areas of low productivity, such as subtropical gyres. To overcome this problem, PCA was applied to $a_{\mathrm{ph}}^{\mathrm{std}}(\lambda)$ together with chl*a*. The input values for the PCA comprised a matrix ($m \times N$) constituted of $a_{\mathrm{ph}}^{\mathrm{std}}(\lambda)$ and chl*a*, where *m* and *N* are the numbers of variables and samples, respectively. The resulting principal component (PC) scores were assumed to correlate with the CSD slope; hence, the CSD slope was quantified as a logistic-type regression model using the *i*-th PC score (S_i) and regression coefficients (β_0 and β_i) between the CSD slope and PC scores as follows:

$$\eta = \left(\beta_0 + \exp\sum_{i=1}^{k} \beta_i S_i\right)^{-1}, \tag{2.10}$$

where k is the number of PCs. Here, S_i can also be expressed as follow:

$$S_i = \sum_{j=1}^{m} v_j w_{i,j}, \tag{2.11}$$

where v_j and $w_{i,j}$ are the *j*-th variables and the loading factors for S_i, respectively. Thus, an equation was obtained by replacing S_i in Eq. (2.10) with Eq. (2.11):

$$\eta = \left(\beta_0 + \exp\sum_{j=1}^{m} C_j v_j\right)^{-1}, \tag{2.12}$$

$$C_j = \sum_{i=1}^{k} \beta_i w_{i,j}. \tag{2.13}$$

Finally, the CSD slope is derived from Eq. (2.12) using the model parameters of β_0 and C_j. To avoid unrealistic values of the CSD slope, the upper and lower limits of the CSD slope were defined as 3.0 and 0.0, respectively. These limits mostly corresponded to 90% of pico- and microplankton dominance to $\mathrm{chl}a_{\mathrm{total}}$.

2.2.5. Evaluation of estimate accuracy of the CSD model

The accuracy of the CSD model was evaluated by comparing *in situ* measured and satellite matchup CSD slope values. Satellite matchup CSD slope values were constructed using the single 9 km pixel from daily images based on sampling date and location. The relative root mean square error (RRMSE) was computed as relative values to provide equal weights to all samples and then expressed as percentages (Ciotti and Bricaud, 2006; Zhang et al., 2009), as described by

$$\mathrm{RRMSE} = 100 \times \sqrt{\frac{1}{N}\sum_{i=1}^{N}[(Meas_i - Sat_i)/Meas_i]^2}, \tag{2.14}$$

where $Meas_i$ and Sat_i are the *i*-th measured and satellite machup values, respectively.

2.2.6. Velocities of the shift

Velocities of the CSD slope, chl*a*, and SST were derived following the method of Burrows et al. (2011). The velocity along angle θ (V_θ), with 0° as North and 180° as South, was calculated on a 1° grid by dividing the temporal trend over the period 2002–2014 by the spatial gradient as follows:

$$V_\theta = \text{Temporal trend}/\text{Spatial gradient} \tag{2.15}$$

The long-term temporal trend was calculated as the slope of the linear regression between monthly anomalies and time. Note that the temporal trend was employed as an absolute value when the velocity was determined using Eq. (2.15) to clarify the local speed of shifting contours. The spatial gradient was derived as the vector angle given by the direction of the gradient, as described by

$$\text{Spatial gradient} = S_{NS}\cos\theta + S_{EW}\sin\theta, \tag{2.16}$$

where S_{NS} is the North–South spatial gradient and S_{EW} is the East–West spatial gradient. The North–South spatial gradient was calculated as the difference in the temporal average for each northern and southern pair divided by the distance between them. The East–West spatial gradient was calculated similarly for each eastern and western adjacent pair divided by the distance between the pixels in each pair.

2.3. Results

2.3.1. Retrieval of the CSD slope from *in situ* chla_{size}

Various filters were used to obtain $\text{chl}a_{\text{size}}$. In general, phytoplankton is partitioned into three size classes: picoplankton (0.7–2.0 μm), nanoplankton (2.0–20.0 μm) and microplankton (>20.0 μm). However, typical filters for dividing phytoplankton into the size classes have not been used during some cruises (e.g., UM0405, OS180 and KH-0904). This fact forces to employ specific combinations of filters used for obtaining $\text{chl}a_{\text{size}}$, resulting in only a part of the dataset can be used together. Thus, the dataset could not be used in its entirely with typical methods such as Brewin et al. (2010) and Devred et al. (2011) that need to fix the size range of each phytoplankton size class. In contrast, it is possible to derive the CSD slope from any combination of $\text{chl}a_{\text{size}}$; hence, the entire dataset was used successfully for developing a CSD model.

To verify the robustness of the CSD slope values determined by various combinations of filters, the CSD slopes derived from different combination of $\text{chl}a_{\text{size}}$ were compared. For this comparison, the data obtained during the MR12-E03 cruise were employed because filters with various pore sizes were used during this cruise. Figure 2.3 shows the

relationships between the CSD slope values derived from three typical chla_{size} (0.7–2.0, 2.0–20.0, and >20.0 μm) and different combination of chla_{size}. The resulting RRMSEs were 4.9% and 4.0%, and therefore the differences in the CSD slope among the combinations of filters were negligible.

2.3.2. Empirical development of the CSD model

The *in situ* CSD slope ranged from 0.42 to 2.43. Note that smaller CSD slope values indicate phytoplankton assemblages with larger size, and vice versa. Figure 2.4 shows the relationship between the CSD slope and spectral shape of $a_{\mathrm{ph}}^{\mathrm{std}}(\lambda)$. It is clear that there are differences in $a_{\mathrm{ph}}^{\mathrm{std}}(\lambda)$ accompanying the variation of CSD slope. For instance, smaller CSD slope values show remarkably higher values of $a_{\mathrm{ph}}^{\mathrm{std}}(\lambda)$ between 400 and 430 nm than do larger values of the CSD slope. In addition, $a_{\mathrm{ph}}^{\mathrm{std}}(\lambda)$ values associated with smaller CSD slope values are higher than those of larger CSD slope values between 660 and 690 nm. These differences in $a_{\mathrm{ph}}^{\mathrm{std}}(\lambda)$ were mainly due to a coupling of the packaging effect and pigment component, which is strongly affected by phytoplankton cell size and species composition, as described by Ciotti et al. (2002) and Wang et al. (2015).

In addition to $a_{\mathrm{ph}}^{\mathrm{std}}(\lambda)$, chl*a* was also employed to conduct PCA for capturing features of phytoplankton assemblage which vary with phytoplankton size structure. Initially, PCA was conducted for $a_{\mathrm{ph}}^{\mathrm{std}}(\lambda)$ at 10 MODIS bands and chl*a*; however, the estimation accuracy of the QAA-v6 became quite poor at longer wavelengths such as 645, 667, and 678 nm with huge RRMSE values of 67.2, 77.9, and 58.1%, respectively (Table 2.3). Therefore, only $a_{\mathrm{ph}}^{\mathrm{std}}(\lambda)$ at the seven shorter wavelengths of 412, 443, 469, 488, 531, 547, and 555 nm and chl*a* were used as input values of $a_{\mathrm{ph}}^{\mathrm{std}}(\lambda)$ for developing the CSD model.

To capture the variances in $a_{\mathrm{ph}}^{\mathrm{std}}(\lambda)$ and chl*a*, PCA was conducted against these two parameters. The first four PC modes explained 98.9% of the total variance in these parameters. The first mode captured 83.1% and its variance was mostly driven by chl*a* (Figure 2.5a). The second mode explained 10.7% of the total variance and $a_{\mathrm{ph}}^{\mathrm{std}}(\lambda)$ shows an positive peak at 443 nm followed by slightly lower values at 412 and 469 nm (Figure 2.5b). The third mode explained 3.6% of the total variance in $a_{\mathrm{ph}}^{\mathrm{std}}(\lambda)$. This mode shows both negative and positive peaks at $a_{\mathrm{ph}}^{\mathrm{std}}(443)$ and $a_{\mathrm{ph}}^{\mathrm{std}}(531)$ (Figure 2.5c). The fourth mode explained only 1.4% of the total variance with an obvious positive peak at $a_{\mathrm{ph}}^{\mathrm{std}}(412)$ (Figure 2.5d).

The first four PC scores derived from $a_{\mathrm{ph}}^{\mathrm{std}}(\lambda)$ at the seven wavelengths and the chl*a*

were used to fit the logistic-type function, following which the model parameters β_0 and C_j were determined. Comparison between the CSD slopes determined from *in situ* chla_{size} and model-derived CSD slopes estimated from *in situ* $a_{\text{ph}}^{\text{std}}(\lambda)$ and chl*a* shows good agreement (RRMSE = 21.6%); however, data scattering for higher CSD slope values is apparent (Figure 2.6a). This might be because single combination of regression coefficients cannot capture the entire relationship between phytoplankton size structure, $a_{\text{ph}}^{\text{std}}(\lambda)$ and chl*a*. When focusing on the average $a_{\text{ph}}^{\text{std}}(\lambda)$ at the MODIS bands, the $a_{\text{ph}}^{\text{std}}(\lambda)$ at 412 nm was higher than at 469 nm for smaller CSD slopes, and vice versa. These spectral features were also found in previous studies, and they were attributed to differences in pigment composition related to phytoplankton cell size (Ciotti et al., 2002). For such practical considerations, the dataset for model parameters was divided into two, according to the relationship between $a_{\text{ph}}^{\text{std}}(\lambda)$ at 412 and 469 nm, and then determined the model parameters for each dataset. Thus, the CSD model is defined as summarized in Table 2.4. The resulting relationship between *in situ* and modeled CSD slopes shows better agreement, for which the RRMSE was reduced significantly to 12.9% (Figure 2.6b). Note that sampling locations of these two dataset were randomly distributed in latitude and longitude, suggesting geographic bias seemed negligible.

The performance of the CSD model was examined by comparing measured CSD slope values determined from *in situ* chla_{size} and matched up MODIS-derived CSD slope values. The resulting RRMSE between the measured and modeled CSD slope values was 25.2% (Figure 2.7). Although the CSD model relies on both the chl*a* and spectral shape of $a_{\text{ph}}^{\text{std}}(\lambda)$, the accuracy of the modeled CSD slope values could improved when more robust IOP algorithms are developed, because estimation of IOPs from satellite is still challenging issue.

2.3.3. Velocities of shifts in CSD slope and chl*a*

Figure 2.8 shows the average CSD slope and chl*a* values during the period from 2002 to 2014. It can be seen that smaller CSD slope values are present in coastal upwelling regions such as in the areas of the Benguela and Humboldt currents, whereas larger CSD slope values are found in oligotrophic regions, especially subtropical gyres. In general, these global patterns of CSD slope exhibit an inverse relationship with chl*a*, suggesting areas of high and low productivity are associated with the relative dominance of larger and smaller phytoplankton assemblages, respectively.

The temporal trend of CSD slope values was derived as a simple linear regression slope of the monthly anomaly of CSD slope against time. Overall, 38.7% of the global oceans had significant increases or decreases during 2002–2017 (Figure 2.9a). An decreasing trend in

CSD slope, indicating a change toward a larger phytoplankton community, was found for 79.3% of these regions. A significant increasing or decreasing trend in chl*a* was found in 32.4% of the global oceans for 2002–2017 (Figure 2.10a), with 84.0% of these regions exhibiting a increasing trend. The spatial gradient of CSD slope was relatively large along coastal regions and subtropical gyres resulting from dynamic changes in CSD slope with modest spatial gradients (Figure 2.9b). This global pattern of spatial gradient was consistent with that of chl*a* (Figure 2.10b).

It appeared that the velocities of CSD slope and chl*a* depended strongly on their spatial gradients rather than on their temporal trends because the velocities showed clear inverse distributions with the spatial gradients. When the rates of temporal change and spatial gradient of the CSD slope were combined, the resulting median velocity of the CSD slope across the ocean was 463.3 km decade^{-1}. This value is slightly higher than that of 383.1 km decade^{-1} for chl*a*, but these velocities are mostly within the range of observed distribution shifts of the phytoplankton community (469.9 ± 115.3 km decade^{-1}) reported by Poloczanska et al. (2013). The directions of shifts both in CSD slope and in chl*a* show a mosaic distribution, suggesting that spatiotemporal variations of CSD slope and chl*a* are non-uniform across the oceans. As species response to climate forcing is specific to the regional scale (Thackeray et al., 2010), a complex mosaic of the spatiotemporal variations of CSD slope and chl*a* has the potential for providing assessments of species shifts that are more accurate.

2.3.4. Comparison of velocities derived from CSD slope, chl*a* and SST

The SST shows significant temporal change in 40.3% of the global oceans, of which regions of warming and cooling account for 86.1 and 13.9%, respectively. The global median velocity of SST was 71.2 km decade^{-1} and this is approximately one fifth that of the CSD slope and chl*a*, suggesting a modest movement of the isotherms compared with the shifts in CSD slope and chl*a*. Note that the velocity of SST in this study was more than three times that reported in Burrows et al. (2011). This discrepancy was caused by differences in methods; i.e., this study used only significant trends ($p < 0.05$), and non-significant trends that result in low velocities were excluded. In fact, the median velocity of SST in this study was 39.1 km decade^{-1} when both significant and non-significant trends were included.

Although the direction of shift in SST also shows a complex pattern, which clearly differs from a simple poleward migration (Figure 2.11d), there are obvious regional differences in the directions of velocities among the CSD slope, chl*a*, and SST. For instance, the directions of shifts in CSD slope and chl*a* are largely consistent (Figure 2.12a), whereas the direction of shift in SST deviates from those of CSD slope and chl*a* (Figure 2.12b and c), as shown in

histograms of angle differences between each pair of these parameters (Figure 2.13). Note that 74.7% of angle difference between CSD slope and chl*a* were within the range of ±45°, whereas those of CSD slope and SST, and chl*a* and SST were 52.0 and 54.4%, respectively. The direction of shift in SST shows a patchy pattern in which some areas are comparable and others dissimilar to those of both CSD slope and chl*a*, and specific patterns were not found in this study. Thus, the rates and directions of shifts in CSD slope and chl*a* could explain the variations in species distribution that deviate from that of SST (Pinsky et al., 2013; Poloczanska et al., 2013).

2.4. Discussion

2.4.1. Advantage of the CSD model for retrieving phytoplankton size structure

Satellite-based estimation of spatiotemporal variation in phytoplankton size structure can contribute to better understanding of the biogeochemical and ecological responses to recent climate forcing (McClain, 2009). In this study, a CSD model was developed based on empirical relationships between the size distribution of chl*a*, the spectral shape of $a_{\mathrm{ph}}^{\mathrm{std}}(\lambda)$ and chl*a* concentration. This method enabled to derive the synoptic size structure of the phytoplankton community with sufficient accuracy using satellite remote sensing, based on the dataset obtained from a wide area of the North Pacific, Southern Ocean and Western Arctic Ocean, despite approximately one third the samples being obtained from the optically complex waters of the Western Arctic Ocean (Cota and Ruble, 2005; Matsuoka et al., 2011). It should be noted that the global distribution of $a_{\mathrm{ph}}(\lambda)$ includes uncertainties in clear waters due to the estimation error by QAA. Although other IOP algorithms for $a_{\mathrm{ph}}(\lambda)$ estimation such as Garver-Siegel-Maritorena (GSM) model might perform well, even in the clearest waters, the fixed shape estimation of $a_{\mathrm{ph}}(\lambda)$ is not applicable to the CSD model.

Compared with existing models, the CSD model has several advantages. First, the CSD model can avoid the estimation errors of $a_{\mathrm{ph}}(\lambda)$ because the method requires $a_{\mathrm{ph}}(\lambda)$ at shorter wavelengths, while the model proposed by Roy et al. (2013) depends on the accuracy of the $a_{\mathrm{ph}}(\lambda)$ estimation at 676 nm, which generally contains significant error because of strong absorption by pure seawater (Lee et al., 2002). Second, the use of the spectral shape of $a_{\mathrm{ph}}^{\mathrm{std}}(\lambda)$ enables to reduce the influence of non-algal components, whereas the $b_{\mathrm{bp}}(\lambda)$-based approach (Kostadinov et al., 2009) can be affected not only by phytoplankton but also by all other suspended particles (Stramski et al., 2004). In addition, the fraction of user-defined phytoplankton size classes can be derived with the CSD model according to Eq. (2.8), while most other models can retrieve only predefined size classes. Furthermore, the CSD model has

been developed using $\mathrm{chl}a_{\mathrm{size}}$, which was determined by size-fractionated filtration. Although diagnostic pigment analysis (DPA) is frequently applied to classify phytoplankton size classes based on the photosynthetic pigment composition (Brewin et al., 2011; Hirata et al., 2011; Roy et al., 2013; Wang et al., 2015; Zhang et al., 2009), Brewin et al. (2014) reported that the DPA method had significant uncertainties. Therefore, the size-fractionated filtration-based method could be useful for obtaining more accurate phytoplankton size structure. Finally, the CSD model can represent the synoptic size structure of the phytoplankton community with one component, and hence the CSD slope is easily applicable to ocean biogeochemical models for retrieving efficiency of the biological pump, and productivity of the marine ecosystem.

2.4.2. Potential of the velocity of shift in phytoplankton size structure

Species distributional shifts have been reported for a variety of organisms such as mollusks, fish, birds, and mammals (Grebmeier et al., 2015a; Przeslawski et al., 2012), and their shifts have often been linked to temperature increases as expectations include simple poleward migration (Chen et al., 2011; Parmesan, 2007). However, in terms of a warming perspective, unexpected equatoward and shallower migrations have been observed (Bates et al., 2014; Lenoir and Svenning, 2015); thus, the complex mosaic of local velocity of SST is believed to represent a powerful tool for evaluating the variability in species distribution (Burrows et al., 2011). Recent studies have applied the velocity of SST to the expectation of species range shifts (Pinsky et al., 2013; Poloczanska et al., 2013). They found that some distributional shifts could be explained clearly by the velocity of SST, whereas others shows independent changes, attributable to the difference sensitivities and strategies of marine organisms (Philippart et al., 2011). VanDerWal et al. (2012) reported that the expectation of shifts in species distributions driven by temperature alone is likely to underestimate the actual shifts. Moreover, Sunday et al. (2015) revealed that the velocity of SST explained some of the variation in the range of shifts; however, including species traits more than doubled the explained variation. These facts suggest that adopting an approach that is more practical than the velocity of SST is required for better prediction of species shifts.

Trophic transfer efficiency describes the efficiency with which energy is transferred from one trophic level to the next (Lalli and Parsons, 1997) and it might control species distribution through changes in the food web structure (Kędra et al., 2015). As the size structure of the phytoplankton community can have considerable effect on determining trophic transfer efficiency, the spatiotemporal variations of CSD slope and chl*a* are considered as important factors that could potentially cause species distribution shifts. In this study, both the rates and directions of the velocities of CSD slope and chl*a* showed clear regional differences with those

of SST. These findings imply that the velocities of CSD slope and chl*a* could constitute powerful tools for predicting species distribution shifts that deviate from isothermal movement. Furthermore, an approach that combines the velocity of phytoplankton size structure with SST might contribute to predicting species distribution shifts that are more accurate than existing approaches, which consider only variations in species thermal niches.

Numerous time series are currently being stored with the aim of monitoring the effects of climate change. Although species responses to climate change have been extremely variable across ocean regions and taxonomic groups (Parmesan and Yohe, 2003; Poloczanska et al., 2013), understanding the pattern of variation and identifying where and when species will respond to climate forcing is essential for managing proactively changes in fisheries resources and to meet conservation goals (Sunday et al., 2015). In consequence, as large proportions of species within marine ecosystem undergo distributional shifts (Sunday et al., 2012), the provision of a cost-effective and relatively rapid integrated assessment of such shifts will be required (Van der Putten et al., 2010). Therefore, techniques for assessing species distribution shifts are currently garnering considerable attention (Bates et al., 2013; Lenoir and Svenning, 2015). In addition to the challenges involved in predicting species shifts, large gaps remain in the knowledge of species responses to climate change. This study provides compelling evidence regarding the potential for using phytoplankton size structure in assessing the persistence and migration of species distributions, which could contribute to the generation of global and regional maps of the expected rates and directions of species shifts that have improved accuracy.

2.5. Conclusions

This chapter proposed a CSD model to derive the synoptic size structure of the phytoplankton community using satellite remote sensing data. The CSD model is based on the relationship between phytoplankton size structure and its spectral absorption properties. The validation results showed that the CSD model performed with sufficient accuracy. Although satellite-derived CSD slope contains uncertainties, especially in clear waters, the CSD model has been demonstrated as a powerful tool for monitoring marine ecosystems through the synoptic size structure of the phytoplankton community. Recent evident deviations from uniform species shifts appear related to various environmental drivers, suggesting that a multifaceted approach, rather than using the velocity of SST, is probably required to assess species migration and persistence properly. Therefore, a new approach combining the velocity of phytoplankton size structure with other factors, including the velocity of SST, might contribute toward producing predictions of species distribution shifts with improved accuracy.

Overall, these results could help generate global and regional maps of the expected rates and directions of species shifts.

Table 2.1. Cruises information and number of data obtained during each cruise.

Cruise period	Cruise ID	Vessel name	Number of data	
			Water sample	Spectral radiation
22 Nov.–12 Dec. 2000	JARE-42	JMSDF Shirase	19	6
16–25 Feb. 2002	JARE-43	JMSDF Shirase	10	9
25 Jan.–9 Feb. 2003	UM0203	T/S Umitaka-maru	15	14
22 Feb.–6 Mar. 2003	JARE-44	R/V Tangaroa	9	6
1–21 Jan. 2005	UM0405	T/S Umitaka-maru	16	11
5–22 Jan. 2006	UM0506	T/S Umitaka-maru	10	7
25 Jul.–14 Aug. 2007	OS180	T/S Oshoro-maru	20	20
27 Dec. 2007–12 Feb. 2008	UM0708	T/S Umitaka-maru	21	15
13–25 Jan. 2009	UM0809	T/S Umitaka-maru	9	7
18 Aug.–18 Sep. 2009	KH-09-4	R/V Hakuho-maru	16	16
11 Sep.–10 Oct. 2009	MR09-03	R/V Mirai	12	12
03 Jun.–07 Jul. 2010	OS216	T/S Oshoro-maru	21	17
04 Sep.–13 Oct. 2010	MR10-05	R/V Mirai	28	28
09–11 May 2011	KT-11-07	R/V Tansei-maru	8	7
08 Jun.–07 Jul. 2011	OS229	T/S Oshoro-maru	25	24
17–18 Jun. 2012	US260	T/S Ushio-maru	8	7
06–08 Aug. 2012	US263	T/S Ushio-maru	10	8
13 Sep.–02 Oct. 2012	MR12-E03	R/V Mirai	12	12
23 Jun.–17 Jul. 2013	OS255	T/S Oshoro-maru	26	24
31 Aug.–04 Oct. 2013	MR13-06	R/V Mirai	32	32
10–12 Oct. 2013	ARAON-EJS	Icebreaker ARAON	9	7
08–30 Jun. 2014	Mu14	R/V Multanovski	16	16
08–23 Mar. 2015	KH-15-1	R/V Hakuho-maru	12	12

Table 2.2. Summary of filters that were used to obtain $\mathrm{chl}a_{\mathrm{size}}$ during each cruise.

Cruise ID	20 μm	10 μm	5 μm	2 μm	GF/F
JARE-42	×	×		×	×
JARE-43	×	×		×	×
UM0203	×	×		×	×
JARE-44	×	×		×	×
UM0405		×		×	×
UM0506		×		×	×
OS180	×		×		×
UM0708	×		×		×
UM0809		×		×	×
KH-09-4		×		×	×
MR09-03		×	×	×	×
OS216		×	×	×	×
MR10-05		×	×	×	×
KT-11-07		×	×	×	×
OS229		×	×	×	×
US260		×		×	×
US263		×		×	×
MR12-E03	×	×	×	×	×
OS255	×			×	×
MR13-06	×	×		×	×
ARAON-EJS	×			×	×
Mu14	×			×	×
KH-15-1	×			×	×

Table 2.3. Summary of performance of QAA-v6 at MODIS bands. R^2 and RRMSE were calculated in log10 space after omitting minus values.

	Wavelength [nm]									
	412	443	469	488	531	547	555	645	667	678
Number of minus value	31	31	36	28	78	77	86	14	44	83
R^2	0.68	0.71	0.59	0.61	0.57	0.62	0.57	0.00	0.01	0.01
RRMSE [%]	20.3	19.0	19.7	21.2	20.5	15.8	15.4	67.2	77.9	58.1

Table 2.4. Model parameters for Eq. (2.12). Note that coefficients for $a_{\mathrm{ph}}^{\mathrm{std}}(\lambda)$ at MODIS bands are from C_1 to C_7, and coefficient for chla is C_8.

	Model parameters								
	β_0	C_1	C_2	C_3	C_4	C_5	C_6	C_7	C_8
$a_{\mathrm{ph}}^{\mathrm{std}}(412) \geq a_{\mathrm{ph}}^{\mathrm{std}}469$	-0.209	0.426	-0.567	0.312	-0.185	0.523	-0.092	-0.418	0.064
$a_{\mathrm{ph}}^{\mathrm{std}}(412) < a_{\mathrm{ph}}^{\mathrm{std}}469$	-0.285	0.215	-0.457	0.404	-0.128	0.300	-0.059	-0.275	0.100

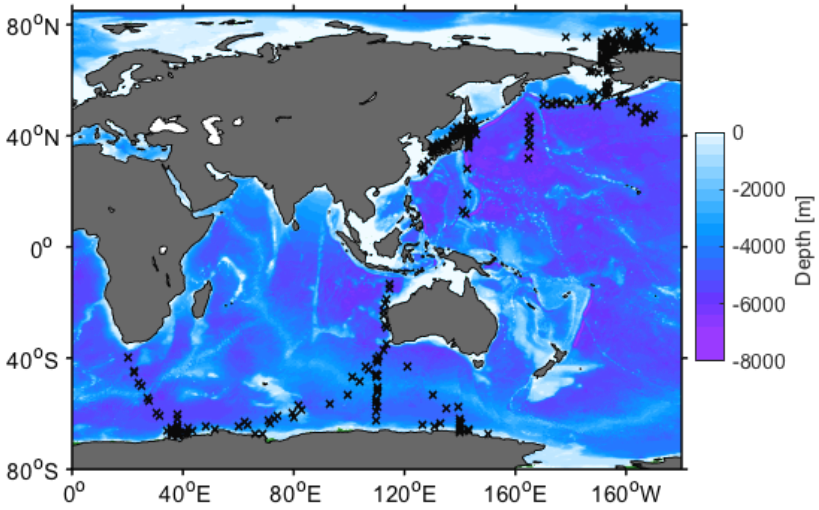

Figure 2.1. Location of sampling stations where *in situ* data were obtained for this study.

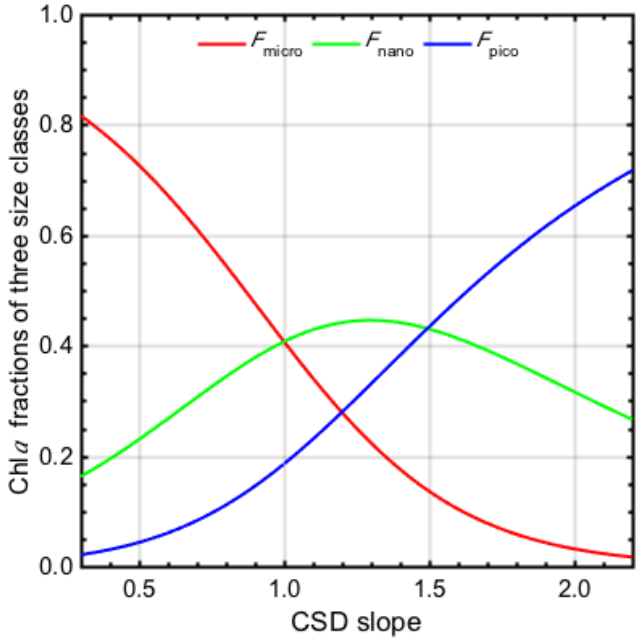

Figure 2.2. Variations in the chl*a* fractions of the three phytoplankton size classes (microplankton (F_{micro}), nanoplankton (F_{nano}) and picoplankton (F_{pico})) as a function of the CSD slope.

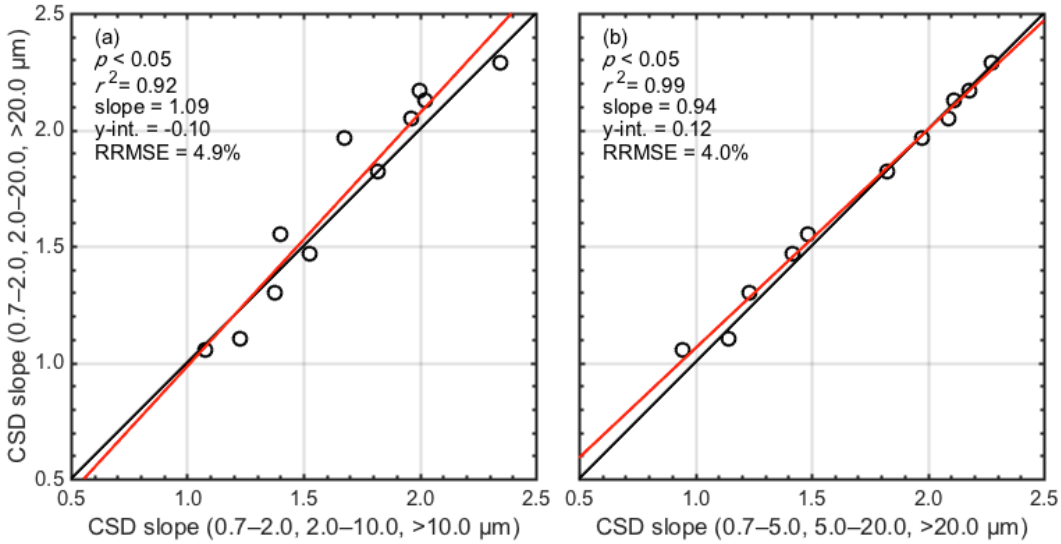

Figure 2.3. The comparison of CSD slope derived from three typical chla_{size} which were divided by the filters of 0.7, 2.0 and 20 µm pore size, and two different combinations of chla_{size}: (a) chla_{size} divided by the filters of 0.7, 2.0 and 10 µm pore size; and (b) 0.7, 5.0 and 20 µm pore size. Solid and dashed lines represent the 1:1 agreements and regression lines, respectively.

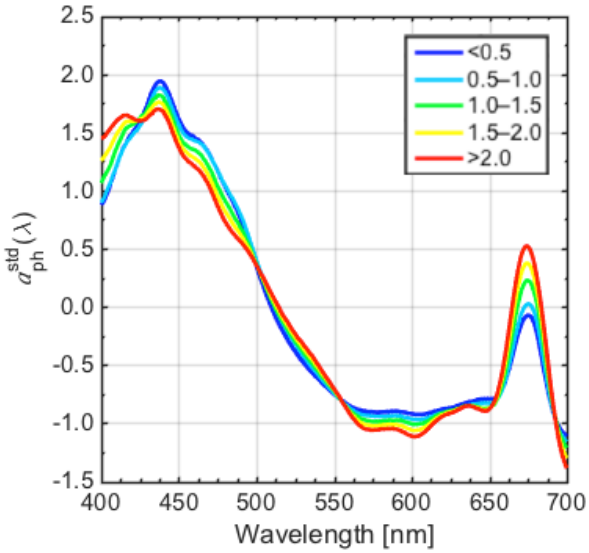

Figure 2.4. The relationship between $a_{\mathrm{ph}}^{\mathrm{std}}(\lambda)$ spectra and CSD slope. Colored solid lines represent average $a_{\mathrm{ph}}^{\mathrm{std}}(\lambda)$ for each CSD slope values; cool colors indicate larger phytoplankton size structure, and vise versa.

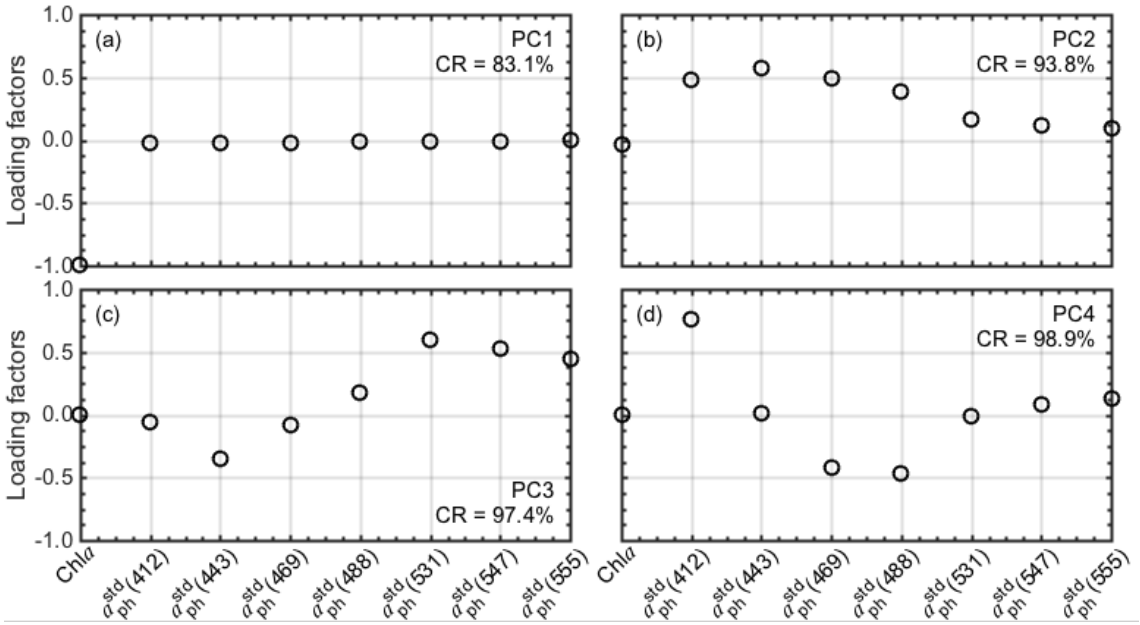

Figure 2.5. Loading factors of the first four PC modes derived from $a_{\mathrm{ph}}^{\mathrm{std}}(\lambda)$ and chl*a*. CR represents the contribution rate of variance.

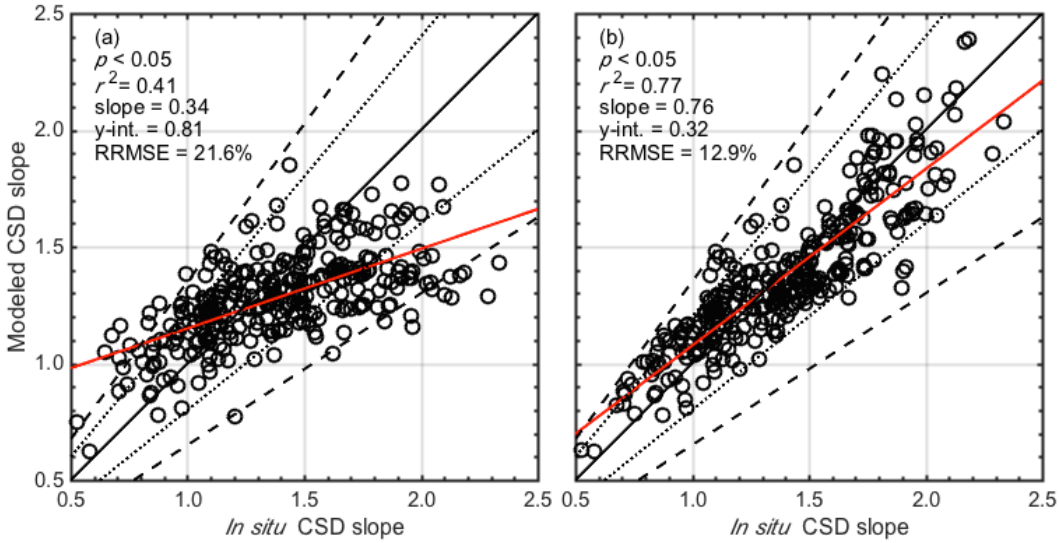

Figure 2.6. Comparison between *in situ* and modeled CSD slope using the CSD slope: (a) before; and (b) after involving a condition branch. Black and red solid lines represent the 1:1 agreements and regression lines, respectively. Dotted and dashed lines represent ±20% and ±35% ranges.

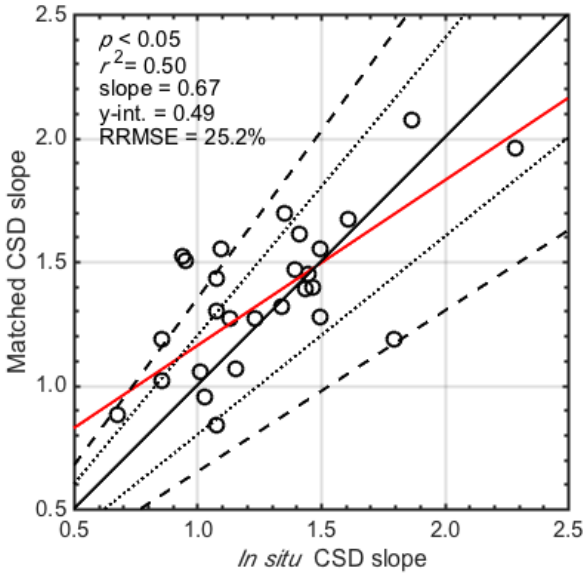

Figure 2.7. Comparison of *in situ* CSD slope values determined from *in situ* chla_{size} and matched CSD slope derived from MODIS-observed satellite data. Black and red solid lines represent the 1:1 agreements and regression lines, respectively. Dotted and dashed lines represent ±20% and ±35% ranges.

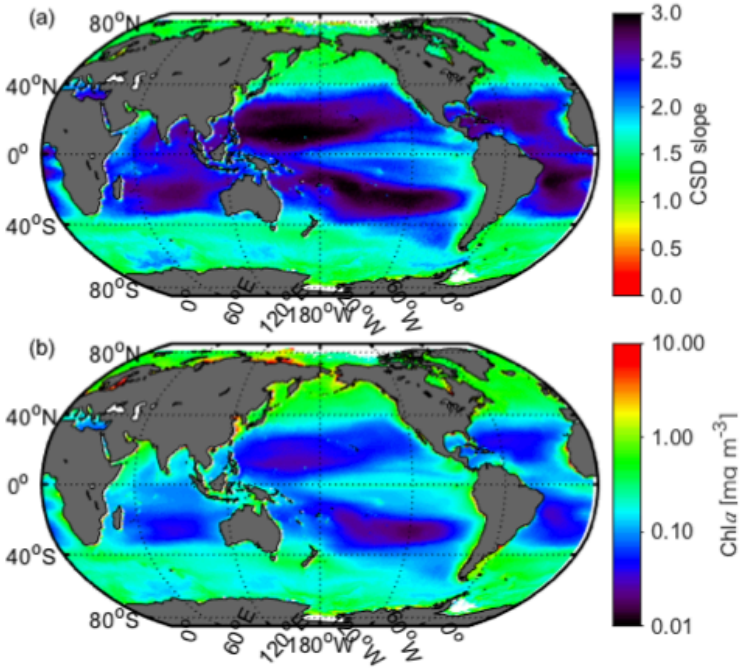

Figure 2.8. Global distribution of average (a) CSD slope and (b) chl*a* over 2002–2017.

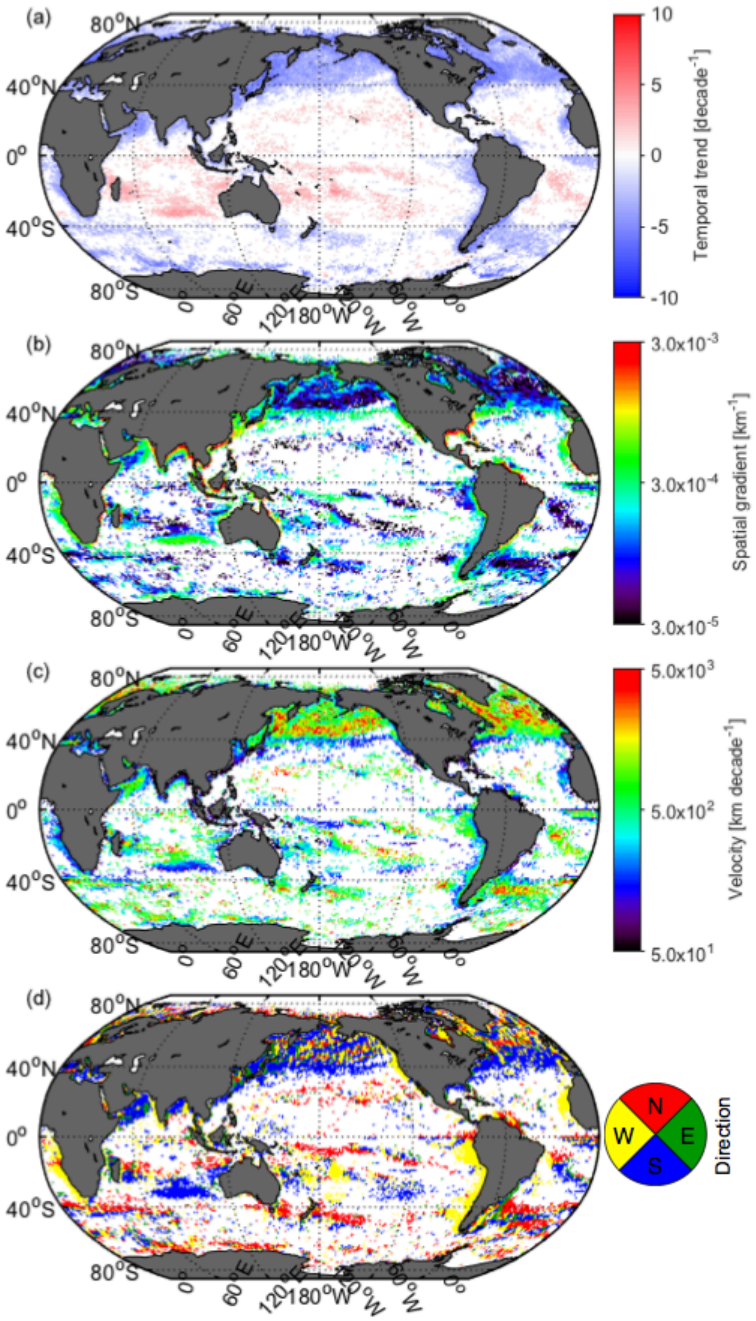

Figure 2.9. Global distribution of (a) temporal trend (b) spatial gradient (c) velocity and (d) direction of CSD slope. White shows the area with non-significant ($p > 0.05$) temporal trend for the period 2002–2017.

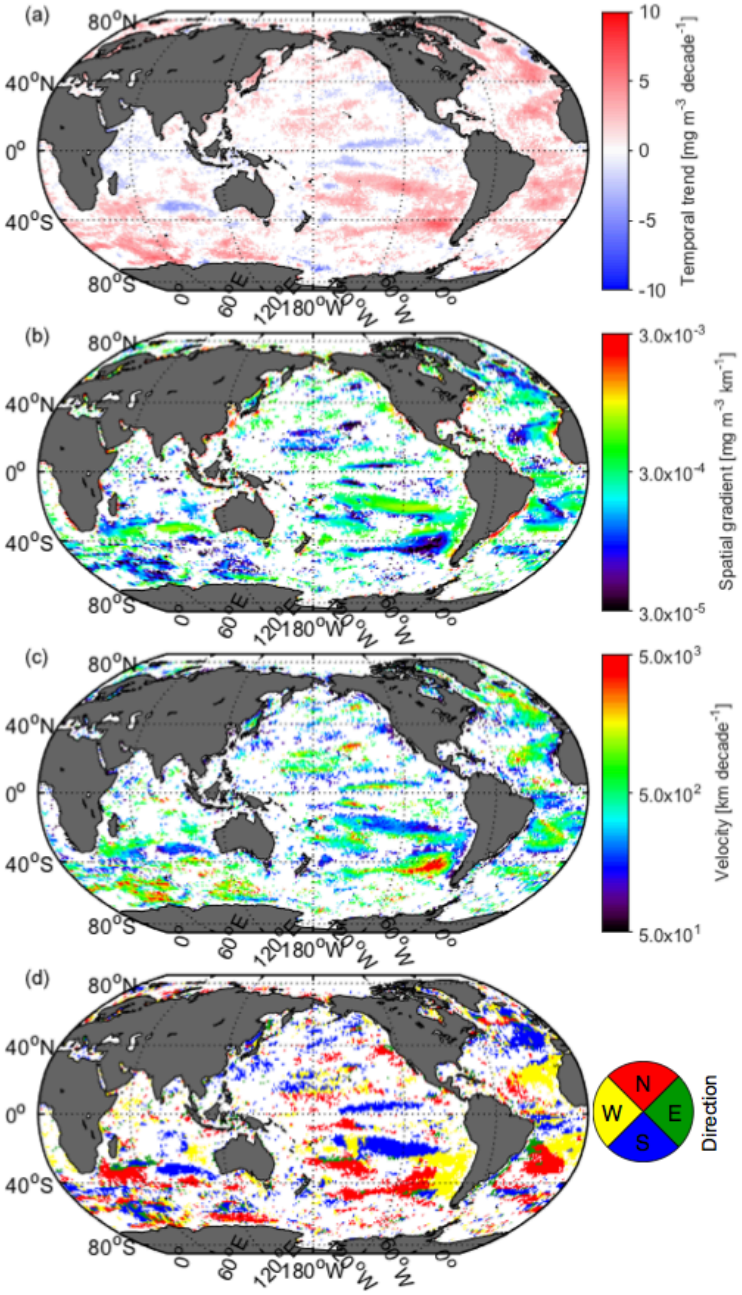

Figure 2.10. Global distribution of (a) temporal trend (b) spatial gradient (c) velocity and (d) direction of chl*a*. White shows the area with non-significant ($p > 0.05$) temporal trend for the period 2002–2017.

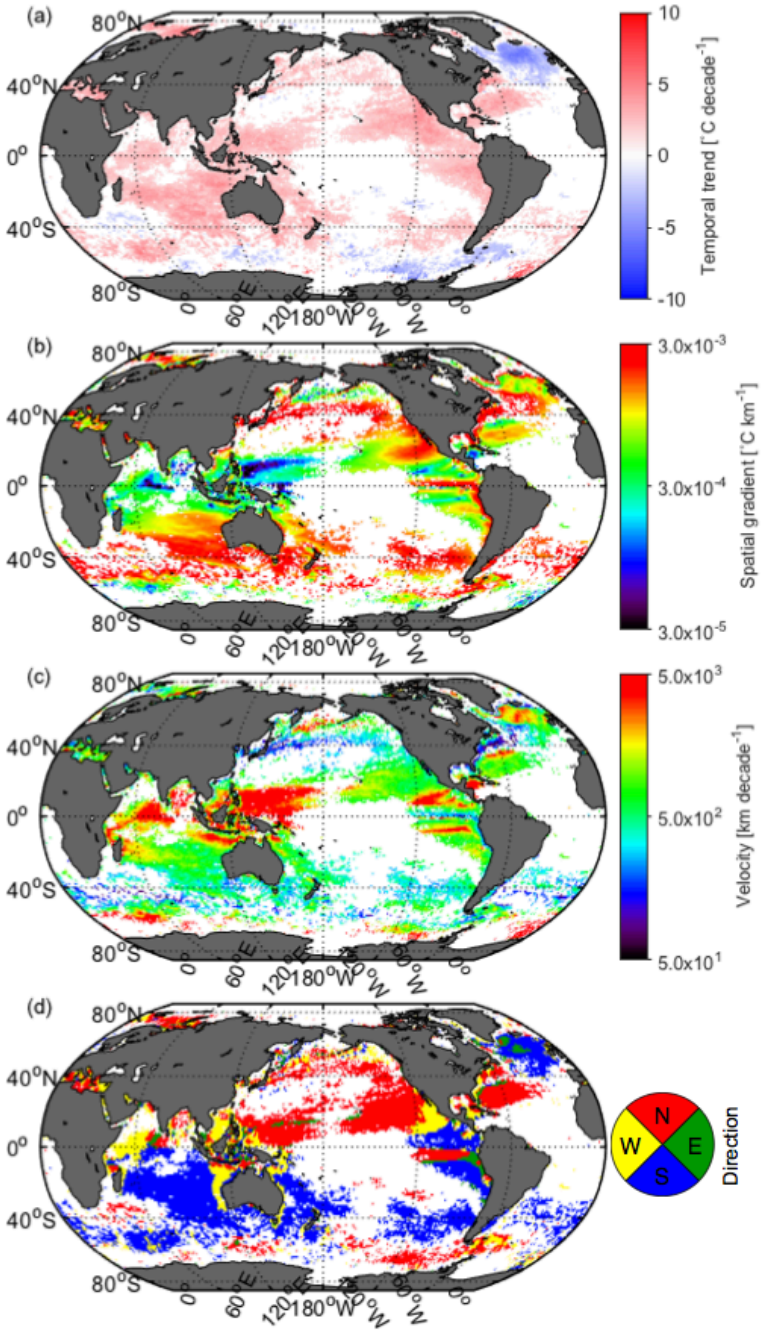

Figure 2.11. Global distribution of (a) temporal trend (b) spatial gradient (c) velocity and (d) direction of SST. White shows the area with non-significant ($p > 0.05$) temporal trend for the period 2002–2017.

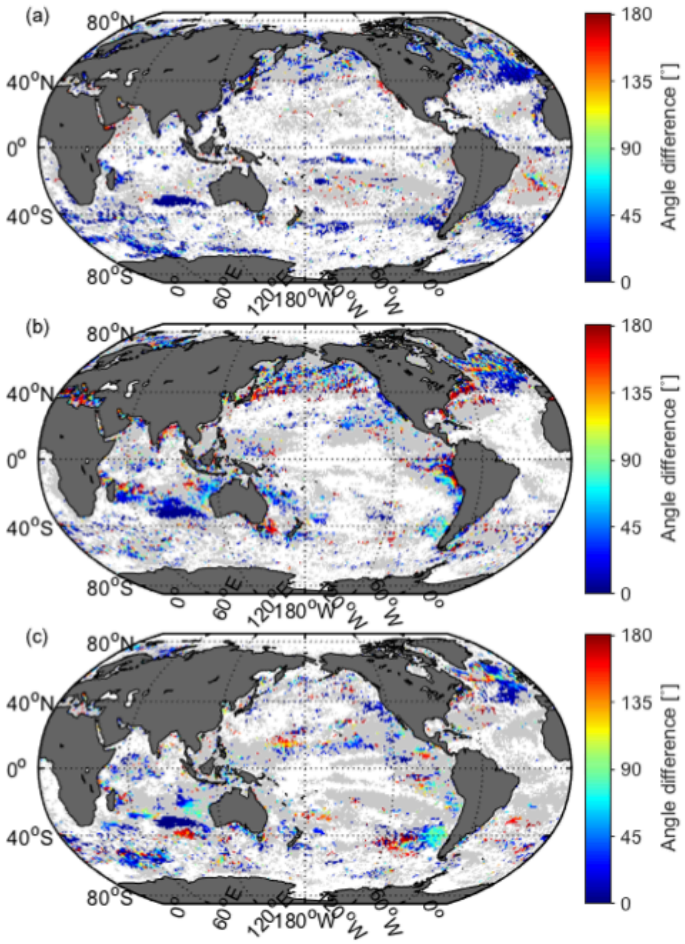

Figure 2.12. Distribution patterns of differences in direction of velocity between: (a) CSD slope and chl*a*; (b) CSD slope and SST; and (c) chl*a* and SST. White and gray areas show the area with non-significant ($p > 0.05$) trend in both and either of two velocities, respectively.

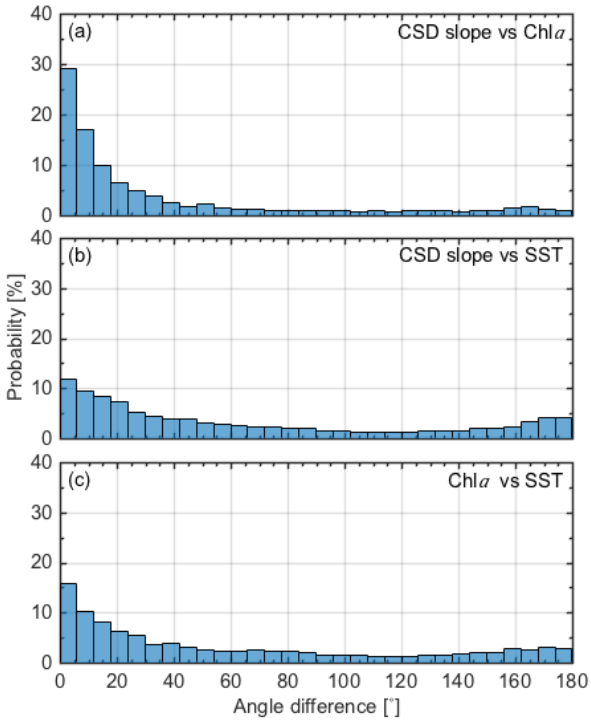

Figure 2.13. Histograms of angle differences shown in Figure 2.12: (a) CSD slope and chl*a*, (b) CSD slope and SST, and (c) chl*a* and SST.

Chapter 3

Impact of spatiotemporal variability in phytoplankton size structure on benthic macrofaunal community in the Pacific Arctic

3.1. Introduction

Growing evidence of changes in the marine environment for the last several decades in the Pacific Arctic has been the focus of the international Distributed Biological Observatory (DBO; Moore and Grebmeier 2017). Recent reductions in Arctic sea ice cover have been most pronounced in the continental shelf region of the Pacific Arctic (Steele et al., 2008; Frey et al., 2015), accompanied by increased ocean temperature, freshwater content, and Pacific water inflow (Wood et al., 2015; Woodgate and Weingartner, 2012). These variations within the marine environment influence the biomass and size structure of the phytoplankton community (Li et al., 2009; Wassmann et al., 2011). In the Pacific Arctic food webs, even small changes in the lower trophic levels would have cascading effects on the higher trophic levels owing to the short and efficient energy transfer pathway (Grebmeier et al., 2010); thus, bottom-up control on higher trophic levels is crucial (Schonberg et al., 2014). However, current knowledge on the changes in phytoplankton community structure and their impact on higher trophic levels is quite scarce. To fully understand the linkages and processes of ongoing changes in the Pacific Arctic ecosystem, it is necessary to clarify the complex biological interactions among the trophic levels. To this end, the spatiotemporal variability of phytoplankton assemblages and their impact on benthic organisms should be investigated.

Benthic macrofauna are normally stationary in marine sediments, and thus their community patterns are strongly impacted by organic carbon transport from the overlying water column as well as lateral advection (e.g., Lovvorn et al., 2013; Mathis et al., 2014; Grebmeier et al., 2015b). Over the last several decades, the high macrofaunal biomass observed in benthic hotspots, ranging from southwest of St. Lawrence Island to Barrow Canyon, have been maintained by transport of large amounts of organic carbon into the sediments (Grebmeier, 2012). Arctic benthic macrofauna rapidly consume the input of fresh algae (McMahon et al., 2006; Sun et al., 2007; Morata et al., 2015); however, several studies have found that the input to the sediment is not consistently consumed by benthic organisms but rather is buried as a food bank by bioturbation or sedimentation (Josefson et al., 2002; Hansen and Josefson, 2003; Pirtle-Levy et al., 2009). In both cases, monitoring of the variations in phytoplankton, which is one of the primary organic carbon materials exported to benthic macrofauna, is a crucial issue to better understand the processes of occurring in changing Arctic ecosystems, although the food

bank process is likely to be dominant in the Pacific Arctic (McTigue and Dunton, 2014; North et al., 2014).

Satellite ocean color remote sensing has been used to address a wide assortment of investigations ranging from local to global scales with various time series data sets (McClain, 2009). Recent efforts have enabled us to monitor the spatiotemporal dynamics of phytoplankton size structure from space as well as chlorophyll-*a* (chl*a*) content (Fujiwara et al., 2011; Hirata et al., 2011). It has been well documented that the inherent optical properties (IOPs) of seawater, such as the phytoplankton absorption coefficient ($a_{ph}(\lambda)$) and the particle backscattering coefficient ($b_{bp}(\lambda)$), are strongly affected by the size structure of the phytoplankton community (Bricaud and Morel, 1986; Ciotti et al., 2002). In the last decade, various IOP-based methods for retrieving the phytoplankton size structure have been proposed and are anticipated to contribute to a better understanding of the diverse responses of marine ecosystem components to climate forcing and associated potential feedback (Wang et al., 2015; Fujiwara et al., 2016). In chapter 2, the chl*a* size distribution (CSD) model which estimates the synoptic size structure of phytoplankton community based on the spectral feature of $a_{ph}(\lambda)$. Although this model performs well in the global ocean, the IOPs are specific to regional water and vary with associated water mass components. A series of papers has suggested that the IOPs of Arctic waters are significantly different from those of temperate waters. For example, Matsuoka et al. (2007) reported that the relative contribution of $a_{ph}(\lambda)$ to total non-water absorption is only 16% at 443 nm, whereas the contribution of absorption by colored dissolved organic matter (CDOM), $a_{CDOM}(\lambda)$, accounts for 76% of the total non-water absorption at that wavelength. They also revealed that the different pigment packaging and pigmentation prevail at higher latitudes compared with those in temperate waters (Matsuoka et al., 2007). Thus, the IOP-based methods developed in other areas should be optimized using *in situ* data obtained from the Pacific Arctic.

In this chapter, influences of surface phytoplankton size structure on benthic macrofaunal biomass and distribution were investigated in the Pacific Arctic. A CSD model for the Pacific Arctic was developed using a dataset obtained in this region to retrieve the size structure of the phytoplankton community from space. In addition, the phytoplankton growth season was divided into two periods (i.e., bloom and post-bloom period), and the relationships of satellite-derived phytoplankton size structure during these two periods with the amount of organic carbon in the sediments were investigated. Based on the relationships, the impact of spatiotemporal variations in phytoplankton size structure on benthic macrofauna was evaluated.

3.2. Materials and methods

3.2.1. *In situ* dataset for optimizing CSD model

The CSD model for the Pacific Arctic was developed using *in situ* data collected during six cruises primarily occurring during late summer from 2007 to 2013 (Table 3.1). The sampling stations were widely spread from the sub-Arctic Bering Sea to the Beaufort Sea (Figure 3.1a). At each station, size fractionated chl*a* (chla_{size}), $a_{ph}(\lambda)$ and spectral radiance were measured. Seawater samples were collected from the sea surface using a clean plastic bucket. Seventy percent of these data were randomly selected for model tuning and the rest were preserved for model validation. Further details of *in situ* dataset for model development are described in section 2.2.1.

3.2.2. *In situ* dataset for evaluating changes in benthic macrofauna

Benthic macrofaunal biomass, sediment chl*a* (top 0–1 cm of sediments), bottom water temperature and salinity were downloaded from the Pacific Marine Arctic Regional Synthesis (PacMARS) archive (http://pacmars.eol.ucar.edu) or the National Science Foundation (NSF) Arctic Data Center (https://arcticdata.io/). The dataset was obtained during the Canadian Coast Guard Ship (CCGS) Sir Wilfrid Laurier (SWL) cruise. In this chapter, macrofaunal dry carbon biomass (using conversion values from wet mass, formalin-preserved samples) was used to reduce the bias of calcium carbonate on the weight values (Grebmeier et al., 2015b). Detailed descriptions of the methods used for determining the macrofaunal biomasses and conversion factors are provided in Grebmeier and Cooper (2014a,b, 2017) and Grebmeier et al. (2015c). The dataset was obtained at 16 fixed, time series observation stations (SLIP1–5, UTBS1–4, and UTN1–7) (Figure 3.1b, Table 3.2) using the Coast Guard icebreaker Sir Wilfrid Laurier that were collected during summer 2000–2013, except in 2009 (Table 3.3). Note that since 2010 these time series stations have been occupied annually as part of the Distributed Biological Observatory (DBO) Sir Wilfrid Laurier field program (Moore and Grebmeier, 2017).

3.2.3. Satellite remote sensing data

The latest (R2014.0) level-3 standard mapped images of remote sensing reflectance ($R_{rs}(\lambda)$) derived by Sea-Viewing Wide Field-of-View Sensor (SeaWiFS) and Moderate Resolution Imaging Spectroradiometer (MODIS)-Aqua were downloaded from the National Aeronautics and Space Administration (NASA) Ocean Biology Processing Group (OBPG). The data durations of $R_{rs}(\lambda)$ were 1998–2007 and 2003–2013 for SeaWiFS and MODIS, respectively. As there are slight differences in the observation bands between SeaWiFS and MODIS, SeaWiFS-derived $R_{rs}(\lambda)$ (λ = 412, 443, 490, 510, 555 and 670 nm) were resampled at 10

MODIS-bands (λ = 412, 443, 469, 488, 531, 547, 555, 645, 667 and 678 nm) using spline interpolation. In addition, the gaps in $R_{rs}(\lambda)$ at each wavelength between the two different sensors were corrected following the method of Fujiwara et al. (2016) to avoid inter-mission bias. The 2003–2007 dataset was selected for the correction, which was the overlap period between missions. The $a_{ph}(\lambda)$ values were derived from $R_{rs}(\lambda)$ using the modified version of quasi-analytical algorithm. These $a_{ph}(\lambda)$ values were then used as input parameters for the CSD model to derive the CSD slopes indicating the synoptic size structure of the phytoplankton community. In addition, chl*a* concentration was computed from $R_{rs}(\lambda)$ using the Arctic-OC4L algorithm (Cota, 2004). All ocean color products are daily averaged values with a 9 km resolution.

Daily sea ice concentrations gridded at a 25 km resolution, which were derived from the Special Sensor Microwave Imager (SSMI)-Defense Meteorological Satellite Program (DMSP) using enhanced NASA Team algorithm (Cavalieri, 2000), were obtained from the National Snow and Ice Data Center (NSIDC) for 2000–2013. Sea ice concentrations were converted to 9 km resolution using nearest-neighbor interpolation to align the spatial resolution of the satellite data (Perrette et al., 2011).

3.2.4. Optimizing of the CSD model

The optimum CSD model for the Pacific Arctic was developed by same procedure with section 2.2.3 using *in situ* data obtained in the Pacific Arctic (Figure 3.1a; Table 3.1). Briefly, the principle component analysis (PCA) was applied to normalized $a_{ph}(\lambda)$ ($a_{ph}^{std}(\lambda)$) and then the CSD slope was quantified as a logistic-type regression model using the *i*-th principle component (PC) score (S_i) and regression coefficients (β_0 and β_i) between the CSD slope and PC scores as follows:

$$\eta = \left(\beta_0 + \exp\sum_{i=1}^{k} \beta_i S_i\right)^{-1}, \tag{3.1}$$

where η and k represent the CSD slope and the number of PCs, respectively. Here, S_i can also be expressed as follow:

$$S_i = \sum_{j=1}^{m} w_{i,j} a_{ph}^{std}(\lambda_j), \tag{3.2}$$

where $w_{i,j}$ and $a_{ph}^{std}(\lambda_j)$ are the loading factors for S_i and $a_{ph}^{std}(\lambda)$ at wavelength j, respectively. Thus, an equation was obtained by replacing S_i in Eq. (3.1) with Eq. (3.2):

$$\eta = \left(\beta_0 + \exp\sum_{j=1}^{m} C_j\, a_{ph}^{std}(\lambda_j)\right)^{-1}, \tag{3.3}$$

$$C_j = \sum_{i=1}^{k} \beta_i w_{i,j}. \quad (3.4)$$

Finally, the CSD slope is derived from Eq. (3.3) using the model parameters of β_0 and C_j.

3.2.5. Evaluation of changes in benthic macrofauna

To evaluate long-term changes in macrofaunal community biomass at the benthic hotspots, average macrofaunal biomass was derived as the mean value of macrofaunal biomass obtained at the benthic hotspots each year from 2000 to 2013. In addition, the centroid of macrofaunal habitat as an indicator of the synoptic macrofaunal distribution, based on biomass, was calculated by following the method described in Pinsky et al. (2013). The latitudinal centroid of the macrofaunal habitat was defined as the biomass-weighted average latitude (lat_c) and was obtained from 16 fixed stations for individual years as follows:

$$lat_c = \sum_{i=1}^{16} biom_i \cdot lat_i / \sum_{i}^{16} biom_i, \quad (3.5)$$

where $biom_i$ and lat_i are macrofaunal biomass and latitude at the ith station, respectively. Note that the lat_c calculation strongly relies on the range of input values. As lat_i varies within a narrow range from 62.01 to 68.00°N (Table 3.2), the variation in lat_i tends to be less sensitive to variations in macrofaunal biomass. Thus, a magnitude of shift in lat_c is not as important as the temporal trend for evaluating synoptic variation in the macrofaunal distribution.

In this chapter, phytoplankton size structure during the bloom and post-bloom period were focused on. Because the sea ice-associated spring bloom generally lasts for two weeks (Niebauer et al., 1995), the bloom period was defined as 14 days from the date of sea ice retreat. In contrast, the post-bloom period was defined as the period from the end of the bloom period to the date of sea ice production. The date of sea ice retreat and sea ice production were defined as the last date when the sea ice concentration fell below 10% (Fujiwata et al., 2016) and one day after the last date when the sea ice concentration below 10% after the sea ice retreat. The CSD slopes during the bloom and post-bloom periods were calculated using daily satellite data across the Pacific Arctic, and the average values within 3 × 3 pixel (27 × 27 km) subsets centered on the macrofaunal sampling location were extracted to investigate the relationships of these satellite-derived CSD values with *in situ* macrofaunal biomass and sediment chl*a*. Additionally, to evaluate the relationship between macrofaunal distribution and the phytoplankton size structure during the bloom and post-bloom periods, the latitudinal centroid values of the CSD slope during these two periods were also derived by Eq. (3.5) using the extracted CSD slope values during the two periods at the macrofaunal sampling location instead of macrofaunal biomass. Note that a variation in lat_c of the CSD slope tends to be unremarkable compared with

the macrofaunal biomass because the range of CSD slope values is much narrower than that of macrofaunal biomass.

3.3. Results

3.3.1. Development of optimized CSD model

A total of 97 of the 139 samples were used to optimize the performance of the CSD model in the Pacific Arctic. PCA was applied to $a_{\mathrm{ph}}^{\mathrm{std}}(\lambda)$ and the first four PC scores were used to determine the model parameters β_0 and C_j by logistic-type multiple regression analysis. The resulting model parameters are summarized in Table 3.4.

The performance of the optimized CSD model was examined by comparing the measured CSD slope, which was determined from *in situ* Chla_{size}, and the modeled CSD slope, which was estimated from *in situ* $R_{\mathrm{rs}}(\lambda)$, using the rest of the 42 samples (Figure 3.2). The resulting relative root mean square error (RRMSE) between the measured and modeled CSD slope was 21.6%, which is slightly lower than the RRMSE of 25.2% reported in chapter 2. In addition, no significant relationship was found between RRMSE and $a_{\mathrm{CDOM}}(\lambda)$ (p = 0.21). Moreover, the CSD model successfully retrieved the CSD slope within ±20% and ±35% ranges from measured the CSD slope value for 71.4% (30 of 42 samples) and 95.2% (40 of 42 samples) of the validated data, respectively. Thus, the CSD model performed with sufficient accuracy for assessing the CSD slope in the Pacific Arctic.

To reduce inter-mission uncertainties, a bias correction was conducted for ocean color products derived from the MODIS and SeaWiFS sensors. Bias and RRMSE were used to evaluate the effect of the conversion. Although there were apparent differences in ocean color products between the MODIS and default SeaWiFS data, the gaps in ocean color products between the MODIS and modified SeaWiFS data decreased after the bias correction (Table 3.5). Thus, an average of the MODIS and modified SeaWiFS data was used for the overlap period between the 2003–2007 missions. In addition, the modified SeaWiFS and MODIS data were adopted for 1998–2002 and 2008–2013, respectively.

Figure 3.3 shows the distribution of the CSD slope and chl*a* values during the bloom and post-bloom periods in the Pacific Arctic averaged for 2000–2013. In general, the CSD slope values during both periods were high/low and coincided with the low/high chl*a* values. In addition, the CSD slope during the bloom period (Figure 3.3a) was apparently lower than that during the post-bloom period (Figure 3.3b). On the other hand, chl*a* was higher during the bloom period (Figure 3.3c) than that during the post-bloom period. (Figure 3.3d) As a higher/lower CSD slope indicates smaller/larger phytoplankton size structure, the pattern in the CSD slope and chl*a* suggests that higher chl*a* is consistent with larger phytoplankton size

structure, and vice versa. Overall, the spatiotemporal variations in CSD slope, namely phytoplankton size structure and chl*a*, showed good agreement in the Pacific Arctic.

3.3.2. Evidence of distributional shifts in benthic macrofauna

Macrofaunal sampling was conducted at the benthic hotspots located on the continental shelf south of St. Lawrence Island (SLI), the Chirikov Basin (Chirikov), and the southeastern Chukchi Sea (Chukchi). These three benthic hotspots showed different patterns of temporal variation in average macrofaunal biomass between 2000 and 2013, with a significant decline south of SLI (Figure 3.4a), an increase further north in Chukchi (Figure 3.4c), and no significant trend in Chirikov (Figure 3.4b). Average macrofaunal biomass across these three regional hotspots exceeded 20 g C m^{-2} during 2000–2013 (Figure 3.4d, Table 3.6), with a significant ($p < 0.05$) increase for the combined dataset. However, average biomass at Chukchi in 2013 was an extreme outlier compared with the other years. A relatively short time series is prone to endpoint bias, which can occur when the first or last points of the time series are exceptionally high or low relative to the series as a whole (Gregg and Rousseaux, 2014). If the 2013 value was removed from the trend analysis at Chukchi and the entire region, the average biomass across the whole region showed an insignificant trend for 2000–2012, whereas that of Chukchi held a significantly increasing trend. Consequently, average macrofaunal biomass across these three regional hotspots exceeded 20 g C m^{-2} during 2000–2013 (Figure 3.4d), accompanied by significant decreasing and increasing trends south of SLI and at Chukchi. These variations in macrofaunal biomass with time resulted in a significant northward shift in the latitudinal centroid of the macrofaunal habitat between 2000 and 2013 at these sites (Figure 3.5), indicating that macrofaunal biomass across the Pacific Arctic is persistently high, but the latitudinal habitat of benthic macrofauna shifted toward the north at a rate of 0.05°N $year^{-1}$ during the study period.

3.3.3. Relationship between CSD slope and sediment chl*a*

In situ sediment chl*a* values obtained at the same stations as the macrofaunal samples ranged from 1.00 to 44.29 mg m^{-2} and were compared with the satellite-derived CSD slope and chl*a* values during both periods. The satellite-derived CSD slope during the bloom and post-bloom periods varied from 0.36 to 1.01 and from 0.51 to 1.79, respectively. Satellite-derived chl*a* was between 2.03 and 57.49 mg m^{-3}during the bloom period, and 1.05 to 18.01 mg m^{-3}during the post-bloom period. The average CSD slope during the bloom period for 2000–2013 was significantly ($p < 0.05$) lower than that during the post-bloom period. On the other hand, the average chl*a* value during the bloom period from 2000 to 2013 was significantly

($p < 0.05$) higher than that during the post-bloom period. Overall, a higher phytoplankton biomass was associated with a larger phytoplankton assemblage during the bloom period. Then phytoplankton biomass decreased with the decline in the proportion of larger phytoplankton to total phytoplankton during the post-bloom period. The satellite-derived CSD slope and chl*a* during the two periods were significantly ($p < 0.05$) correlated with *in situ* sediment chl*a* (Figure 3.6). However, Spearman's rho statistic indicated that the satellite-derived CSD slope during the post-bloom period was better correlated with *in situ* sediment chl*a* than with the others. This finding indicates that the spatiotemporal patterns in the size structure of phytoplankton are strongly related to patterns in the sediment chl*a*. Therefore, the CSD slope during the post-bloom period was considered as an important correlate of the amount of food supplied to benthic macrofauna.

3.3.4. Impact of phytoplankton size structure on macrofaunal distribution

Temporal trends in the CSD slope during the bloom period at each benthic hotspot, and in the combined dataset, showed clearly increasing trends, except at the Chirikov hotspot (Figure 3.7), suggesting that the size structure of the phytoplankton community shifted toward smaller assemblage. On the other hand, the CSD slope during the post-bloom period significantly increased and decreased south of SLI and at Chukchi, whereas no variation was observed at Chirikov and the whole region. These results suggest that the phytoplankton assemblages south of SLI and Chukchi shifted toward domination by smaller and larger cells during 2000–2013, respectively. Specifically, the CSD slope values during the post-bloom period in 2000 and 2013 were 0.90 ± 0.17 and 1.29 ± 0.15 south of SLI, and 0.99 ± 0.10 and 0.64 ± 0.07 at Chukchi, indicating that the F_{micro} value derived using Eq. (2.8) decreased from 0.48 ± 0.12 to 0.24 ± 0.08 south of SLI and increased from 0.41 ± 0.07 to 0.65 ± 0.04 at Chukchi. Consequently, the latitudinal centroid of the CSD slope during the post-bloom period shifted southward (Figure 3.8b) owing to the increasing and decreasing trends south of SLI and at Chukchi (Figure 3.7), whereas no significant variation was observed in the latitudinal centroid of CSD slope during the bloom period (Figure 3.7a).

A significant relationship was detected between the CSD slope during the post-bloom period and macrofaunal biomass, although the relationship was not consistent over the Pacific Arctic owing to outliers observed at Chukchi: extremely high macrofaunal biomass (> 70 gC m^{-2}) was observed at UTN-5 in 2006–2013 and UTN-2–4 in 2013 (Figure 3.9a). A direct comparison of the latitudinal centroid of the macrofaunal habitat with that of the CSD slope during the post-bloom period showed a clear inverse relationship (Figure 3.9b). These results suggest that macrofaunal biomass co-varied with phytoplankton size structure during the

post-bloom period and was strongly related with the spatiotemporal pattern in sediment chl*a*. Additionally, the impact of variations in bottom water temperature and salinity on the macrofaunal biomass distribution was also investigated; however, no observable relationship was observed between the spatiotemporal variations of these factors and macrofaunal biomass due to the negligible temporal variation in both bottom temperature and salinity at each hotspot during 2000–2013 (Table 3.7).

3.4. Discussion

3.4.1. Remote estimation of phytoplankton size structure

Because the size structure of phytoplankton is one of the most important factors affecting biogeochemical processes, various local and global methods for retrieving phytoplankton size structure from satellite data have been developed in the last decade. For example, an algorithm for deriving the ratio of algal biomass larger than 5 μm to the total phytoplankton biomass in the Pacific Arctic was developed by Fujiwara et al. (2011) and was used to understand the spatiotemporal variation in phytoplankton size structure in response to environmental changes (Fujiwara et al., 2016). However, this kind of knowledge is quite limited in the Pacific Arctic. Therefore, the results found in this chapter will contribute to a better understanding of the spatiotemporal variation in the phytoplankton size structure in the Pacific Arctic.

A modified version of the CSD model was developed to successfully estimate the phytoplankton size structure in the Pacific Arctic from satellite data. In general, owing to the large amount of CDOM in coastal waters, the retrieved inherent optical properties, such as $a_{ph}(\lambda)$ and $b_{bp}(\lambda)$, tend to include more errors in coastal areas compared with those in open ocean areas (Kostadinov et al., 2007). As the Pacific Arctic receives large amounts of freshwater containing CDOM delivered from rivers and the Bering Sea (Holmes et al., 2002; Eisner et al., 2012), global bio-optical algorithms do not often perform well in this region (Wang and Cota, 2003; Matsuoka et al., 2007). In this study, a modified version of the quasi-analytical algorithm proposed by Fujiwara et al. (2016) was applied to estimate $a_{ph}(\lambda)$, and the validation results suggest that the modified CSD model performed with sufficient accuracy regardless of the magnitude of $a_{CDOM}(\lambda)$ (Figure 3.2). It has also been reported that pigment packaging and pigmentation at higher latitudes are different from those in temperate waters (Matsuoka et al., 2007), resulting in estimation errors of the satellite algorithm based on inherent optical properties. The CSD model depends on the spectral shape of normalized $a_{ph}(\lambda)$ for estimating the size structure of phytoplankton, and the variation in normalized $a_{ph}(\lambda)$ is mainly caused by a coupling of the packaging effect and pigment composition (Wang et al., 2015). Because the

modified CSD model was developed using a dataset that covers a wide area and over several seasons in the Pacific Arctic (Figure 3.1a, Table 3.1), the model comprehensively captures the relationship between phytoplankton size structure and normalized $a_{ph}(\lambda)$ controlled by the packaging effect and pigment composition in the study area. Therefore, the modified CSD model could be a powerful tool to estimate spatiotemporal variation in phytoplankton size structure in the Pacific Arctic.

3.4.2. Current and future perspective of variations in phytoplankton community

Micro-sized diatoms dominate the community composition during the spring bloom (Aizawa et al., 2005; Sukhanova et al., 2009), and a large part of annual primary production in the Pacific Arctic occurs at this time (Sakshaug, 2004). Therefore, the phytoplankton size structure during the bloom period was initially expected to largely be responsible for the amount of sediment chl*a*. Nevertheless, the phytoplankton size structure during the bloom period was not well correlated with sediment chl*a* (Figure 3.6a). Instead, a clear relationship was observed between phytoplankton size structure during the post-bloom period and sediment chl*a* (Figure 3.6b). Two factors could help explain this difference. First, the possibility that the difference in sediment chl*a* was driven not by the amount of transported chl*a* during the bloom period but that during the post-bloom period. The CSD slope during the bloom period was significantly ($p < 0.05$) lower than that during the post-bloom period. In addition, the range of the CSD slope values was relatively narrow during the bloom period (0.36–1.01) than that during the post-bloom period (0.51–1.79), and coefficients of variation in the CSD slope across the whole region were significantly ($p < 0.05$) lower during the bloom period than those during the post-bloom period, with averages for 2000–2013 of 20.0% and 26.2% during the bloom and post-bloom periods, respectively. These findings suggest that the large phytoplankton size structure was distributed homogeneously during the bloom period, whereas that of the post-bloom period exhibited a large variation among stations. The uniformly large phytoplankton size structure during the bloom period could have potential to transport chl*a* to the sediments at all stations, resulting in a comparable distribution of sediment chl*a* due to the equivalent ability of the biological pump. In contrast, the CSD slope during the post-bloom period varied within a wide range, and differences in phytoplankton size structure among stations could drive variations in sediment chl*a* at each station. Based on these results, efficient carbon transport to the sediments driven by uniformly large phytoplankton size structure may occur all over the Pacific Arctic during the bloom period, and regionally small/large size structure of phytoplankton community could restricts/allows further carbon transport at the region in the post-bloom period. Second, the bloom and post-bloom periods were defined as 14

days from the date of sea ice retreat, and from the end of the bloom period to the date of benthic sampling, respectively. As benthic sampling was conducted in mid to late July (Table 3.3) and the sea ice retreated before mid-May in the study area, the time lag between the end of the bloom period and the date of benthic sampling was generally more than 1 month. During this time, benthic organisms would quickly assimilate some of the freshly settled chl*a* during the bloom period (Ambrose and Renaud, 1995), and the rest could be buried as a food bank by bioturbation or sedimentation (Josefson et al., 2002; Hansen and Josefson, 2003; Pirtle-Levy et al., 2009). Sediment chl*a* was determined by surface (top 0–1 cm) sediment samples; hence, chl*a* content in the deeper layers was not reflected as sediment chl*a*.

Chl*a* during both periods showed significant but weak relationship with sediment chl*a* (Figure 3.6). In the Arctic, the seasonal drawdown of nutrients drives the seasonal shift in the phytoplankton sizes structure, from larger assemblage dominating in the spring to smaller assemblages in the summer (Moran et al., 2012). These variations in size structure associated with changes in species composition are linearly related with total biomass of the phytoplankton community (Eisner et al., 2016). However, Brugel et al. (2009) reported an exception of a different proportion of larger cells (>5 μm) in the phytoplankton community despite the same amount of its biomasses, suggesting that the typical relationship between biomass and size structure of a phytoplankton community does not always hold true. These findings may explain the reason why chl*a* was less correlated with sediment chl*a* than CSD slope, which is a more direct index of phytoplankton size structure. It is noteworthy that, according to Stoke's Law, terminal velocity of sinking particle increases with the square of particle diameter if other parameters such as density and fluid of the particles are constant. Indeed, the CSD slope during the post-bloom period south of SLI varied from 1.04 ± 0.13 in 2000–2006 to 1.15 ± 0.17 in 2007–2013 (Table 3.6), representing the terminal velocity became approximately one quarter in 2007–2013 compared with in 2000–2006. Similarly, the CSD slope during the post-bloom period at Chukchi varied from 1.02 ± 0.14 in 2000–2006 to 0.79 ± 0.14 in 2007–2013 (Table 3.6), indicating the terminal velocity in 2007–2013 was more than two and a half times as large as that in 2000–2006. These facts exhibit the importance of phytoplankton size structure in terms of phytoplankton settlement to the seafloor.

Consequently, these findings suggest the importance of monitoring phytoplankton size structure in terms of the biogeochemical cycle in the Pacific Arctic. Notably, several studies have revealed continuous increases in annual primary production associated with a reduced extent of sea ice and the longer phytoplankton growth season in the Arctic (Arrigo et al., 2008; Arrigo and van Dijken, 2011, 2015); however, it may not be directly linked with increases in food supply for benthic organisms because of the importance of the phytoplankton size

structure to organic carbon influx to the sediments. Although the spatiotemporal monitoring of phytoplankton size structure via satellite remote sensing has not been widely used in the Pacific Arctic, it has the potential to provide more effective conservation and prediction of marine ecosystem function. Moreover, modeling approaches integrating these satellite and field findings will be able to better address the response of the marine ecosystem to ongoing environmental changes associated with warming temperatures (Woodgate and Weingartner, 2012; Woodgate et al., 2015) and sea ice loss (Stroeve et al., 2014).

3.4.3. Factors driving the temporal variation in phytoplankton size structure

Phytoplankton blooms in the seasonally ice-covered area in the Arctic were believed to begin after the sea ice retreats and the water column stratifies, providing sufficient light for photosynthesis (Sakshaug, 2004; Hill et al., 2005). In this chapter, the bloom period was defined as 14 days from the date of sea ice retreat to detect the blooms occurring in the marginal ice zone, which is the area where ice melt has just recently occurred. However, the recent shift from multi-year ice to thin first-year ice (Comiso et al., 2008; Stroeve et al., 2014) accompanying a significantly higher melt pond fraction in the Pacific Arctic (Polashenski et al., 2012) allows sufficient sunlight to penetrate for phytoplankton growth in the water column under the ice (Frey et al., 2011). Accordingly, a massive under-ice phytoplankton bloom has been frequently detected and widely occurs in recent years (Arrigo et al., 2012; Lowry et al., 2014), implying that under-ice phytoplankton blooms may utilize nutrients in the surface layer before the sea ice retreats (Fujiwara et al., 2016). This observation likely explains why the phytoplankton size structure during the bloom period shifted toward a smaller assemblage in the Pacific Arctic (Figure 3.7). Although the under-ice bloom has been growing in importance in this area, direct observations of the under-ice bloom from a satellite are a technically difficult issue. Therefore, a novel approach to monitor the spring bloom occurring under the sea ice could improve our knowledge of the biogeochemical and ecosystem dynamics in this region.

Temporal trends in the phytoplankton size structure showed regional patterns during the post-bloom period (Figure 3.7). The phytoplankton size structure shifted toward a smaller assemblage with time south of SLI, whereas the opposite pattern was found in Chukchi. In the northern Bering Sea shelf south of the SLI hotspot, a less sharply stratified water column permits entrainment of nutrients into the surface layer in response to wind-induced mixing (Stabeno et al., 2010). As such a physical process is one of the most important factors related to biomass and size structure of the phytoplankton community in the region (Eisner et al., 2016), variations in the wind field would explain the variation in phytoplankton size structure south of the SLI hotspot. On the Chukchi shelf, Danielson et al. (2017) suggested a positive relationship

between nutrients and northward volume flux through the Bering Strait. As the annual average volume flux through Bering Strait exhibited an increase in northward transport of ~50% from 2001 to 2013 (Woodgate and Weingartner, 2012; Woodgate et al. 2015), the Chukchi hotspot could receive more nutrients from the northern Bering Sea shelf over time. Therefore, this increasing nutrient availability would support a larger size structure of the phytoplankton community in this region.

3.4.4. Response of benthic macrofauna to food input

There is a clear relationship between the phytoplankton size structure during the post-bloom period and macrofaunal biomass distribution in the Pacific Arctic, suggesting that the continuous influx of organic carbon to the seafloor through the bloom and post-bloom periods has an important influence on macrofaunal biomass in this region. In this study, higher/lower macrofaunal biomass was observed in the hotspot areas with larger/smaller size structure of coincident phytoplankton during the post-bloom period (Figure 3.9). However, extremely high macrofaunal biomasses were found at Chukchi during 2006–2013. In the Pacific Arctic, in addition to export of organic carbon from the overlaying water column to benthic organisms, lateral advection of organic carbon also plays important roles as a food source for benthic organisms (Grebmeier et al., 2015a,b; Lovvorn et al., 2016; Moore et al., in press). Strong currents through the Bering Strait slow down at Chukchi, and advected organic carbon from the Bering Sea is deposited to the seafloor at this site. Notably, stations that observed extremely high macrofaunal biomass are located at the western part of Chukchi, which are strongly influenced by productive Anadyr Water (Grebmeier et al., 2015b), resulting in a large amount of advected organic carbon settling in the sediments at the stations (Grebmeier et al., 2015b). Considering recent increases in the northward flow through the Bering Strait (Woodgate et al., 2012, 2015), a combination of influx from the overlaying water column and lateral advection may explain the unclear process of extremely high macrofaunal biomass at these stations.

The latitudinal centroid of the macrofaunal habitat shifted northward (Figure 3.5) because of the significant decrease and increase south of SLI and at Chukchi, respectively, with an insignificant trend at Chirikov during 2000–2013 (Figure 3.4). It is noteworthy that the pace of the northward shift in the macrofaunal habitat at the rate of 0.05°N year^{-1} was much faster than that of marine taxa in temperate regions of ~0.015°N year^{-1} (Pinsky et al., 2013), suggesting a drastic shift in macrofauna habitat in the Pacific Arctic compared with the global average. These spatiotemporal variations were clearly opposite to the phytoplankton size structure during the post-bloom period; namely, a significant decrease and increase in the

phytoplankton size structure south of SLI and at Chukchi, respectively (Figure 3.7). As the size structure of the phytoplankton community during the bloom period was homogeneously large (Figure 3.3 and 3.6), the continuous influx of organic carbon throughout the bloom and post-bloom periods could occur at the region that also exhibits a large phytoplankton size structure during the post-bloom period. During the ice-covered season, benthic macrofauna in the Pacific Arctic must rely on the food bank produced during in ice-free season and/or lateral advection of organic carbon from the ice-free area (Pirtle-Levy et al., 2009; Grebmeier et al., 2015b), although the food bank likely predominates as the food source because of the negligible upstream production in winter (Shiomoto et al., 2002). Therefore, it is logical that the macrofaunal habitat shifted along with the variation in phytoplankton size structure during the post-bloom period to satisfy their year-round food demand.

Based on the food bank hypothesis, the results found in this chapter suggest the importance of continuous influx of organic carbon for benthic macrofuana through a longer period in the Pacific Arctic. However, a conflicting hypothesis is the quick consumption of newly settled algae by benthic organisms. McMahon et al. (2006) and Sun et al. (2007) reported rapid consumption of fresh algae by benthic organisms in the Svalbard archipelago. Furthermore, Morata et al. (2015) reported results consistent with previous studies that benthic organisms increase their activities in response to the addition of fresh algae resulting in quick consumption of the input in the same region. Although the cause for these different hypotheses has not been provided, such findings seem reasonable for both hypotheses: most of the settled organic carbon is likely preserved in the sediments as a food bank for later utilization by benthic organisms based on the food bank hypothesis, whereas continuous influx of organic carbon may continue to satisfy the food demand of benthic organisms despite rapid consumption of fresh algae by benthic organisms based on conflicting studies. Overall, many intricacies exist in the benthic community in the Arctic and require integrated process studies to properly evaluate the dynamics of the food web, community structure, and the ocean system.

3.5. Conclusions

The Pacific Arctic has a unique food web structure in which a large proportion of primary productivity generated in the upper layer falls directly to the sea floor with little or no zooplankton grazing, resulting in a high benthic biomass and thereby a large proportion of benthic-feeding species. There was a significant relationship between sediment chl*a* and phytoplankton size structure during the post-bloom period, suggesting that the continuous influx of organic carbon to the sediments during the bloom and post-bloom periods provides more food for benthic macrofauna. Indeed, the latitudinal shifts in macrofauna and phytoplankton size

structure were well correlated during 2000–2013. These results indicate that bottom-up forcing by the size structure of the phytoplankton community via vertical transport of surface organic carbon to the seafloor influences the benthic macrofaunal and, therefore, potentially impacts the upper trophic levels, such as marine mammals and diving seabirds, in the Pacific Arctic. Consequently, remote estimates of phytoplankton size structure will contribute to our understanding of the response of the Pacific Arctic ecosystem to ongoing environmental changes.

Table 3.1. Cruise information and number of samples (*N*) obtained during each cruise where size fractionated chlorophyll-*a* (chla_{size}), the phytoplankton absorption coefficient ($a_{ph}(\lambda)$), and spectral radiance of a total of 139 samples were collected. Note that the cruise period indicates the data span.

Cruise period	Cruise ID	Vessel name	*N*
25 Jul.-14 Aug. 2007	OS180	T/S Oshoro-maru	20
11 Sep.-10 Oct. 2009	MR09-03	R/V Mirai	13
04 Sep.-13 Oct. 2010	MR10-05	R/V Mirai	28
13 Sep.-02 Oct. 2012	MR12-E03	R/V Mirai	12
23 Jun.-17 Jul. 2013	OS255	T/S Oshoro-maru	35
31 Aug.-04 Oct. 2013	MR13-06	R/V Mirai	32

Table 3.2. List of station names and locations of the sampling stations for the benthic macrofaunal and environmental data at each hotspot.

Hotspot	Station	Latitude (°N)	Longitude (°W)
SLIP	SLIP1	62.01	175.06
	SLIP2	62.05	175.21
	SLIP3	62.39	174.57
	SLIP5	62.56	173.55
	SLIP4	63.03	173.46
Chirikov	UT-BS5	64.67	169.92
	UT-BS2	64.68	169.10
	UT-BS4	64.96	169.89
	UT-BS1	64.99	169.14
SECS	UTN1	66.71	168.34
	UTN2	67.05	168.73
	UTN3	67.30	168.97
	UTN4	67.50	168.91
	UTN5	67.67	168.96
	UTN6	67.74	168.49
	UTN7	68.00	168.93

Table 3.3. Cruise information and number of data (*N*) for benthic macrofaunal biomass and conductivity–temperature–depth (CTD) data used in this study for the Canadian Coast Guard Ship (CCGS) Sir Wilfrid Laurier (SWL) cruises from 2000 to 2013 (excluding 2009, no data collected). CTD data were used for determining bottom water temperature and salinity.

Cruise period	Cruise	*N*	
		Infauna	CTD
19–23 Jul. 2000	SWL00	16	15
17–20 Jul. 2001	SWL01	16	16
15–18 Jul. 2002	SWL02	16	16
14–18 Jul. 2003	SWL03	16	16
15–19 Jul. 2004	SWL04	16	16
14–18 Jul. 2005	SWL05	16	16
12–17 Jul. 2006	SWL06	16	16
14–17 Jul. 2007	SWL07	16	16
16–21 Jul. 2008	SWL08	15	15
16–19 Jul. 2010	SWL10	16	16
15–18 Jul. 2011	SWL11	16	16
14–16 Jul. 2012	SWL12	16	16
13–20 Jul. 2013	SWL13	16	16

Table 3.4. Model parameters (β_0 and C_j in Eq. (3)) for estimating the CSD slope using $a_{\mathrm{ph}}^{\mathrm{std}}(\lambda)$.

	Model parameters							
	β_0	C_1	C_2	C_3	C_4	C_5	C_6	C_7
$a_{\mathrm{ph}}(412) > a_{\mathrm{ph}}(443)$	-0.291	0.324	0.018	-0.921	0.203	1.720	-0.194	-1.313
$a_{\mathrm{ph}}(412) < a_{\mathrm{ph}}(443)$	-0.342	0.302	0.031	-0.723	0.196	1.842	-0.201	-1.289

Table 3.5. Statistics of differences in ocean color products between the SeaWiFS and MODIS data; average ± standard deviation. Original SeaWiFS and modified SeaWiFS represent differences in each product derived from the SeaWiFS data against the MODIS products before and after bias correction, respectively. Statistics of chl*a* and $a_{\mathrm{ph}}(443)$ were compared in log10 space.

Product	Original SeaWiFS	Modified SeaWiFS
Chl*a*	0.07 ± 0.15	0.02 ± 0.12
$a_{\mathrm{ph}}(443)$	-0.05 ± 0.16	-0.03 ± 0.13
CSD slope	-0.08 ± 0.08	0.00 ± 0.06

Table 3.6. Statistics of macrofaunal biomass (gC m^{-2}), CSD slope during the bloom and post-bloom periods at each hotspot and the entire region; average ± standard deviation (coefficient of variance).

Hotspot	Macrofaunal biomass [gC m^{-2}]			CSD slope [no unit]					
				Bloom period			Post bloom period		
	2000–2006	2007–2013	2000–2013	2000–2006	2007–2013	2000–2013	2000–2006	2007–2013	2000–2013
South of SLI	19.1 ±3.9 (20.4)	15.7 ± 7.3 (46.5)	17.5 ± 6.0 (34.3)	0.72 ± 0.15 (20.8)	0.84 ± 0.12 (14.3)	0.78 ± 0.15 (19.2)	1.04 ± 0.13 (12.9)	1.27 ± 0.11 (8.9)	1.15 ± 0.17 (14.8)
Chirikov	23.5 ± 10.5 (44.7)	18.9 ± 13.5 (71.4)	21.5 ± 12.2 (56.7)	0.60 ± 0.11 (18.3)	0.65 ± 0.16 (24.6)	0.62 ± 0.14 (22.6)	0.76 ± 0.11 (14.5)	0.83 ± 0.12 (13.9)	0.80 ± 0.12 (14.8)
Chukchi	28.0 ± 15.2 (54.3)	40.7 ± 35.5 (80.8)	33.8 ± 27.3 (80.8)	0.64 ± 0.13 (20.3)	0.73 ± 0.14 (19.2)	0.68 ± 0.14 (20.6)	1.02 ± 0.14 (13.7)	0.79 ± 0.14 (17.9)	0.91 ± 0.18 (20.0)
Whole	24.1 ± 12.2 (50.6)	27.5 ± 27.5 (100.0)	25.7 ± 20.8 (80.9)	0.65 ± 0.12 (18.5)	0.74 ± 0.15 (20.3)	0.70 ± 0.14 (20.0)	0.96 ± 0.17 (18.2)	0.95 ± 0.25 (26.4)	0.96 ± 0.25 (26.2)

Table 3.7. Temporal trends in bottom water temperature and salinity at each hotspot and the entire region for 2000–2013.

Hotspot	Temperature [˚C]				Salinity [psu]			
	Slope	Y-int.	r^2	p	Slope	Y-int.	r^2	p
South of SLI	-0.01	25.6	0.02	0.64	0.00	35.2	0.00	0.92
Chirikov	0.00	9.5	0.00	0.95	-0.02	63.1	0.07	0.37
Chukchi	-0.04	73.1	0.02	0.64	-0.01	58.6	0.09	0.32
Whole	-0.02	38.5	0.01	0.71	-0.01	52.3	0.08	0.36

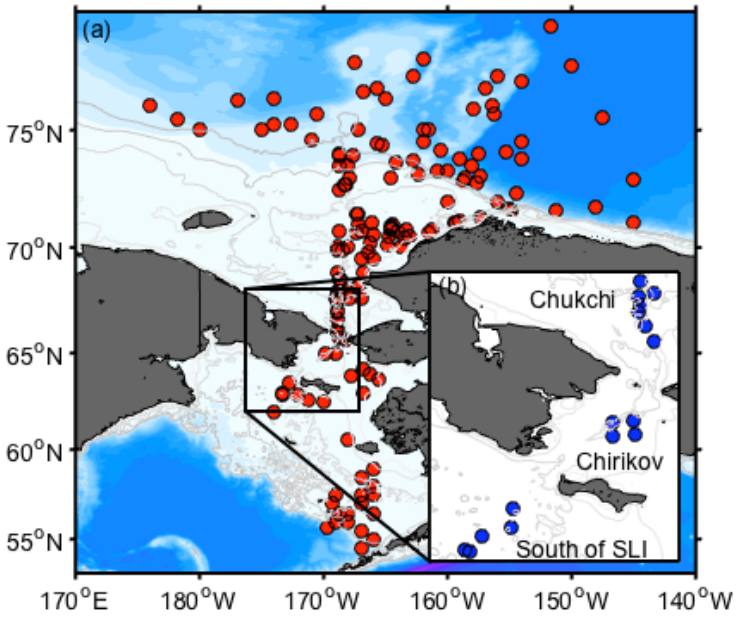

Figure 3.1. *In situ* observation stations for (a) optimizing the chlorophyll-*a* (chl*a*) size distribution (CSD) model and (b) evaluating of changes in biomass and distribution of the benthic macrofauna.

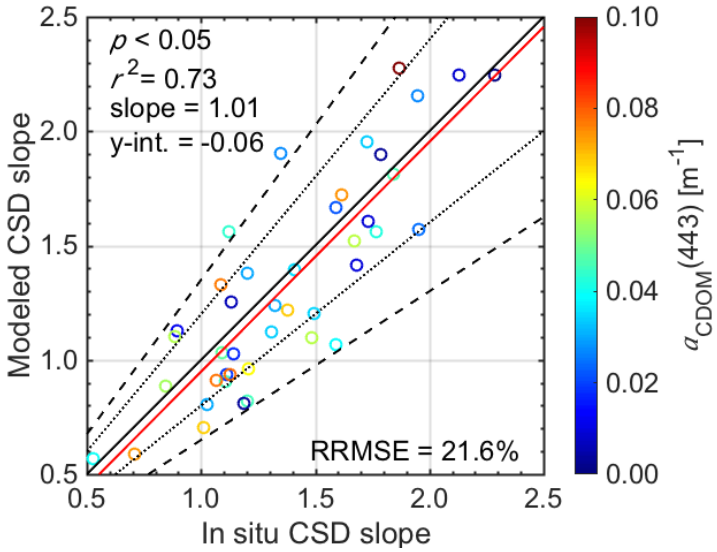

Figure 3.2. Comparison of *in situ* CSD slope values determined from *in situ* chla_{size} and modeled CSD slope derived from estimated $a_{ph}^{std}(\lambda)$ through a modified quasi-analytical algorithm using the *in situ* PRR data. Black and red solid lines represent the 1:1 agreements and regression lines, respectively. Dotted and dashed lines represent ±20% and ±35% ranges. Color of markers represents *in situ* measured $a_{CDOM}(443)$.

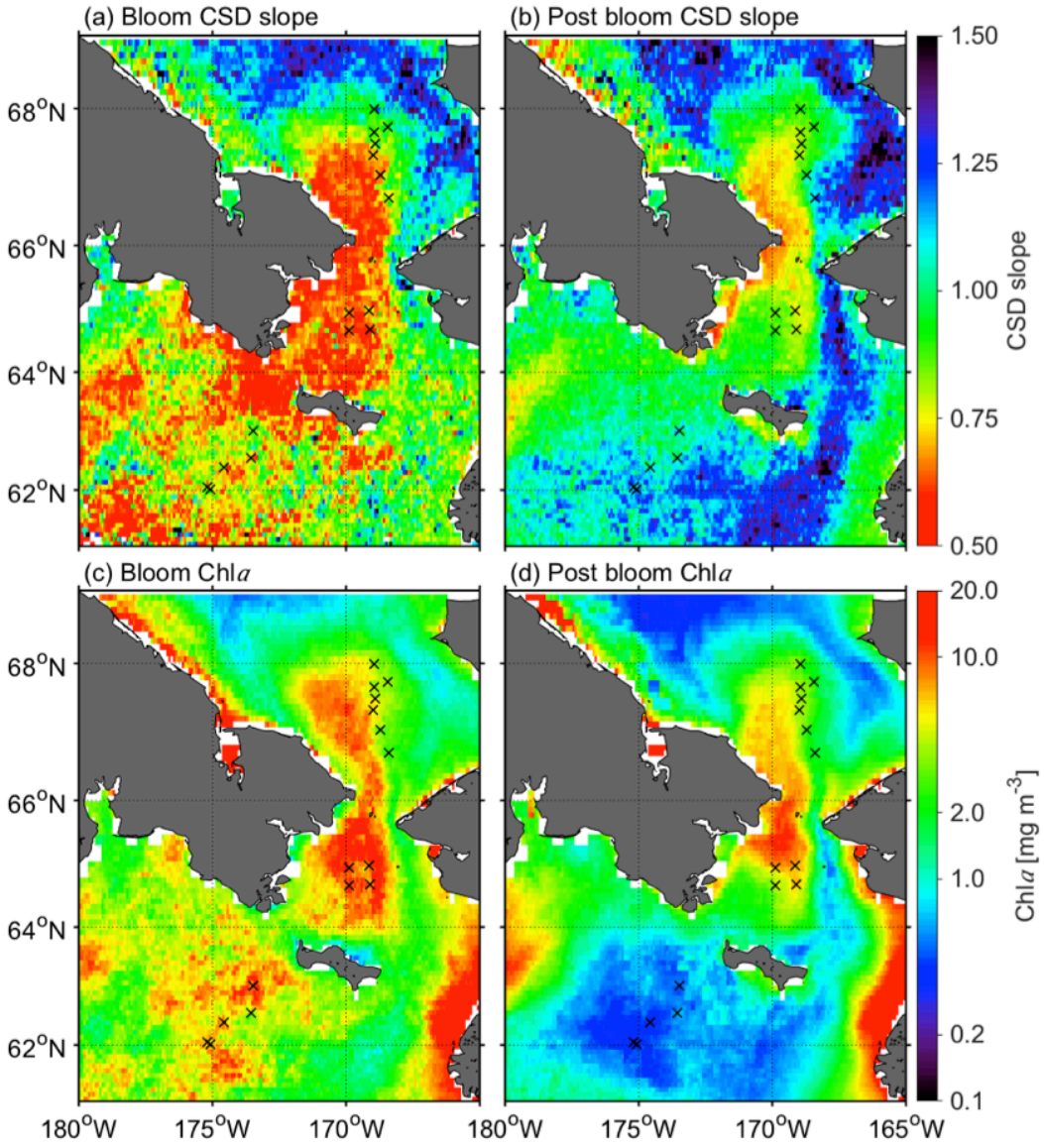

Figure 3.3. Average CSD slope and chl*a* during the bloom and post-bloom periods for 2000–2013: (a) The CSD slope during the bloom and (b) post-bloom periods, and chl*a* during (c) the bloom and (d) post-bloom periods. Crosses represent the location of the time series observation stations. Here, the post bloom-period was defined as the period from the end of the bloom period to the date of sea ice was produced.

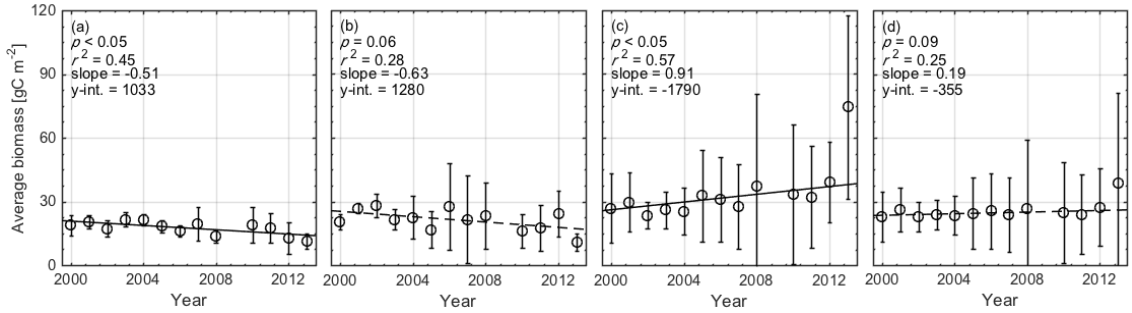

Figure 3.4. Temporal trends in the average macrofaunal biomass with standard error bars at (a) south of SLI, (b) Chirikov, (c) Chukchi, and (d) the whole region during 2000–2013. Solid and dashed lines indicate significant ($p < 0.05$) and insignificant ($p \geq 0.05$) trends, respectively. Statics and regression lines in (c) and (d) were derived as time-series of 2000–2012 because outlier was observed at Chukchi in 2013.

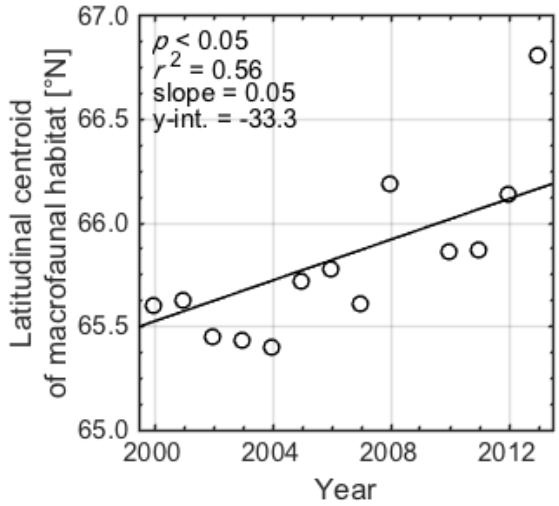

Figure 3.5. Temporal variation in the latitudinal centroid of the macrofaunal habitat. Black line and annotations represent regression line and statistics for 2000–2012 because outlier was observed at Chukchi in 2013.

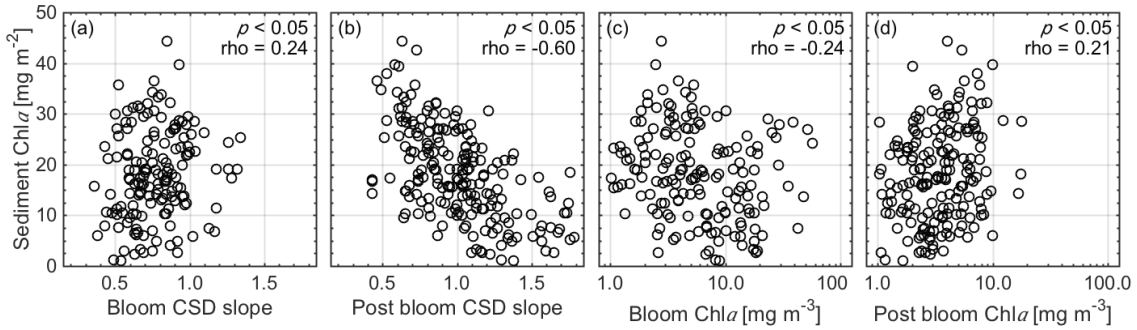

Figure 3.6. Relationship of *in situ* sediment chl*a* (top 0–1 cm of sediments) with the satellite-derived CSD slope during (a) the bloom and (b) post-bloom periods and satellite-derived chl*a* during (c) the bloom and (d) post-bloom periods.

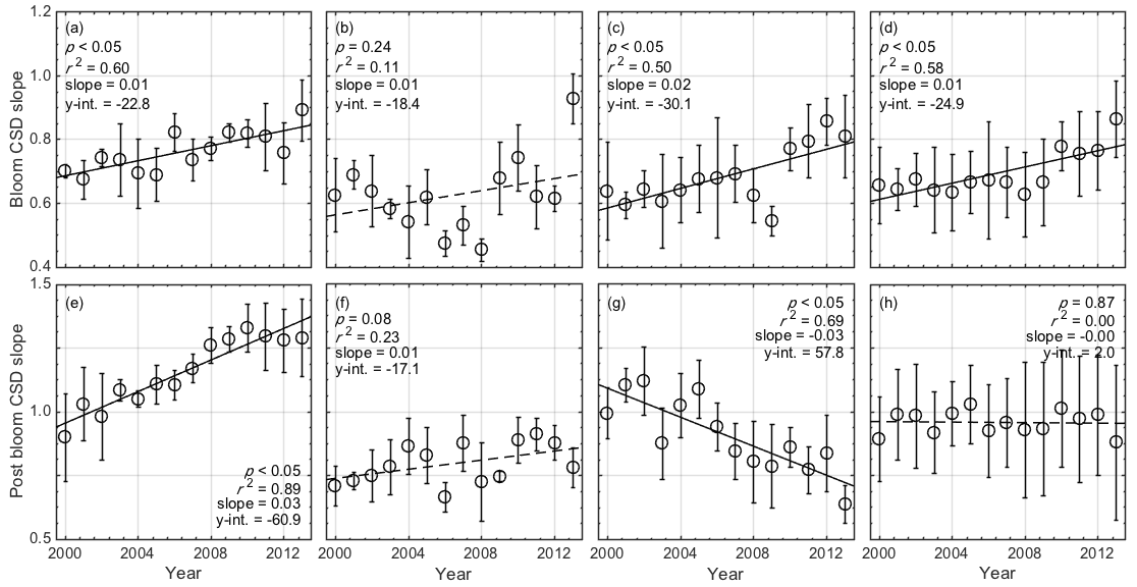

Figure 3.7. Temporal trends in the average CSD slope during the bloom (upper row) and post-bloom period (lower row) with standard error bars at south of SLI (a, e), Chirikov (b, f), Chukchi (c, g), and the entire region (d, f) for 2000–2013. Solid and dashed lines indicate significant ($p < 0.05$) and insignificant ($p \geq 0.05$) trends.

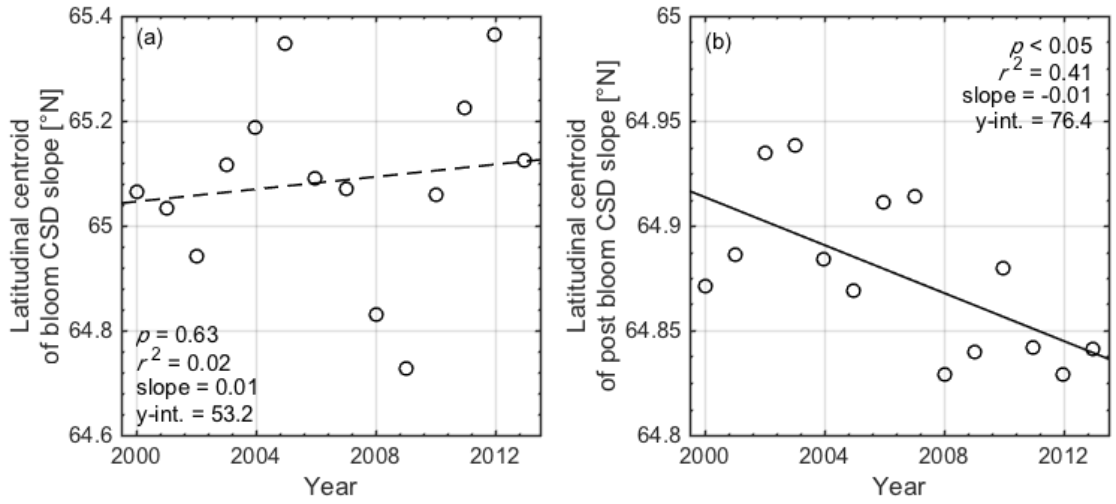

Figure 3.8. Tenporal trends in latitudinal centroid of CSD slope during (a) the bloom and (b) post-bloom periods. Solid and dashed lines indicate significant ($p < 0.05$) and insignificant ($p \geq 0.05$) trends.

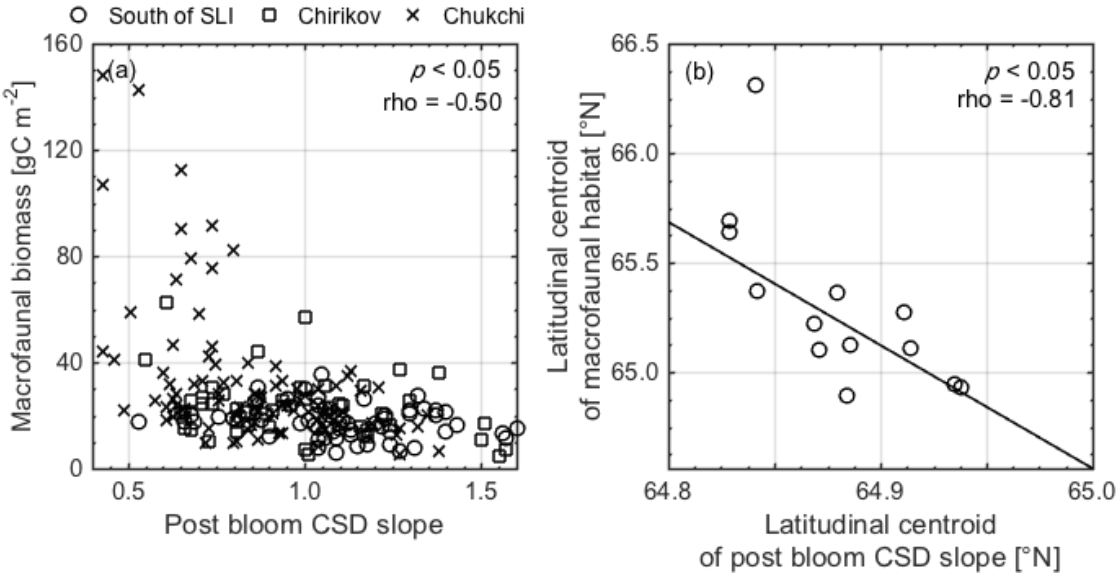

Figure 3.9. Relationships between (a) macrofaunal biomass and CSD slope during the post-bloom period, and (b) latitudinal centroids of the macrofaunal habitat and CSD slope during the post-bloom period. Latitudinal centroids in 2013 were removed in (b).

Chapter 4

Growth and physiological responses of a common Pacific Arctic bivalve to different food supplement patterns

4.1. Introduction

Climate warming has accelerated over the past several decades, causing increases in global surface temperatures of about 0.2 °C per decade (Hansen et al., 2006). The greatest changes have been recorded in the Arctic, where the temperatures have risen at approximately three times the global average rate (Steele et al., 2008). Such ocean warming promotes shrinking ice coverage (Comiso et al., 2008) and earlier ice retreat in the Arctic (Perovich and Richter-Menge, 2009). The initiation of sea ice retreat is important for the timing, quality and quantity of primary production, and subsequently food webs by influencing the standing stock of zooplankton (Hunt et al., 2002; 2011), which will in turn affect the direct, ungrazed deposition of phytoplankton and subsequently benthic organisms (Grebmeier, 2012; Nelson et al., 2009). Indeed, Moran et al. (2012) reported that with sea-ice cover the spring blooms were characterized by a less recycling with little or no grazing by zooplankton and greater export and, therefore, stronger pelagic–benthic coupling; on the contrary, in the case of open-water conditions, blooms were characterized by a greater carbon cycling in the water column via grazing impact of zooplankton and lower export to the seafloor, and consequently reduced pelagic–benthic coupling. Historically, the Pacific Arctic is characterized by tight pelagic–benthic coupling (Grebmeier and McRoy, 1989; Grebmeier et al., 1988) and up to 70% of primary production reached the seafloor in the Chukchi Sea (Walsh et al., 1989), while ongoing reduction of sea ice and earlier sea ice retreat would result in more intensive grazing by zooplankton and then less fresh algal settles to the bottom (Grebmeier et al., 2006; Lalande et al., 2007). Thus, the character of food web structure in the Pacific Arctic is expected to shift toward pelagic-oriented because of the earlier onset of ice melt (Kędra et al., 2015).

Dependence of benthic macrofauna on a large pool of persistence sediment organic matter referred to as a food bank has been documented in a range of environments at polar latitudes (Byrnes, 2006; Josefson et al., 2002; Mincks et al., 2005; North et al., 2014). However, fresh ice algae and phytoplankton may be important sources of certain essential fatty acids (FAs) required for benthic macrofaunal growth and reproduction (Hayakawa et al. 1996, McMahon et al. 2006, Sun et al., 2007, 2009), whereas reworked organic matter comprising major part of food bank are less nutritious than fresh microalgae, with higher C:N ratio (Turner, 2002) and lower content of polyunsaturated fatty acids (PUFAs) (Najdek et al., 1994). Although major pulses of settling fresh algae had little effect on the consistent fraction of sediment

organic matter assimilated by benthic deposit-feeders year-round (North et al., 2014), variation in pattern of phytoplankton settled to the seafloor could be crucial factor in terms of biomass and abundance of benthic macrofauna in the Pacific Arctic.

In chapter 3, the size structure of phytoplankton during the post-bloom period was significantly correlated with sediment chlorophyll-*a* (chl*a*) concentration, suggesting that the amount of phytoplankton settlement to the seafloor was strongly related to phytoplankton size structure after the spring bloom. In addition, the distribution of benthic macrofuna was shifted toward north for 2000–2013 in the Pacific Arctic, which was well correlated with the phytoplankton size structure during the post-bloom period. Following two processes would explain this fact. First, more food bank that supports more benthic macrofaunal biomass could be made in the region where larger phytoplankton size structure was maintained not only during the bloom period but also during the post-bloom period, and vice versa. Second, larger phytoplankton size structure during the post-bloom period could keep providing PUFAs by continuous influx of fresh phytoplankton for longer duration, resulting in better growth and reproduction succession of benthic macrofauna. To the best of current knowledge, it is remain unclear that either or both of these two processes have driven distributional shift in benthic macrofauna, but the issue is required for better understanding about variations in marine ecosystem in the Pacific Arctic.

The goal of this chapter is to examine the effects of variation in food availability on the growth and physiological condition of benthic macrofauna in the Pacific Arctic. To investigate the response of benthic macrofauna to different patterns in availability, in addition to *in situ* and satellite observations, a factorial experiment was conducted exposing a common Pacific Arctic bivalve *Macoma calcarea* (Gmelin, 1791) to differences among several experimental setups. The density of *M. calcarea* is a key indicator of food availability for benthivorous upper trophic levels in both the northern Bering Sea (Jay et al., 2012) and northern Chukchi Sea (Beatty et al., 2016; Young et al., 2017); hence, understanding growth and physiological response of *M. calcarea* to environmental variations is considered as one of the most crucial factors for evaluating changes in marine ecosystem in the Pacific Arctic.

4.2. Materials and methods

4.2.1. Study site

Field observations were conducted at the Pacific Arctic around St. Lawrence Island, Chirikov Basin, and Bering Strait during a cruise of the T/S Oshoro-maru in the summer 2017. During the cruise, bivalve was collected at five stations (Figure 4.1, Table 4.1) using a Smith McIntyre Grab sampler. At each station, at least three grabs were collected for bivalve

collection. In addition, conductivity–temperature–depth (CTD) measurements were collected with a calibrated Sea-Bird Electronics, Inc. (SBE) CTD sensor from 5 m above of seafloor to 5 m beneath of sea surface at each station.

4.2.2. Bivalve collection and pre-experimental holding conditions

A common Pacific Arctic bivalve *Macoma calcarea* was employed in this chapter as one of the most typical benthic macrofauna in the Pacific Arctic. At least 20 individuals obtained at each five station were immediately stored frozen for post-cruise measurements. The rest of clams collected at sea were maintained in groups at most 50 individuals in 10 L tanks with bubbling at 4 °C for the reminder of the cruise. Daily maintenance for the bivalves included alternating water changes, in which half the volume of water was removed every other day and replaced with fresh seawater. During the cruise and also post-cruise experiment, artificial seawater, made from Instant Ocean™ (Spectrum Brands, Inc., Blacksburg, Virginia) sea salt and then controlled to be a similar salinity (32.5 psu) as the bottom water in which the clams were collected, was used.

4.2.3. No-incubation measurements

Shell length and weight of *in situ* obtained clams were measured at laboratory. Shell length (to the nearest hundredth of a mm) was measured as length from anterior to posterior side using a stainless steel digital caliper for three times and the mean of three lengths was employed in this chapter. In addition, ash-free dry weight (AFDW) calculated by subtracting the ash weight (AW) from the dry weight (DW) was used as weight of clams. AFDW is typically regarded as the most accurate predictor of macrofauna biomass, as it only includes biologically active tissue, although AFDW determinations require the incineration of dried samples in a furnace at high temperature, adding considerable time and costs to analyses. Additionally, AFDW/DW ratio was also calculated as an index of physiological condition of clams. Determinations of AFDW and DW were processed based on the procedures of Eklöf et al. (2017). Following size measurements, the measured individuals were transferred to pre-dried and -weighted (to the nearest hundredth of a mg) porcelain crucibles. Samples were then dried at 60 °C for >48 h (until constant biomass), and then cooled to room temperature in a desiccator before weighting of DW. After DW measurements, the crucibles were transferred to a muffle furnace, incinerated (550 °C for 3 h), cooled and weighted again for AW measurements. Finally, AFDW was determined as DW minus AW. AFDW/DW ratio was derived as AFDW divided by DW and expressed in %.

To compare shell length and weight of clams obtained at each station with spatial

distribution of phytoplankton size distribution during the post-bloom period, the chl*a* size distribution (CSD) model developed in chapter 3 was applied to satellite data. Details of material and methods were as described in section 3.2, but the period was expanded to 1998–2017 in this chapter. As high latitude bivalves have lifespans of decades (Ambrose et al., 2006; Carroll et al., 2011) to centuries (Butler et al., 2009, 2011; Schöne et al., 2005, 2011; Wanamaker et al., 2008), the CSD slope during the post-bloom period was averaged for 1998–2017. Then the average value within 3 × 3 pixel (27 × 27 km) subsets centered on the bivalve sampling station were extracted and then compared with shell length and weight of clams.

4.2.4. Factorial incubation measurements

A factorial experiment involving exposure clams to four different setups was run from August 19 to November 4 (eleven-weeks duration) at laboratory. Clams were randomly assigned to one of four 40 L tanks controlled at 4 °C. Within each tank, 25 polyethylene containers (5 cm diameter × 10 cm height) filled to the rim with sand collected from the Pacific Arctic were established and assigned one individual for each plastic container (25 individuals per tank). Prior to begin the experiment, the sand was rinsed with deionized water three times and then was soaked for 72 h in Instant Ocean™ seawater to acclimate it to experimental conditions and to allow for development of microbial flora associated with the incubated bivalves (Goethel et al., in press). Tanks were covered with polyethylene covers to reduce evaporation and endure in dark. Moreover, seawater within each tank was kept circulating moderately by pump and was kept bubbling over the course of the experiment.

Here, 2 × 2 factorial experiments were conducted as follows: a tank with a strong pulse of phytoplankton supplement for the first two weeks and also large amount of continuous influx of phytoplankton for subsequent period (treatment A); a tank without a strong pulse of phytoplankton supplement and instead high amount of continuous influx of phytoplankton throughout the experiment period (treatment B); a tank with a strong pulse of phytoplankton supplement for the first two weeks without phytoplankton supplement for subsequent period (treatment C); a tank with neither a strong pulse of phytoplankton supplement nor continuous influx of phytoplankton throughout the experiment period (treatment D). Long-term food bank in the Pacific Arctic is believed that is generally formed during ice-related bloom, including under-ice and ice-edge blooms (Hansen and Josefson, 2003; Josefson et al., 2002; Pirtle-Levy et al., 2009), and the sea-ice associated bloom typically lasts for two weeks (Niebauer et al., 1995). In chapter 3, the chl*a* concentration during the bloom period was 15.53 ± 1.35 mg m^{-3} at the benthic hotspots. In addition, the highest chl*a* concentration during post-bloom period was found at the southeastern Chukchi Sea hotspots at the average for 2000–2013 of 3.17 ± 1.35 mg

m^{-3}. These chl*a* concentrations corresponded with 270 and 50 μL of Shellfish Diet 1800™ per 10 L of seawater. Therefore, the tanks categorized as presence of strong pulse of phytoplankton supplement was fed 270 μL of Shellfish Diet 1800™ per 10 L of seawater during the first two weeks, and the tanks with continuous influx of phytoplankton were fed 50 μL of Shellfish Diet 1800™ per 10 L of seawater for the period without strong pulsed phytoplankton supplement. Feeding was conducted every other day (totally 38 times). Half the volume of seawater within each tank was removed every other day and replaced with fresh seawater. Prior to water replacements, bubbling and circulation were stopped for 3 h to sink the phytoplankton within seawater in order to reduce phytoplankton discharge from tanks accompanying with water exchange. Note that the amount of Shellfish Diet 1800™ fed on treatment B and C were 1.89 and 1.90 mL per 10 L of seawater, respectively, indicating that total amount of Shellfish Diet 1800™ fed on these tanks was mostly consistent.

Changes in shell length and weight of clams were determined by differences between directly before and after experiment. Shell length was measured by same procedure with no-incubation samples and percent change in shell length over the course of the experiment was calculated as follows:

$$\text{Change in shell length} = \frac{\text{Final shell length} - \text{Initial shell length}}{\text{Initial shell length}} \times 100. \quad (4.1)$$

Following size measurements before and after experiment, each clam was patted dry with a paper towel and then weighted. A similar percent change formula to Eq. (4.1) was applied to wet weight. Furthermore, AFDW/DW ratio of each clam was derived after the experiment based on same procedure of no-incubation samples.

4.3. Results

4.3.1. Linkage between body size of bivalve and phytoplankton size structure

There were significant differences in shell length, AFDW and AFDW/DW ratio among the sampling stations (Steele-Dwass: $p < 0.05$) (Figure 4.2). The largest shell length and AFDW were observed at St001 located at the north of Bering Strait, with second and third largest values were observed at Chirikov Basin (St007) and west of St. Lawrence Island (St019), respectively. These values observed southeast and south of St. Lawrence Island (St021 and St023) were relatively lower than others. On the other hand, AFDW/DW ratio showed inverse relationship with both shell length and AFDW. This is because that, in general, the proportional mass of biologically active vs. non-active tissue (shell, hard mouth parts, etc.) decreased with body size (Eköf et al., 2017), and thus body size is often used as conversion factor of AFDW/DW ratio in macrofauna studies (e.g., Brey et al., 1988; Ricciardi and Bourget, 1998).

Hence, spatial pattern in AFDW/DW ratio was not appropriate as an index of physiological condition owing to significant variations in size and weight of bivalve among the stations.

Figure 4.3 shows the distribution of CSD slope during the post-bloom period averaged for 1998–2017. As the CSD slope during the post-bloom is an important index of the amount and/or continuous phytoplankton settlement to the seafloor, the lower/higher CSD slope (i.e., larger/smaller phytoplankton size structure) during the bloom period suggests the region that bivalve enable to obtain more/less fresh phytoplankton from overlying water column. Obviously, the CSD slope during the post-bloom period exhibited clear contrast between western and eastern side of the region and lower/higher CSD slope were found in western/eastern side. Such pattern consists with typical water mass distribution in the Pacific Arctic: nutrient-rich Anadyr Water flows along the eastern coast of Siberia, nutrient-poor Alaskan Coastal Water passes along the western coast of Alaska, and those mediated Bering Shelf Water flows toward north between Anadyr Water and Alaskan Coastal Water (Coachman et al., 1975).

The CSD slope during the post-bloom period was ranged from 0.72 ± 0.02 to 1.17 ± 0.11 at the locations of bivalve sampling stations, indicating that the fractional contribution of microplankton (>20 μm) to the total phytoplankton assemblage derived using Eq. (2.8) varied from 0.60 ± 0.01 to 0.24 ± 0.02, respectively. The lowest and highest CSD slope during the post-bloom period was found at St001 and St023, where the highest and smallest body size in clams was observed. Despite of the very small number of samples (N = 5), the CSD slope during the post-bloom period showed significant (spearman's $\rho = -1.00$, $p < 0.05$) relationship with shell length and AFDW. These results clearly indicate that the larger shell length and weight were associated with a larger amount and/or continuous influx of phytoplankton to the seafloor in the Pacific Arctic. Note that bottom water temperature observed just before the bivalve sampling showed insignificant relationship with shell length ($p < 0.133$) and AFDW ($p < 0.133$). However, ship-based observed bottom temperature was a snapshot condition at the stations, whereas the bivalve in the Pacific Arctic could have longer lifespan of decades to centuries (Ambrose et al., 2006; Schöne et al., 2005, 2011; Wanamaker et al., 2008; Butler et al., 2009, 2011; Carroll et al., 2011). Thus, the linkages of habitat environment with body condition of bivalve should be evaluate more appropriately in terms of time scales of lifespan.

4.3.2. Growth and physiological conditions of bivalve

No significant difference among treatments was confirmed in both shell length and wet weight (one-way ANOVA: shell length, $p = 0.72$; wet weight, $p = 0.83$) before the factorial experiment. Thus, the difference in AFDW/DW ratio associated with body size could be

negligible though it was unable to measure and verify the statistical difference in AFDW/DW ratio among the treatment before the experiment. Comparing changes in shell length and wet weight before and after the experiment, there were significant differences in both of them among treatments (one-way ANOVA: $p < 0.05$) (Figure 4.5). Growths in shell length and wet weight were clearly consistent with each other: the largest growths in both shell length and wet weight were found in treatment A, followed by treatment B, C, and D. In addition, AFDW/DW ratio also showed same pattern that the largest and lowest values were observed in treatment A and D, respectively, suggesting that better physiological condition promotes growth in shell length and weight of clams. Furthermore, these differences in growth and AFDW/DW ratio were likely to be attributed to the positive influences of the amount of phytoplankton supplement during the bloom and continuous influx of phytoplankton during the post-bloom period (two-way ANOVA: $p < 0.05$), without the interaction between them (two-way ANOVA: changes in shell length, $p = 0.78$; changes in wet weight, $p = 0.64$; AFDW/DW ratio, $p = 0.99$), indicating that both the amount of phytoplankton supplement during the bloom and continuous influx of phytoplankton during the post-bloom period were important for bivalve in terms of its better growth and physiological condition. It is noteworthy that treatment B showed better growth and physiological conditions than those of treatment C (Table 4.3), suggesting that the continuous influx of phytoplankton during the post-bloom period was more important for growth and physiological condition of bivalve than strong pulse of phytoplankton supplement during the bloom period.

4.4. Discussion

4.4.1. Spatial pattern in body size of bivalve and its potential drivers

The shell length and AFDW of *M. calcarea* collected from the five sites between south of St. Lawrence and Bering Strait showed clear spatial differences. Larger body size (i.e., larger shell length and AFDW) of clams found at the northern two stations (St001 and St007) may be a result of the larger amount and/or continuous influx of fresh phytoplankton to the seafloor. Because the high latitude regions including the Pacific Arctic has established long-term food bank, settled phytoplankton to the sediment has been preserved for several weeks to months and support high benthic macrofaunal biomass year-round (Hansen and Josefson, 2003; Josefson et al., 2002; Pirtle-Levy et al., 2009). However, much of settled phytoplankton as food bank is processed by bacteria or by repeated passage through the guts of deposit-feeders before being assimilated by macrofauna in the Pacific Arctic (Lovvorn et al., 2005; North et al., 2014), and thus food bank likely to be less nutrition than fresh ice algae and phytoplankton. The long-chain eicosapentaenoic acid (EPA) and docosahexaenoic acid (DHA)

are omega-3 fatty acids produced exclusively by marine algae, and these PUFAs play a key role in reproduction, growth, and physiology for all organisms in marine ecosystems not only bivalve (Hayakawa et al. 1996; McMahon et al. 2006; Sun et al., 2007, 2009). The size structure of phytoplankton community during the post-bloom period can be an important index of the amount of settled phytoplankton to the seafloor as well as the continuous influx of phytoplankton to the sediment during the period, and it was not clear which process primary drove spatial pattern in body size of clams found. Consequently, the only certain was the results in section 4.3.1 support the findings of chapter 3 that benthic macrofaunal biomass shifted toward north accompanied by the variation in the phytoplankton size structure during the post-bloom period. Note that the influence of bottom water temperature should be also considered as one of the factors affecting spatial pattern in body size of bivalve in the region. As shown in Table 4.1, bottom water temperatures at the bivalve sampling stations were varied from −1.26 to 3.38 °C. Growth and survival rate of bivalve often well correlate with temperature especially during the growing season (Dekker and Beukema, 1999) and thus the spatial pattern in body size of bivalve may reflect the variation in water temperature, while intra- and interannual variations in bottom water temperature were not investigated. In the Pacific Arctic, the ice-derived cold pool (defined as the region in which the early summer bottom temperature is <2 °C) expands over the entire middle shelf from Bering Strait almost to the Alaska Peninsula especially in cold years (Stabeno et al., 2012), and may have restricted bivalve growth at St019, St021 and St023 owing to the presence of cold bottom water throughout the year. In addition, the impact of zooplankton grazing on the amount of phytoplankton settlement to the seafloor has not been considered in this chapter. Although several factors including bottom water temperature and grazing impact of zooplankton could affect directly or indirectly on growth and in turn body size of bivalve, the significant relationship between the size structure of phytoplankton community during the post-bloom period and body size of bivalve is one of the important findings in this chapter.

4.4.2. Responses of bivalve to different food availability

Growths in shell length and wet weight of bivalve as well as AFDW/DW ratio showed statistically similar and/or different variations among treatments (Table 4.4). These facts indicate a relative importance of continuous influx of phytoplankton during the post-bloom period than the strong single pulse of phytoplankton settlement such as ice-edge bloom occurring in spring (Niebauer, 1981; Sakshaug, 2004; Perrette et al., 2011), although both of these phytoplankton supplies contributed better growth and physiological condition of clams without specific interaction. Sun et al. (1993) reported half-life of sediment chl*a* (probably also

be true of PUFAs such as EPA and DHA) was within 31 d at 5 °C, and thus there was enough time during the experimental period to be degraded and decomposed the single pulse supplement of phytoplankton provided for the first two weeks at 4°C. Therefore, it is considered that bivalve in treatment C seemed to less assimilate nutrition required for better growth and physiological condition when comparing with treatment B, which was continuous influx of fresh phytoplankton but without strong pulse. Indeed, growth and physiological condition of bivalve in treatment A, which was same level of continuous fresh phytoplankton supplement as treatment B in addition to strong pulse for the first two weeks, showed the best growth and physiological condition than the others. Hence, continuous influx of phytoplankton to the sediment and then longer duration of fresh phytoplankton availability likely to be important for both growth and physiological condition of bivalve in the Pacific Arctic, and the amount of reworked and less nutritious food bank in the sediment might be less important. Note that the Shellfish Diet 1800™ is a mixture of PUFA-rich algae such as diatoms and flagellates (Hayawaka et al., 1996; Falk-Petersen et al., 1998, Leu et al., 2006, Sun et al., 2007), and the diet likely to contain more PUFAs than natural phytoplankton even when the same level of chl*a* concentration. Thus, changes in shell length and weight in addition to difference in physiological condition among the treatments were likely to be emphasized than natural condition for the same level of phytoplankton availability and the same duration.

4.4.3. Implications of benthic macrofaunal community in the future Pacific Arctic

Coupling between phytoplankton and zooplankton stocks during spring bloom is likely to be particularly weak when water temperature are cold (<2 °C), as under-ice and ice-edge blooms, because zooplankton reproduction and population growth will be retarded (Napp et al., 2000). In contrast, in the case of open water bloom that occurs in warm water temperature (>4 °C), zooplankton reproduction and population growth will become higher rates (Hunt et al., 2002; 2011). In the Pacific Arctic, tight pelagic–benthic coupling processes associated with ice related blooms have been believed that it maintained benthic hotspots in the Pacific Arctic (Grebmeier et al., 2015a). The results found in this chapter demonstrated the importance of continuous influx of phytoplankton than single-pulsed supplement of phytoplankton to the sediment in terms of growth and physiological condition of benthic macrofauna, although the presence of these two food sources was more appropriate than alone either of two. Therefore, shift in character of food web structure from pelagic–benthic to pelagic-oriented system likely to be not directly fatal for benthic macrofauna in the Pacific Arctic, if only they able to obtain continuous influx of phytoplankton from overlying water column and/or by lateral advection. However, on average, increased standing stock of

zooplankton in summer following the spring bloom consume large part of the daily primary production resulting in less phytoplankton flux to benthic organisms than during the spring bloom when the grazers unable to control prodigious growth of phytoplankton population (Springer et al., 1989), and it is uncertain that benthic macrofauna in the Pacific Arctic can obtain continuous influx of phytoplankton during the post-bloom period. If it were impossible, long-term food bank would support high biomass of benthic macrofauna, although the nutrition required for growth and reproduction such as DHA and EPA likely to be less contain in it. It should be noted that the several studies suggested the strong influence of earlier sea ice retreat on size structure and species composition of phytoplankton community not only during the bloom period but also during the post-bloom period (Li et al., 2009; Fujiwara et al., 2014, 2016). As the species composition of phytoplankton community varies with the phytoplankton size structure (e.g., Vidussi et al., 2001; Hirata et al., 2011), both sinking rate and PUFAs content likely to be determined by the size structure of phytoplankton community. Thus, variations in size structure of phytoplankton community should be considered for assessing the impact of climate change on benthic macrofaunal community in the Pacific Arctic.

4.5. Conclusions

Historically, the Pacific Arctic has been characterized by tight pelagic–benthic coupling processes that a large part of water column production will be transported to the seafloor with little or no grazing by zooplankton, resulting in persistent high benthic macrofaunal biomass in the region; however, recent studies have expected that the character of food web structure at the area shifts toward pelagic-oriented in near future owing to climate forcing such as drastic reduction of sea ice and warming water temperature. The results in this chapter provides useful evidences that growth and physiological condition of a common Pacific Arctic bivalve *M. calcarea* reflect a duration of fresh phytoplankton availability rather than total amount of organic material, suggesting that the shift in food web structure from pelagic–benthic to pelagic–pelagic system likely not to be directly fatal for benthic macrofauna in the Pacific Arctic if only benthic macrofauna able to obtain continuous influx of phytoplankton from overlying water column and/or by lateral advection. Since climate forcing significantly affects on ocean properties including sea ice dynamics and in turn phytoplankton community not only during the bloom period but also the post-bloom period, focused experimental studies on biological and physiological responses of sentinel species, such as bivalves, are needed to forecast future marine ecosystem structure. Such experimental work in addition to *in situ* observation would enable more accurate evaluation of detailed mechanisms that have occurred or would occur in the Pacific Arctic.

Table 4.1. General information of sampling stations. Bottom water temperature and salinity were determined by a calibrated SBE CTD sensor as the deepest value acquired a few meters above the bottom.

Station	Date	Latitude [°N]	Longitude [°W]	Depth [m]	Bottom water	
					Temperature [°C]	Salinity [psu]
St001	09 Jul.	66.2758	66.2758	57	3.38	32.7
St007	12 Jul.	65.0622	65.0622	51	3.76	32.9
St019	19 Jul.	63.4992	63.4992	66	−0.60	32.5
St021	20 Jul.	62.9102	62.9102	56	−1.26	32.2
St023	21 Jul.	62.1665	62.1665	47	−1.07	32.0

Table 4.2. Statistics of shell length, AFDW, AFDE/DW ratio, and post-bloom CSD slope at each station; average ± standard deviation (median).

	Length	AFDW	AFDW/DW	Post-bloom CSD slope
St001	28.08 ± 2.10 (28.66)	0.32 ± 0.06 (0.34)	20.08 ± 2.25 (20.24)	0.75 ± 0.03 (0.75)
St007	21.73 ± 4.41 (22.89)	0.18 ± 0.16 (0.11)	23.10 ± 3.10 (21.41)	0.87 ± 0.03 (0.87)
St019	19.49 ± 2.42 (19.47)	0.11 ± 0.04 (0.10)	28.44 ± 1.33 (28,22)	1.04 ± 0.05 (1.04)
St021	14.48 ± 0.89 (14.54)	0.05 ± 0.01 (0.05)	30.01 ± 0.89 (29.48)	1.11 ± 0.05 (1.10)
St023	14.42 ± 2.10 (13.34)	0.04 ± 0.02 (0.03)	32.88 ± 2.94 (30.90)	1.17 ± 0.11 (1.16)

Table 4.3. Statistics of changes in shell length and wet weight, and AFDE/DW ratio at each treatment; average ± standard deviation (median).

	Change in		AFDW/DW ratio [%]
	Shell length [%]	Wet weight [%]	
A	1.58 ± 1.75 (1.30)	2.19 ± 2.41 (1.30)	25.53 ± 2.89 (24.90)
B	0.92 ± 1.36 (0.57)	1.05 ± 0.72 (1.48)	24.25 ± 2.64 (24.61)
C	0.38 ± 1.33 (0.26)	0.43 ± 1.54 (0.39)	23.74 ± 2.93 (23.00)
D	−0.13 ± 0.97 (−0.20)	−0.38 ± 1.59 (−0.26)	22.48 ± 2.45 (21.46)

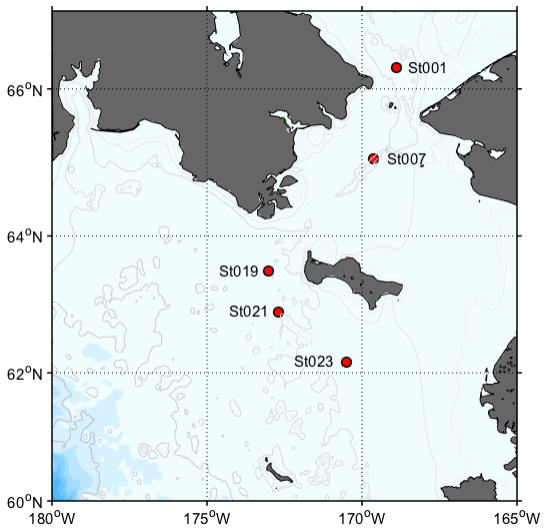

Figure 4.1. Location of sampling stations that bivalve was collected during the cruise.

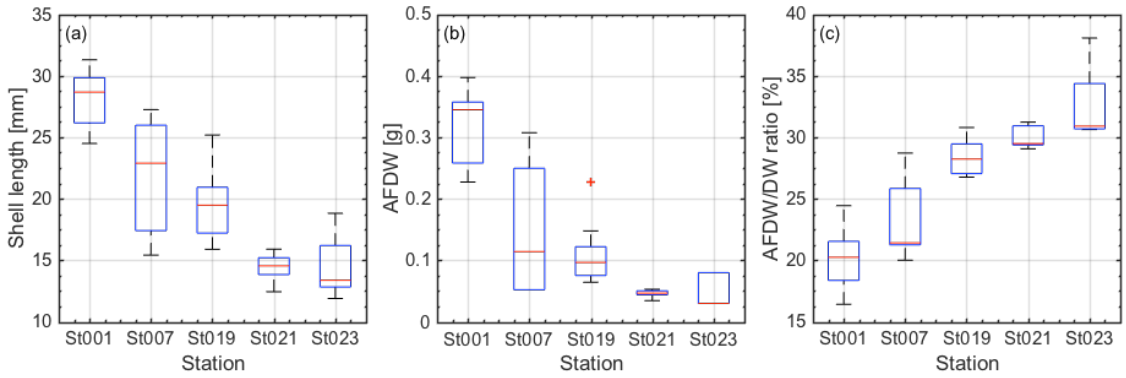

Figure 4.2. Boxplots of shell length (a), AFDW (b) and AFDW/DW ratio (c) at each station.

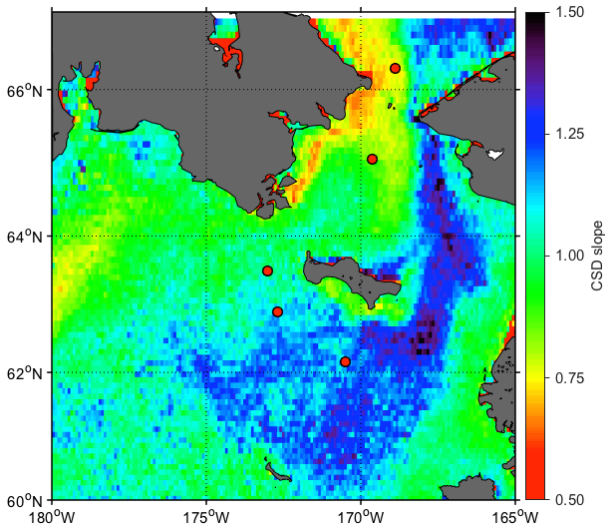

Figure 4.3. Average CSD slope during the post-bloom period for 1998–2017. Red plots represent the location of the bivalve sampling stations.

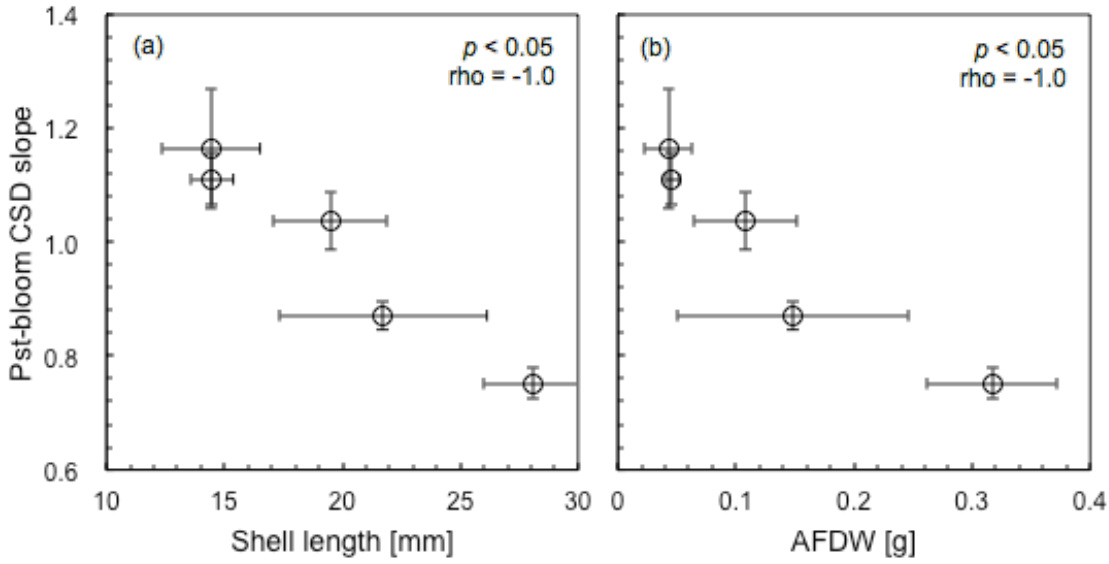

Figure 4.4. Relationships between the CSD slope during the post-bloom period and (a) shell length, and (b) AFDW at each station.

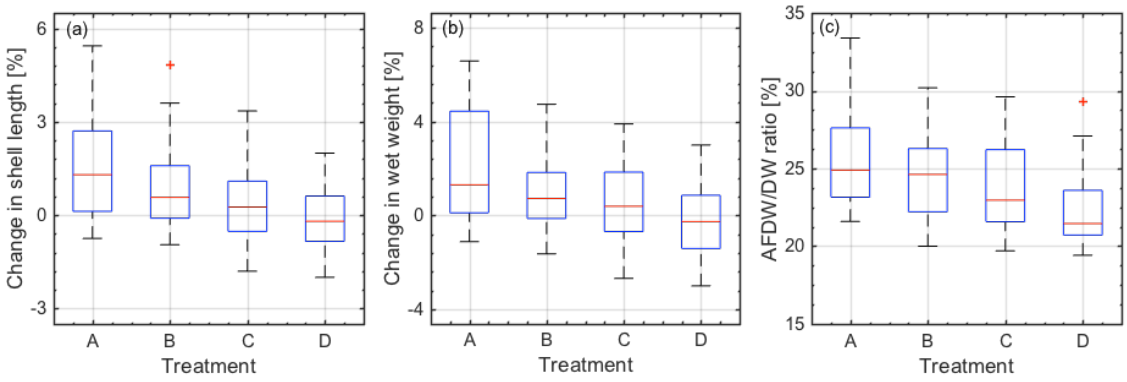

Figure 4.5. Boxplots of changes in shell length (a) and AFDW (b), and AFDW/DW ratio (c) at each treatment.

Chapter 5

Species invasion and diversity in benthic macrofaunal community in the Pacific Arctic

5.1. Introduction

The Bering Strait, where narrow (~85 km wide) and shallow (~50 m depth) channel, is the only ocean gateway between the Pacific and the Arctic ocean (Figure 5.1). Although the current through the strait is modest in global term, the impact of the Bering Strait throughflow is substantial in the Arctic (Woodgate et al., 2015). For instance, the heat flux through the Bering Strait acts as a trigger for sea-ice retreat in the Chukchi and western Arctic, and a major source of heat to about half of the Arctic Ocean (Woodgate et al., 2010). In addition, the freshwater flux in Bering Strait takes account ~40% of the total freshwater input to the Arctic Ocean (Aagaard, 2005). Beside its physical function, the Pacific water transiting across the Bering Strait also plays central roles in biogeochemical and biological environmental state in the Pacific Arctic. Water masses through the Bering Strait include the relatively colder, saltier and more nutrient-rich water of the Anadyr Current in the west, Bering Shelf water in the middle, and warmer, fresher and nutrient-poor Alaskan Coastal Current waters in the east (Pickart et al., 2010). The area, which are to a largely influenced by high nutrient concentrations in Anadyr Water, have comparatively higher standing stocks of phytoplankton, benthic macrofauna and demarsal fish (Grebmeier et al., 2015a).

Time series data obtained by the recent high-resolution mooring arrays indicate the Bering Strait throughflow increases ~50% from 2001 (~0.7 Sv) to 2013 (~1.1 Sv) (Woodgate and Weingartner, 2012). It has been believed that the variation in northward flow through Bering Strait is set by the sea level pressure gradient between the Pacific and Arctic oceans, often termed as pressure head, and local wind (Danielson et al., 2014; Woodgate and Aagaard, 2005; Woodgate and Weingartner, 2012). The pressure head primarily drives the background flow to the north through Bering Strait, whereas strong wind forcing in this region resulting in short term transport variability which is much larger than the background flow (Coachman and Aagaard, 1966). More specifically, the pressure head and local wind account for 2/3 and 1/3 of the variation in northward volume transport, respectively (Woodgate and Weingartner, 2012) By a recent study of Danielson et al. (2014), an integrated conceptual model of the Bering-Chukchi circulation was constructed: the northward transport through Bering Strait changes on inter-annual time scales in response to meridional sea level gradient associated with pressure head variations, where synoptic to monthly time scale variations in shelf currents result from local wind forcing as well as remotely generated continental shelf waves. Consequently,

there are growing knowledge on the processes of resent variation in Pacific water transport through the Bering Strait to the Arctic.

Climate changes are affecting polar ecosystems faster and stronger than the ecosystems in other regions (Doney et al., 2012), and climate-forced distribution shifts are likely to present a major challenge in the Arctic (Mueter, 2008). One of the logical predictions for a future Arctic characterized by increased northward volume transport is that new taxa will expand or invade Arctic ecosystem. Since the Arctic ecosystem is characterized as a low biodiversity relative to temperate and tropical communities (Hueffer et al., 2011; Kutz et al., 2013), the communities should be less resistible to invasion because of a less complete utilization of resources (Byrnes, 2006). However, well-documented examples are still scarce because of the very small number of time-series measurements in the Arctic, particularly for benthic organisms (Renaud et al., 2015). Although benthic organisms are normally stationary and less mobile than fish, it seems relevant that benthic organisms with pelagic life stages will be less limited in their expansion abilities than those with benthic dispersal stages (Renaud et al., 2015). Shifting species have potential to seriously affect biological system by robbing of food and/or habitat of native species, resulting in disruption of existing biological interaction and food web (Sorte et al., 2010). Since the Pacific Arctic is important foraging area for benthic feeding species (Grebmeier et al., 2006), the impact of changes in benthic community can propagate to upper trophic levels through the trophic cascades. Thus, evaluating these changes is crucial for better understanding about the Pacific Arctic ecosystem.

In this chapter, the variations in benthic community and those relationships with the volume transport of Pacific water into the Arctic were investigated. To achieve this objective, the spatiotemporal variations in benthic biomass, number of benthic taxa and species diversity for evaluating the species invasion was examined. In addition, temporal variations in meridional sea level gradient and local wind as indices of the northward volume transport of Pacific water were also investigated. Finally, this chapter examined the impact of SSH and local wind on benthic community in the Pacific Arctic.

5.2. Material and methods

5.2.1. Benthic macrofaunal data

Benthic macrofaunal biomass, number of family, biomass-based Shannon-Weaver diversity index (SWI) from the Pacific Marine Arctic Regional Synthesis (PacMARS) archive (http://pacmars.eol.ucar.edu) or the National Science Foundation (NSF) Arctic Data Center (https://arcticdata.io/). The dataset was obtained during the Canadian Coast Guard Ship (CCGS) Sir Wilfrid Laurier (SWL) cruise. In this chapter, macrofaunal dry carbon biomass (using

conversion values from wet mass, formalin-preserved samples) was used in order to reduce the bias of calcium carbonate on weight values (Grebmeier et al., 2015b). Detailed descriptions of methods used for determining macrofaunal biomasses and conversion factors are provided in Grebmeier and Cooper (2014a,b, 2017) and Grebmeier et al. (2015c). SWI is a commonly used diversity index that takes into account both the type (e.g. number of family or species) in a data set and evenness of those types (e.g. abundances in each family) present in the community. The value of a diversity index increases both when the number of types (families) increases and when evenness of entities measured (e.g, abundance within each family) increases. The data was obtained at 16 fixed, time series observation stations (SLIP1–5, UTBS1–4, and UTN1–7) (Figure 3.1, Table 3.1) using the SWL that were collected during summer 2000–2013, except the year 2009 (Table 3.1). Note that since 2010 these time series stations have been occupied annually as part of the Distributed Biological Observatory (DBO) SWL field program (Moore and Grebmeier, 2017).

5.2.2. Satellite altimetry data

Monthly mean gridded satellite altimetry data for 2000–2013 were downloaded from the Archiving, Validation, and Interpretation of Satellite Oceanographic (AVISO) data website (http:// www.aviso.oceanobs.com/), which combines data from the Topex/Poseidon mission along with other satellites to generate global gridded sea surface height (SSH) anomalies. The merged data are mapped on a 1/3° global grid. These data was provided by the Centre National d'Etudes Spatiales (CNES). This processing also includes an extended Low Resolution Mode (LRM) and a Doppler Synthetic Aperture Rader (SAR) pseudo-LRM mode, which allow extended high latitude coverage over seasonally ice-covered shelves. Expected accuracy (<2 cm) is <5% of the signal variance for multi-satellite month-long averages (Le Traon and Dibarboure, 1999), but variance increases in seasonally ice-covered waters and many grid cells therefore contain no usable data. The annual cycle was removed by subtracting each month's mean at each grid cell from the appropriate time steps (Danielson et al., 2014).

5.2.3. Atmospheric reanalysis data

The North American Regional Reanalysis (NARR) model (Mesinger et al., 2006) computes variable products containing temperatures, winds, moisture, soil data, and dozens of other parameters on a ~35 km grid with 3 h time steps from 1979–2014. The data was obtained from the National Climate Data Center's National Operational Model Archive & Distribution System (http://nomads.ncdc.noaa.gov/) for 2000–2013, and used daily averaged values of 10 m height wind vector components (*u* and *v*) for the region.

5.3. Results

5.3.1. Regional differences in benthic macrofaunal community among hotspots

Macrofaunal sampling was conducted at benthic hotspots located on the continental shelf in south of St. Lawrence Island (south of SLI), the Chirikov Basin (Chirikov), and the southeastern Chukchi Sea (Chukchi). Average macrofaunal biomass for 2000–2013 (Figure 5.2a–c) was significantly ($p < 0.05$) high at Chukchi (33.8 ± 12.5 gC m^{-2}), followed by Chirikov (21.5 ± 4.8 gC m^{-2}) and south of SLI (17.5 ± 3.1 gC m^{-2}). In addition, Chirikov hotspot exhibited the significantly ($p < 0.05$) largest average number of macrofaunal family of 39.9 ± 3.02 (Figure 5.2e), whereas those of south of SLI (Figure 5.2d) and Chukchi (Figure 5.2f) were 37.8 ± 3.58 and 34.8 ± 3.34, respectively. Furthermore, average SWI (Figure 5.2g–i) was the significantly ($p < 0.05$) highest at south of SLI (2.70 ± 0.11), with the second highest SWI of 2.20 ± 0.20 at Chirikov and the lowest SWI of 1.97 ± 0.19 at Chukchi. Overall, south of SLI was the region where the highest benthic macrofunal diversity among the three benthic hotspots accompanied with the lowest macrofaunal biomass, although the number of family was highest at Chirikov hotspot. On the other hand, both number of family and diversity were the lowest at Chukchi, while the macrofaunal biomass was the highest at the region.

5.3.2. Spatiotemporal variations in benthic macrofaunal community

There were significant ($p < 0.05$) increasing and decreasing trends in average macrofaunal biomass at Chukchi and south of SLI for 2000–2013, with insignificant temporal trend at Chirikov. At south of SLI and Chirikov, average number of family showed significant ($p < 0.05$) increasing trend over the period, while that of Chukchi exhibited no significant increase or decrease. On the other hand, Chukchi was the only region where showed significant ($p < 0.05$) temporal variation in SWI for 2000–2013: average SWI at Chukchi showed significant decreasing trend, whereas the rest of hotspots exhibited no significant trends ($p = 0.18$ and 0.11 at south of SLI and Chirikov, respectively). Since the number of family and evenness of biomass within each family drive a variation in SWI, a decreasing trend in SWI at Chukchi indicates a shift of macrofauna community from balanced biomass among each family to predominance of certain family in biomass. In contrast, insignificant variations in SWI were found at south of SLI and Chirikov where number of family showed increasing trend for 2000–2013, indicating that new families come into the regions but the biomass of these families were negligible and less affect on SWI. Note that the decrease in biomass at south of SLI might have been drove by uniform reduction in biomass within each family rather than reduction in biomass within certain family, because SWI showed insignificant temporal trend despite increase and decrease in number of family and whole biomass at the region.

5.3.3. Long-term variations in meridional sea level gradient and local winds

Figure 5.3a shows the difference in SSH between 2000 and 2013, suggesting a broad area of higher SSH in 2013 compared with that of 2000. Indeed, temporal variation in SSH was significant in the North Pacific and Aleutian Basin, whereas the continental shelves extending from the northern Bering Sea to the Chukchi Sea exhibited insignificant trend over the period (Figure 5.3b). Thus, when investigating variations in difference in SSH (ΔSSH) between the Aleutian Basin (SSH_{AB}; 50°–55°N and 170°E–180°) and southwestern Chukchi Sea (SSH_{CS}; 66–70°N and 180°–170°W), there was a significant ($p < 0.05$) increasing trend in ΔSSH (Figure 5.4) due to the increased SSH in the Aleutian Basin with negligible trend in southwestern Chukchi Sea. These spatiotemporal patterns in SSH represent increased meridional sea level gradient down to the north, suggesting that greater annual mean northward volume transport from the Pacific to the Arctic oceans. Additionally, long-term variations in local winds at each benthic hotspot were also investigated. According to previous studies, there are slight differences in surface wind direction that gives the best correlation with the northward current (Danielson et al., 2012; Woodgate et al., 2005). Hence, temporal variations in local winds heading 315°, 330° and 0° were examined at south of SLI, Chirikov and Chukchi hotspots, respectively. Comparing the local winds at each hotspot between 2000 and 2013, it was clear that opposite and compatible winds toward the best correlate directions were declined and increased in 2013 than 2000 (Figure 5.5), respectively. There were significant increased winds heading toward the best correlate directions within three regions (Figure 5.6). These results suggest that the reductions in the opposite wind stress against the northward currents at each hotspot, which indicate increased northward currents at the regions. Consequently, the northward volume transport at each region could exhibit increasing trend for 2000–2013 due to the positive impacts of variations in meridional sea level gradient and local winds.

5.3.4. Relationship between number of macrofaunal family and physical forcing

Direct comparisons between number of macrofaunal family and the meridional sea level gradient showed significant positive relationships at south of SLI and Chirikov hotspots (Figure 5.7), where the regions exhibited increasing trends in number of family for 2000–2013 (Figure 5.2). On the other hand, relationships between number of family at each hotspot and local winds at the regions were significant south of SLI and Chirikov, whereas Chukchi showed insignificant relationship between them during the study period (Figure 5.7). These results suggested that the increased northward volume transport associated with increased meridional sea level gradient and decreased southward winds promoted introduction of new macrofaunal organisms from southern region into the Pacific Arctic.

5.4. Discussion

5.4.1. Evidence of species invasion in benthic macrofaunal community

In this chapter, increasing trends in number of benthic macrofaunal family at the south of SLI and Chirikov Basin were found in accordance with the increased meridional sea level gradient as well as decreased opposite local winds. Since variation in northward flux at the Bering Straight is primary controlled by the meridional sea level gradient and local winds (Woodgate et al., 2015; Woodgate and Weingartner, 2012), the findings of the increased trans-basin sea level gradient and decreased opposite local winds could result in increased northward volume flux from south to north at each hotspot. To the best of our knowledge, this chapter reported the species invasion of benthic macrofauna in the Pacific Arctic for the first time, suggesting the benthic macrofaunal community in this region may be experiencing the beginning of community reconstruction from Arctic to sub-Arctic in response to increased Pacific water transport. However, it could not distinguish which family joined the benthic macrofaunal community and where is the origin. Additionally, this chapter could not preclude a possibility that not only invasion of exotic family but also withdraw of native family have been occurred in benthic macrofaunal community at the Pacific Arctic. These issues should be regarded as future research needs in the Pacific Arctic.

One of the possible reasons of insignificant variation in number of family at Chukchi is that larval settlement of benthic macrofauna could be occurred before arriving Chukchi hotspot. Many benthic invertebrate species have a dispersive larval stage in their life cycles (Thorson, 1950). Although larvae of benthic invertebrates in a water column behave as passive particles that are transported to a given site on large spatial scales, larvae can reject one site and select another appropriate site for settlement (Qian, 1999). Settlement and subsequent metamorphosis in marine invertebrates typically occur in response to environmental, chemical and physical cues and involve extremely rapid and irreversible changes in both morphology and habitat (Hadfield et al., 2001), suggesting settlement of exotic larvae transported from southern region could have been triggered in response to a common cue or a mixture of cues emitted at south of SLI and/or Chirikov hotspots. Numerous studies have demonstrated macrofaunal composition vary regionally due to current structure that influences sediment grain size in the Pacific Arctic (Blanchard and Feder, 2014; Grebmeier et al., 2015b; Schonberg et al., 2014). Both the south of SLI and Chukchi hotspots have fine-grained, silty and clayey sediments that are dominated by bivalves and polychaetes, whereas the macrofaunal community of the Chirikov hotspot occurs in sandy-mud sediments and are dominated by amphipods along with bivalves (Grebmeier et al., 2015b). Since the bottom environment is similar between south of SLI and Chukchi hotspots, larvae appropriate such environment could be triggered the cues at

south of SLI and the rest of larvae could be triggered the cues at Chirikov.

5.4.2. Benthic macrofaunal diversity associated with species invasion

Variations in SWI that represents biomass-based diversity in macrofaunal community showed regional differences, as with number of macrofaunal family. At south of SLI and Chirikov hotspots, SWI showed insignificant variation in spite of increased number of macrofaunal family, suggesting biomasses of invaded macrofauna into the regions seemed to be negligible compared with total macrofaunal population and resulted in quite little or no variation in evenness of each family's biomass. Following two factors could help explain the negligible variation in evenness of each family's biomass observed at south of SLI and Chirikov. First, the exotic families come from southern region could not be able to reproduce at the Pacific Arctic because of difficulty in survive within an extreme environment at the region. Foremost, the near-bottom water with temperatures less than 2°C associated with sea ice formation, which is commonly called as cold pool, persists from winter until the water column is homogenized in the fall by wind mixing and cooling. The cold pool acts as a barrier to many temperate species that are intolerant of the low temperatures of ice-associated bottom water (Sigler et al., 2016), and therefore determines the boundary between arctic and subarctic communities (Grebmeier et al., 2006; Wyllie-Echeverria and Wooster, 1998). Indeed, Fetzer and Arntz (2008) reported that nearly half of larvae of benthic organisms found in the Kara Sea are not represented in the adult communities of the region, indicating that arrival of propagules alone is not sufficient for successful colonization (Renaud et al., 2015). Thus, pelagic dispersal of larvae is only able to bridge the barrier of cold pool and doesn't always succeed in survival and reproduction at the region. Second possible cause is the population would be regulated by a carrying capacity of benthic macrofaunal population. In chapter 3, strong relationship between the amount of food supply and macrofaunal biomass have been reported, suggesting the carrying capacity in benthic macrofaunal community at the Pacific Arctic has been determined by food availability rather than spatial margin. Therefore, decreasing and consistent carrying capacities at south of SLI and Chirikov hotspots have prevented from growing of each family's population because of a complete utilization of food material by well-established native population.

A decreased SWI observed at Chukchi could not have been drove by decreased number of family, but by decrease in evenness of each family's biomass without decline in number of family. Considering the fact that macrofaunal biomass at Chukchi has increased for 2000–2013, this decrease in evenness of each family's biomass likely to be driven by drastic increase in biomass of specific family. At Chukchi hotspot, increased food supply

accompanying with shift toward large size structure of phytoplankton community (chapter 3) and also gyre structure trapping food materials (Sirenko and Gagaev, 2007) likely to support higher carrying capacity in terms of food availability that promote increment of macrofaunal biomass. Although it was impossible to distinguish which family exhibited drastic increase in their biomass in this chapter, feeding strategy likely to be important in deciding the winner the race to secure supplies of foods and other resources (North et al., 2014). Therefore, not only *in situ* time-series observations but also laboratory experiments dealing such difference among different feeding strategy would be largely improve our understanding of ongoing ecosystem variations in benthic macrofaunal community in the Pacific Arctic.

5.4.3. Increased northward volume transport and its subsequent impacts

Danielson et al. (2014) reported that eastward displacement of the Aleutian Low into the Gulf of Alaska from over the Bering Sea results in more northward volume transport at Bering Strait owing to combination of two factors: the increased the Pacific-Arctic basin dynamic height at inter-annual timescales, and increased southeasterly wind over the Bering shelf on synoptic storm timescales. There was a significant relationship of meridional sea level gradient and number of benthic macrofaunal family south of SLI and Chirikov where the areas would be exposed to species invasion from southern region, although local winds are significant only south of SLI. As meridional sea level gradient and local winds account for 2/3 and 1/3 of the variation in northward volume transport at Bering Strait (Woodgate and Weingartner, 2012) and probably also at each hotspot in the Pacific Arctic, number of macrofaunal family could be associated with meridional sea level gradient that is the most important factor controlling northward volume transport at each hotspot. In addition, such increased volume transport may influences on population composition of benthic macrofauna. Several studies reported that community pattern of benthic macrofauna varies regionally due to varying strength of the flow field that influences sediment grain size (Grebmeier and McRoy, 1989; Schonberg et al., 2014). As the increased volume flux would flush out fine-grained, silty and clayey sediments, benthic community likely to shift from deposit feeding species to suspension feeding species. Thus, not only species diversity but also population composition of benthic macrofaunal community in the Pacific Arctic will vary or have already varied in response to increased northward volume flux.

There is evidence of ~50% of the heat flux and ~90% of the freshwater flux changes are due to changes in the volume flux at Bering Strait, suggesting the heat and freshwater flux through Bering Strait has increased over the last decade (Woodgate and Weingartner, 2012). Physiological constrains associated with cold temperature in the Arctic has been one of the most obvious barriers for boreal organisms (Renaud et al., 2015). Even small levels of ocean

warming, however, could reduce physiological barriers for boreal immigrants. Aronson et al. (2007) predicted a rise in bottom temperatures of only 1 °C would be sufficient for invasion of decapod predators with a feeding strategy unknown to shelf regions around Antarctica. At the same time, a warming Arctic can present novel problems for resident Arctic fauna adapted to low temperatures. High-latitude taxa have temperature ranges of two to six times smaller than temperate and tropical taxa (Peck and Conway, 2000). Projected temperature increases in shallow (<200 m) waters of many Arctic's marginal seas exceed 2–3 °C by 2100 (Renaud et al., 2015), suggesting thermal conditions may soon become suitable and may inadequate for boreal and arctic taxa, respectively. Invaders might have competitive advantages over resident fauna if the latter have physiological constraints in adjusting to warmer temperatures (Peck and Conway, 2000). Therefore, warming of ocean temperature in the future Arctic will have significant implications for immigrant and resident Arctic benthos both directly and indirectly through species interactions (Renaud et al., 2015).

5.5. Conclusions

The Pacific Arctic has been exhibited drastic variation in macrofaunal community in response to increased northward volume transport from the Pacific to Arctic. This chapter reported the species invasion of benthic macrofauna in the Pacific Arctic for the first time, suggesting the benthic macrofaunal community in this region may be experiencing the beginning of community reconstruction from Arctic to sub-Arctic in response to increased Pacific water transport. Shifting species have potential to seriously affect biological system by robbing of food and/or habitat of native species, resulting in disruption of existing biological interaction and food web. As the Pacific Arctic is important foraging area for benthic feeding species, the impact of changes in benthic community can propagate to upper trophic levels through the trophic cascades. It is likely the future Pacific Arctic ecosystem will be very different from the past ecosystems before the major wave of biological invasions of the benthic macrofauna, which plays important roles in the food web structure in the Pacific Arctic ecosystem.

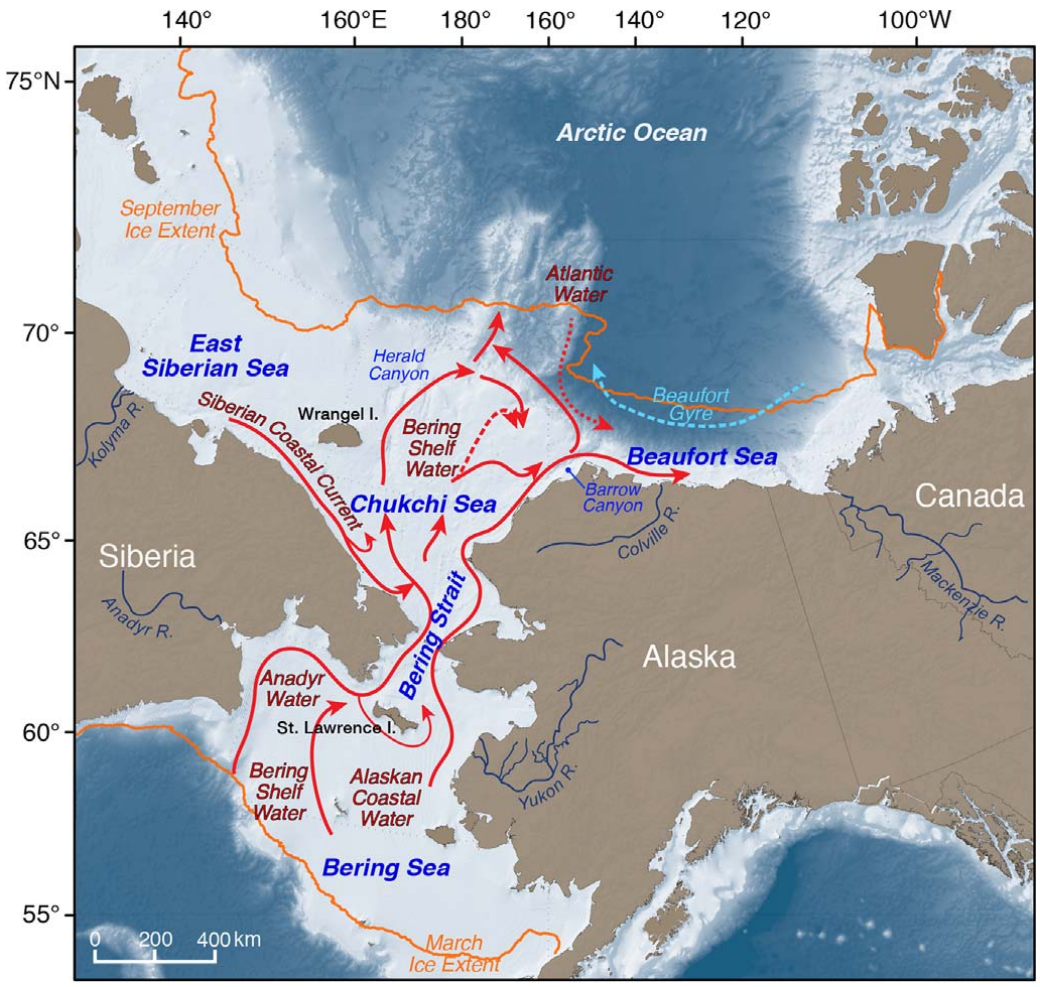

Figure 5.1. Schematic of general current patterns in the Pacific Arctic sector (Moore et al., in press).

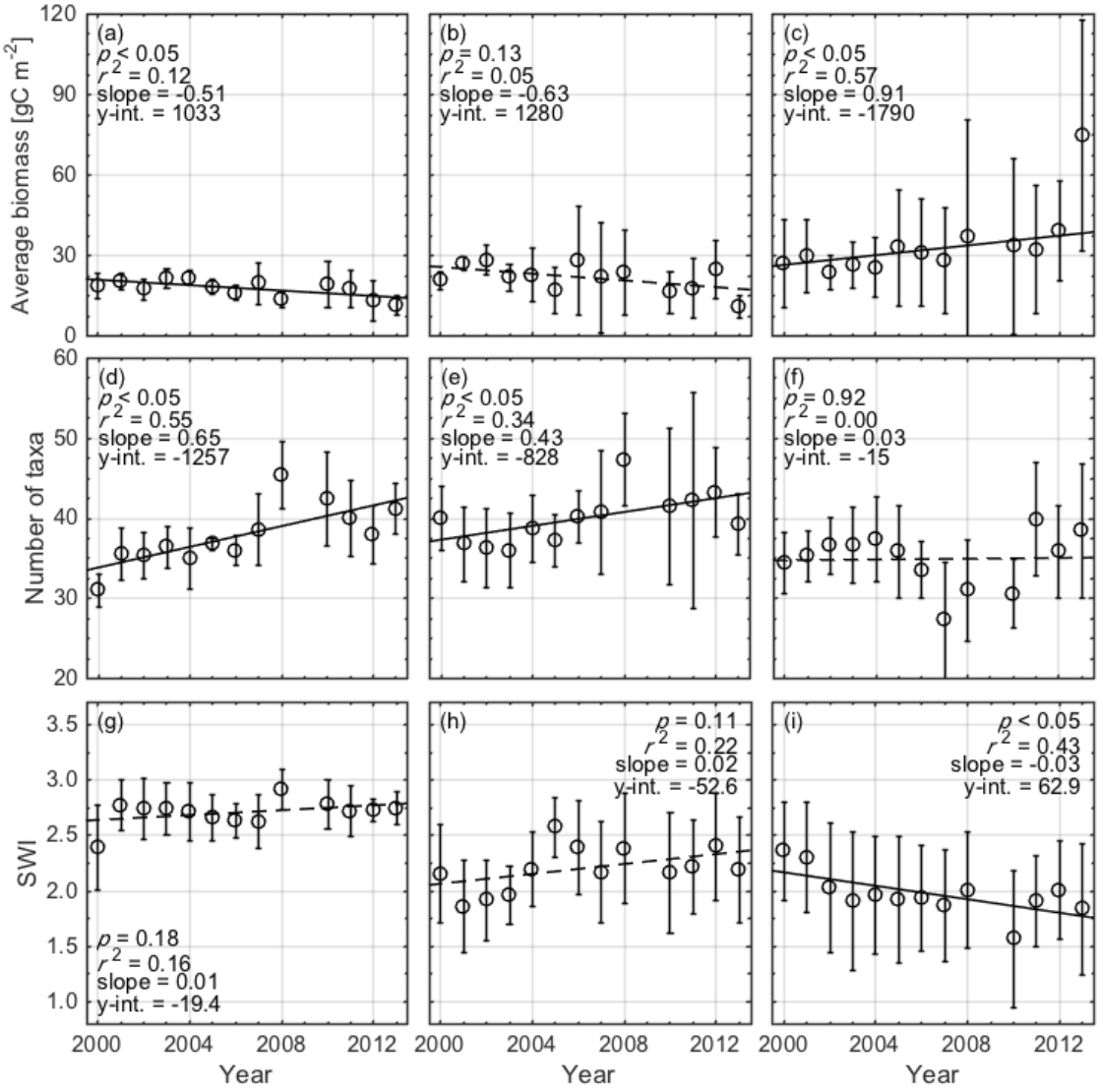

Figure 5.2. Temporal trends in the average macrofaunal biomass (a–c), number of taxa (d–f), and SWI (g–i) with standard error bars at south of SLI (left), Chirikov (middle), and Chukchi (right) during 2000–2013. Black lines indicate regression lines for 2000–2013. Solid and dashed lines indicate significant ($p < 0.05$) and insignificant ($p \geq 0.05$) trends, respectively.

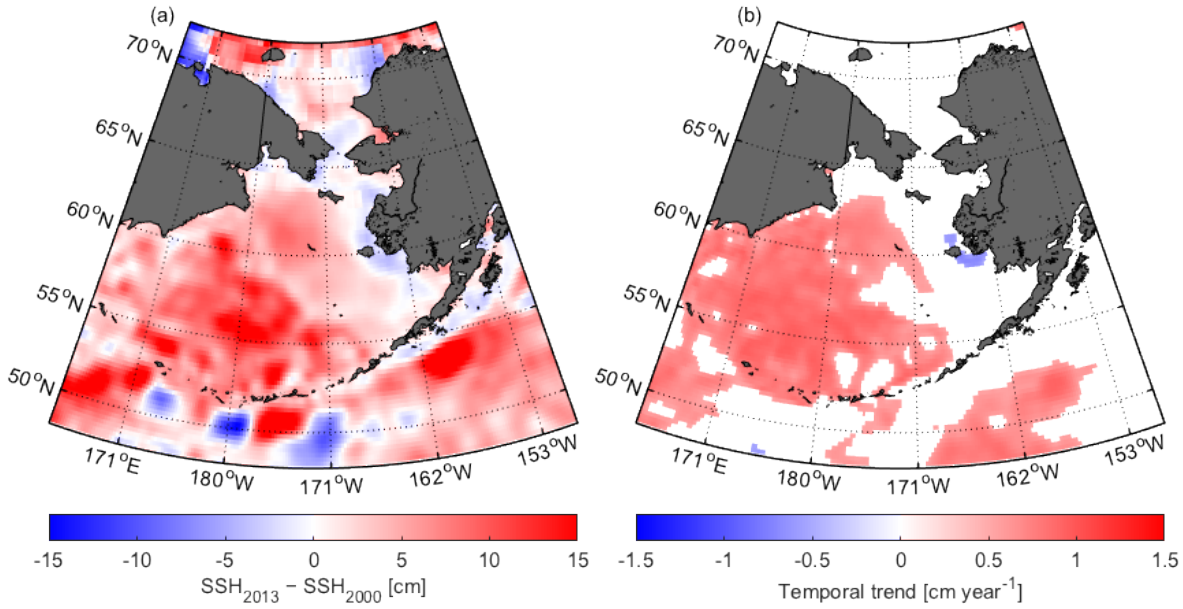

Figure 5.3. (a) The difference in SSH between 2000 and 2013 (SSH_{2013} − SSH_{2000}), and (b) temporal trend in SSH for 2000–2013. White in (b) shows the area with non-significant trend ($p \geq 0.05$).

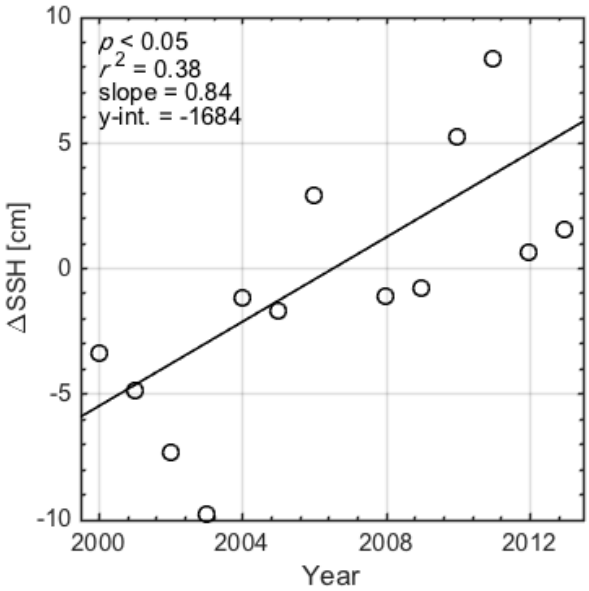

Figure 5.4. Temporal trend in ΔSSH derived as $\Delta SSH = SSH_{AB} - SSH_{CS}$ for 2000–2013. Solid line represents regression line.

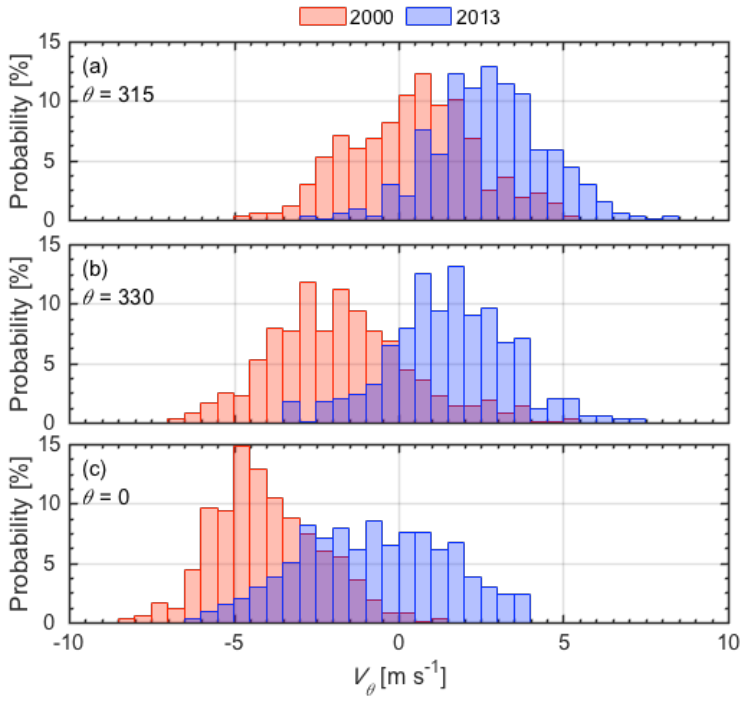

Figure 5.5. Histograms of local wind velocities along best correlate directions (V_θ) at (a) south of SLI, (b) Chirikov, and (c) Chukchi. θ were 315°, 330° and 0° for south of SLI, Chirikov and Chukchi. Red and blue bars represent winds in 2000 and 2013, respectively.

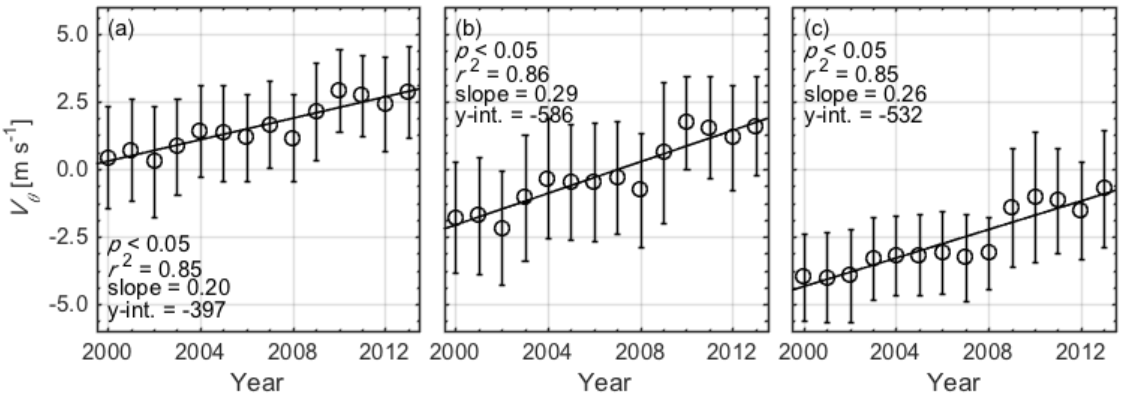

Figure 5.6. Temporal trends in local wind velocities along best correlate directions (V_θ) at (a) south of SLI, (b) Chirikov, and (c) Chukchi for 2000–2013. θ were 315°, 330° and 0° for south of SLI, Chirikov and Chukchi. Black solid lines represent regression lines.

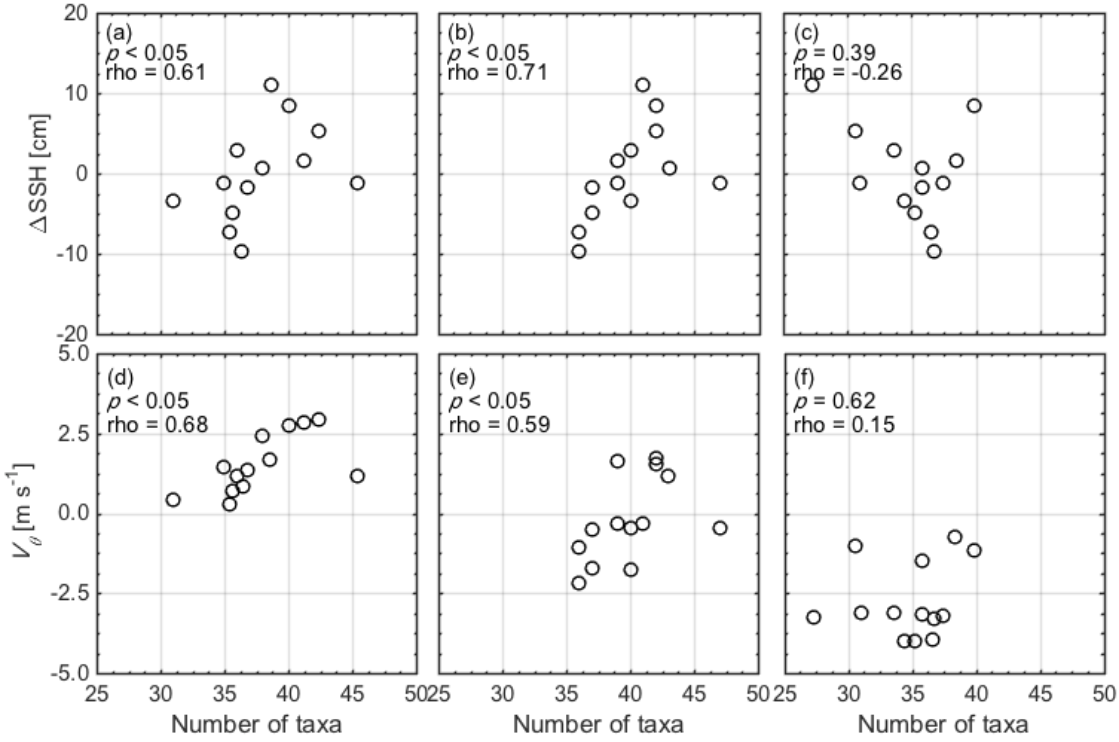

Figure 5.7. Comparison results between number of taxa and ΔSSH derived as $\Delta SSH = SSH_{AB} - SSH_{CS}$ (a–c), and number of taxa and V_θ (d–f) south of SLI (left), at Chirikov (middle) and Chukchi (right) hotspots. Black lines indicate regression lines. Solid and dashed lines indicate significant ($p < 0.05$) and insignificant ($p \geq 0.05$) trends, respectively.

Chapter 6

Overall discussion and conclusions

6.1. Summary and synthesis of individual chapters

Finally, this chapter combines the results and insights derived from individual chapters to provide a holistic discussion. This work documented reliable evidences of relationships between phytoplankton and benthic macrofauna, and also species invasion at benthic hotspots in the Pacific Arctic. The findings of this work could fill the lack of knowledge about the detailed processes how phytoplankton community influence on benthic macrofauna via benthic–pelagic coupling, and would contribute to offering a solid foundation for assessing future changes in the area. Thus, integrating the results provided in individual chapters arranges biological and ecological implications vital in making informed management decisions.

In chapter 2, a chlorophyll-*a* size distribution (CSD) model was developed by basing on biomass and optical property of phytoplankton, and enabled to derive the synoptic size structure of the phytoplankton community with sufficient accuracy using satellite remote sensing. Compared with existing models, the CSD model has several advantages: use of phytoplankton absorption coefficients ($a_{ph}(\lambda)$) at shorter wavelengths that reduce uncertainties by strong absorption by pure seawater, employment of the spectral shape of $a_{ph}(\lambda)$ avoiding the influence of non-algal components, retrieval of user-defined phytoplankton size classes calculated from the CSD slope, development by using size fractionated chlorophyll-*a* (chl*a*) without the use of the diagnostic pigments such as fucoxanthin and peridinin, and user-friendly index that the CSD slope represent the synoptic size structure of the phytoplankton community with one component. In consequence, satellite-based estimation of spatiotemporal variation in phytoplankton size structure by the CSD model can contribute better understanding of the biogeochemical and ecological responses to recent climate forcing. In fact, chapter 3 built a constructive linkage between phytoplankton size structure and biomass of benthic macrofauna at the benthic hotspot in the Pacific Arctic. As the Pacific Arctic has a tight pelagic–benthic coupling that surface production directly transported to the sediment with little or no grazing by zooplankton, spatiotemporal variation in satellite-derived phytoplankton size structure was an important index of pattern in food supply to benthic macrofauna. Although average macrofaunal biomass through three benthic hotspots in the Pacific Arctic, i.e., south of St. Lawrence Island (south of SLI), Chirikov Basin (Chirikov), and southeastern Chukchi Sea (Chukchi), sustained high value (> 20 gCm^{-2}) throughout 2000–2013, those observed south of SLI and Chukchi showed decreasing and increasing trends for the period. Coincidently, size structure of

phytoplankton during the post-bloom period shifted smaller and larger community south of SLI and Chukchi, respectively, suggesting that the macrofaunal distribution seemed to be driven by the amount of settled phytoplankton to the sediments and/or continuous supplement of fresh phytoplankton. To examine which or both of these processes contribute to determining spatiotemporal variations in macrofaunal biomass at benthic hotspots in the Pacific Arctic, a factorial laboratory experiment, in addition to *in situ* and satellite observations, was conducted in chapter 4. Spatial distribution in body size of a common bivalve in the Pacific Arctic *Macoma calcarea* showed significant relationship with size structure of phytoplankton community during the post-bloom period, supporting the results in chapter 3 that higher benthic macrofaunal biomass coincide with larger phytoplankton size structure during the period. In addition, the factorial experiment suggested that growth in body size and physiological condition of *M. calcarea* reflected the available duration of fresh phytoplankton rather than total amount of available organic materials. These results further imply that the shift in food web from pelagic–benthic to pelagic-oriented system likely not to be directly fatal for benthic macrofauna in the Pacific Arctic if only benthic macrofauna able to obtain continuous influx of phytoplankton from overlying water column and/or lateral advection. Moreover, chapter 5 demonstrated that the species invasion seemed to have been already occurred in benthic macrofaunal community in the Pacific Arctic, accompanying with increasing northward volume transport controlled by meridional sea level gradient and local winds. As the variation in northward volume transport has been expected to keep increasing, species invasion could be amplified in future.

6.2. Current status and trend of marine ecosystem in the Pacific Arctic

The quality and quantity of primary production, including ice algae and phytoplankton, reaching the seafloor have a strong impact on benthic communities (McMahon et al., 2006; Sun et al., 2007, 2009; North et al., 2014), which further cascades on upper trophic levels such as diving spectacled eiders (*Somateria fischeri*), bearded seals (*Erignathus barbatus*), walrus (*Odobenus rosmarus*) and grey whales (*Eschrichtius robustus*) (Lovvorn et al., 2003; Grebmeier et al., 2006; Grebmeier, 2012). During the spring bloom period, almost 70% of the water column organic carbon reaches the seafloor in the Pacific Arctic characterized by tight pelagic–benthic coupling owing to high primary production and low grazing by zooplankton (Walsh et al., 1989), supporting high biomass of benthic macrofauna (Grebmeier and McRoy, 1989). In contrast, theoretical grazing of phytoplankton by zooplankton may reach up to 50–150% of the daily water column primary production in the Pacific Arctic (Springer et al., 1989), suggesting the amount of daily influx of phytoplankton to the sediment would much

lower than that of during the bloom period because of relatively lower primary production and high grazing by zooplankton. In addition to these facts, a robust food bank theory lead recent trend in way of thinking that water column primary production especially in spring supports persistent benthic hotspots in the Pacific Arctic; however, this work revealed a shift in benthic macrofaunal biomass coincided with phytoplankton size structure during the post-bloom period in the Pacific Arctic because of positive influences of continuous influx of fresh phytoplankton on growth and physiological condition of a common bivalve in the Pacific Arctic *Macoma calcarea*. As the high sinking rate likely allow escaping from grazing by zooplankton, it is considered that larger phytoplankton size structure leads substantial settlement of fresh phytoplankton even if zooplankton-rich water during the post-bloom period. In areas with reduced summer sea ice, grazing pressure by zooplankton will be higher resulting in pelagic-oriented systems (Kędra et al., 2015). The Pacific Arctic, where is experiencing drastic sea ice reduction (Steele et al., 2008), is one of the areas that food web structure may shift from pelagic–benthic to pelagic-oriented systems. Indeed, it is regarded as a mainstream prediction that biomass and abundance of benthic organisms decrease in future Pacific Arctic in response to ongoing sea ice reduction (Kędra et al., 2015), although this study propose an alternative hypothesis that the region exposed large phytoplankton size structure during the post-bloom period (e.g., southeastern Chukchi hotspot) may not drive decreasing in benthic biomass even if in pelagic-oriented systems.

Recently, fall blooms have been observed in wide regions of the Arctic Ocean. In temperate regions, wind-driven mixing and the incidental upward supply of nutrients trigger fall blooms (Chiswell et al., 2013), whereas the presence of sea ice prevents wind-driven mixing even during strong storms in the Arctic. However, the impact of local storms on the upper ocean is becoming more prominent due to the drastic reduction of sea ice extent (Rainville and Woodgate, 2009). In fact, weak but evident fall blooms have already been observed in the eastern Bering Sea and the southern Chukchi Sea (Sigler et al., 2014; Nishino et al., 2016). While the present pattern of single phytoplankton blooms occurred in spring is currently the major primary production period in the Pacific Arctic, phenological shifts from single to double blooms (i.e., both spring and fall) may be amplified in the future (Ardyna et al., 2014). Although this work have not examined occurrence of fall blooms at benthic hotspots in the Pacific Arctic, such event promote fresh phytoplankton settlement into the sediment and hence encourage the hypothesis that pelagic-orient food web may no directly drive decrease in biomass and abundance of benthic organisms in the Pacific Arctic.

Another logical prediction for a future Arctic characterized by increased Pacific water intrusion into the Arctic (Woodgate et al., 2010, 2015; Woodgate and Weingartner, 2012)

and reduced sea ice (Steele et al., 2008) is that new taxa will expand or invade Arctic seafloor habitats (Renaud et al., 2015). While it remains unclear that which family joined benthic macrofaunal community and where is the origin, this work proposed a possibility that new macrofaunal taxa have already invaded benthic macrofaunal community in the Pacific Arctic. In general, the alien species have potential to seriously affect biological system by robbing of food and/or habitat of native species (Sorte et al., 2010), and therefore disruption of existing linkage in food web may occur in the Pacific Arctic in near future as a consequence of reconstruction from Arctic to sub-Arctic community. Furthermore, there is a possible prediction that benthic community in the Pacific Arctic shift from deposit feeding species to suspension feeding species in response to varying sediment grain size, suggesting not only species diversity but also population composition of benthic macrofaunal community in the Pacific Arctic will vary or have already varied in response to increased northward volume flux. As the Pacific Arctic is important foraging area for benthic feeding species (Grebmeier et al., 2006), the impact of changes in benthic community can propagate to upper trophic levels through the trophic cascades. Indeed, gray whales primarily used the Chirikov Basin with dense aggregations of amphipod (Highsmith and Coyle, 1992), whereas population of gray whales decline their population in 2002 due to the reduction in prey biomass as much as 50% relative to the 1980s, resulting in an extension of their foraging area to the southern Chukchi Sea (Moore et al., 2003). In addition, spectacled eiders, which overwinter in the open-water leads in pack ice south of St. Lawrence Island to feed on productive bivalve populations (Lovvorn et al., 2003), have drastically decreased their population size coincident with declines in prey density during the last few decades (Lovvorn et al., 2014). Although it remain unclear that declines in prey availability were directly linked with species invasion and/or variation in community composition, these facts substantially suggest that benthic community pattern strongly influences on biomass and distribution of upper trophic levels. Therefore, if the alien species replace native species and subsequently disrupt existing linkage in food web, marine ecosystem in the future Pacific Arctic will be considerably different than those we see today.

6.3. Research needs and ways forward

There is a sturdy prediction that the duration of open water in the Chukchi and Beaufort seas shifts from 3 to 4 months in 2010 to a projected ~5 months by 2040s (Wang and Overland, 2015), and a sea ice free Arctic in summer may occur as early as the late 2020s (Wang and Overland, 2009). In addition, time series data obtained by the recent high-resolution mooring arrays indicate the Bering Strait throughflow increases ~50% from 2001 (~0.7 Sv) to 2013 (~1.1 Sv) (Woodgate and Weingartner, 2012). To understand the response of marine

ecosystem to such extreme events, a novel conceptual model named the Arctic Marine Pulses (AMP) model has developed (Moore et al., in press) in the course of the Synthesis of Arctic Research (SOAR) project focusing on an integrated synthesis of conditions in the Pacific Arctic. The AMP model depicts biophysical pulses by linking processes such as sea ice dynamics, pelagic–benthic coupling and also lateral advection on spatiotemporal scales extending from 1 to 1000 km over days to months during an annual cycle (Moore et al., in press). In the model, timing and pace of sea-ice retreat across the Chukchi Sea drives pulses of organic material either to the benthos, or toward the pelagic system; however, the results reported in chapters 3 and 4 imply that not only pulse of organic material influx occurred in blooms but also that of during the post-bloom period is substantially important for benthic community at benthic hotspots in the Pacific Arctic. Therefore, in addition to pulsed influx of organic materials during the bloom period, continuous influx of organic materials after the bloom should be considered as one of the important sources of organic materials in the Pacific Arctic. Such improvement of the AMP model would facilitate holistic understanding of ocean dynamics and complex trophic linkages from primary production to humans providing a foundation required for policy decisions of the sustainable ecosystem services in the Pacific Arctic. Note that this dissertation did not examine the influence of advected organic carbon brought into the region by Pacific water transiting northward from upstream sources, although such process as well as *in situ* production likely to important for the persistence of benthic hotspots especially sea ice covered seasons (Grebmeier, 2012; Grebmeier et al., 2015a,b).

Compared with other trophic levels such as phyto- and zooplankton, fish, seabirds, and marine mammals, basic information of benthic organisms in the Arctic is largely unclear, especially reproduction strategy (Fetzer and Arntz, 2008), while those could clearly important in modeling and predicting benthic community structure as well as whole ecosystem. Some studies suggest that temperature and salinity may trigger reproduction of benthic organisms (Hoegh-Guldberg and Pearse, 1995), whereas conflicting study reported that water temperature has no direct effect on timing of reproduction (Pearse and Lockhart, 2004). Hence, more detailed quantifications of the timing of reproduction in benthic organisms are necessary to obtain a broader view of Arctic life history strategies (Kuklinski et al., 2013); however, year-round monitoring of benthic community is not easy owing to sea ice dynamics and extreme storms in the region. One of the solutions is a long-term laboratory experiment. To the best of my knowledge, Goethel et al. (in press) is the only example of laboratory experiment in the Pacific Arctic, examining the response of growth in bivalve to different PH conditions. Because such experiments improve our understanding about detailed response of target organisms to experimental conditions, we need more effort on laboratory experiment especially for benthic

organisms.

The Conservation of Arctic Flora and Fauna (CAFF) placed that ecosystem services in the Arctic are important economically, environmentally and culturally (CAFF, 2013). These services not only benefit for Arctic residents directly, providing essential food and cultural keystones (Moore and Stabeno, 2015). In addition, the Arctic ecosystem also serves the rest of the world, as a destination for tourism in various forms and icons of the Arctic region, and by providing a large amount of food from commercial fisheries (CAFF, 2013). Recognition of the importance of these services, and an assessment of how they are changing, is vital to design effective Arctic conservation strategies (CAFF, 2013). Consequently, to facilitate development of management strategies now and in the future, research strategies should focus on process studies investigating the detailed processes of ecosystem variations via trophic interaction and/or cascading impact, as well as monitoring observations and development of conceptual models.

Acknowledgements

This dissertation would have not been possible without inputs, support and encouragements from countless individuals. Firstly, I would like to express my sincere appreciation to my supervisor Dr. Toru Hirawake (Associate Prof., Hokkaido University) for his stimulations and helpful discussions throughout my study. My gratitude is also extended to Drs. Yutaka Watanuki (Prof., Hokkaido University), Yasuzumi Fujimori (Prof., Hokkaido University), Hiroto Abe (Assistant Prof., Hokkaido University), and Amane Fujiwara (Research Scientist, Japan Agency for Marine-Earth Science and Technology: JAMSTEC) for their valuable comments and suggestions on this work. Likewise, I am grateful to Drs. Sei-Ichi Saitoh (Prof., Hokkaido University), Koji Suzuki (Prof., Hokkaido University), Masahiro Nakaoka (Prof., Hokkaido University), Takafumi Hirata (Associate Prof., Hokkaido University), Jun Nishioka (Associate Prof., Hokkaido University) and Shigeto Nishino (Senior Research Scientist, JAMSTEC), Tomonori Isada (Assistant Prof., Hokkaido University), Takashi Kikuchi (Senior Research Scientist, JAMSTEC), Makoto Sampei (Assistant Prof, Hokkaido University), Shintaro Takao (Assistant Prof., National Institute of Polar Research) and Jacqueline M. Grebmeier (Research Prof., University of Maryland Center for Environmental Science) for their valuable time in going through the contents of this work. Their respective expertises were equally important in the foci of this thesis. Similarly, I wish to thank the captains and crews of the T/S Oshoro-maru, T/S Ushio-maru, T/S Umitaka-maru, JMSDF Shirase and R/V Tangaroa for their cooperation during the cruises. I also thank the staffs of JAMSTEC and Marine Work Japan, Ltd., for their support to obtain and analyze the data. Furthermore, I am extending my thanks to members of Akkeshi Marine Station of Hokkaido University for their helpful supports of bivalve collections and measurements. Special acknowledgements are also to Drs. Kohei Mizobata (Assistant Prof., Tokyo University of Marine Science and Technology), Takahiro Iida (Second Officer, Ushio-maru), Liu Yang (Prof., Ocean University of China), Hiroko Sasaki (Research Scientist, National Research and Development Agency), Yoshiyuki Abe (P.D., Hokkaido University) and Bungo Nishizawa (P.D., Hokkaido University). I am also extending my thanks to colleagues at laboratory, especially Tomomi Yagi, Seira Suzuki, Yukiko Kudo, Ryosuke Futsuki and Yuta Yoshino for their helpful supports and meaningful conversations. Finally, I would like to express my deepest gratitude to my family for being patient and understanding while I chase after my dreams.

This study was supported by the Green Network of Excellence (GRENE) Arctic Climate Change Research Project and Arctic Challenge for Sustainability (ArCS) Project, which were founded by he Ministry of Education, Culture, Sports, Science and Technology of Japan (MEXT). This study was also supported by the Global Change Observation Mission–Climate

(GCOM-C) mission by the Japan Aerospace Exploration Agency (JAXA). The ocean color data were produced and distributed by the Distributed Active Archive Center (DAAC) at the Goddard Space Flight Center (GSFC). Sea ice concentration data were provided by the National Snow and Ice Data Center (NSIDC) at the University of Colorado. I am grateful to the individuals and organization that have contributed to the Pacific Marine Arctic Regional Synthesis (PacMARS) Data Archive and National Science Foundation (NSF) Arctic Data Center.

References

Aagaard, K., 2005. Revising the Bering Strait freshwater flux into the Arctic Ocean. Geophys. Res. Lett. 32. doi:10.1029/2004GL021747

Aizawa, C., Tanimoto, M., Jordan, R.W., 2005. Living diatom assemblages from North Pacific and Bering Sea surface waters during summer 1999. Deep-Sea Res. II 52, 2186–2205. doi:10.1016/j.dsr2.2005.08.008

Alvain, S., Moulin, C., Dandonneau, Y., Bréon, F.M., 2005. Remote sensing of phytoplankton groups in case 1 waters from global SeaWiFS imagery. Deep-Sea Res. I 52, 1989–2004. doi:10.1016/j.dsr.2005.06.015

Ambrose, W.G., Carroll, M.L., Greenacre, M., Thorrold, S.R., McMahon, K.W., 2006. Variation in Serripes groenlandicus (Bivalvia) growth in a Norwegian high-Arctic fjord: evidence for local- and large-scale climatic forcing. Glob. Chang. Biol. 12, 1595–1607. doi:10.1111/j.1365-2486.2006.01181.x

Ambrose, W.G., Renaud, P.E., 1995. Benthic Response to Water Column Productivity Patterns - Evidence for Benthic-Pelagic Coupling in the Northeast Water Polynya. J. Geophys. Res. 100, 4411–4421. doi:10.1029/94JC01982

Ardyna, M., Babin, M., Gosselin, M., Devred, E., Tremblay, J.-É., 2014. Recent Arctic Ocean sea ice loss triggers novel fall phytoplankton blooms. Geophys. Res. Lett. 41, 6207–6212. doi:10.1002/2014GL061047

Aronson, R. B., Thatje, S., Clarke, A., Peck, L. S., Blake, D. B., Wilga, C. D., Seibel, B. A., 2007. Climate Change and Invasibility of the Antarctic Benthos, Annu. Rev. Ecol. Evol. Syst. 38, 129–154, doi:10.1146/annurev.ecolsys.38.091206.095525.

Arrigo, K.R., Perovich, D.K., Pickart, R.S., Brown, Z.W., van Dijken, G.L., Lowry, K.E., Mills, M.M., *et al.*, 2012. Massive Phytoplankton Blooms Under Arctic Sea Ice. Science 336, 1408–1408. doi:10.1126/science.1215065

Arrigo, K.R., van Dijken, G.L., 2015. Continued increases in Arctic Ocean primary production. Prog. Oceanogr. 136, 60–70. doi:10.1016/j.pocean.2015.05.002

Arrigo, K.R., van Dijken, G.L., 2011. Secular trends in Arctic Ocean net primary production. J. Geophys. Res. Oceans 116, C09011. doi:10.1029/2011JC007151

Arrigo, K.R., van Dijken, G., Pabi, S., 2008. Impact of a shrinking Arctic ice cover on marine primary production. Geophys. Res. Lett. 35, L19603. doi:10.1029/2008GL035028

Auad, G., Miller, A., Di Lorenzo, E., 2006. Long-term forecast of oceanic conditions off California and their biological implications. J. Geophys. Res. Oceans 111. doi:10.1029/2005JC003219

Bader, H., 1970. The hyperbolic distribution of particle sizes. J. Geophys. Res. 75, 2822–2830. doi: 10.1029/JC075i015p02822

Barbier, E.B., 2012. Progress and Challenges in Valuing Coastal and Marine Ecosystem Services. Rev. Environ. Econ. Policy 6, 1–19. doi:10.1093/reep/rer017

Bates, A.E., McKelvie, C.M., Sorte, C.J.B., Morley, S.A., Jones, N.A.R., Mondon, J.A., Bird, T.J., *et al.*, 2013. Geographical range, heat tolerance and invasion success in aquatic species. Proc. R. Soc. B 280, 20131958. doi:10.1098/rspb.2013.1958

Bates, A.E., Pecl, G.T., Frusher, S., Hobday, A.J., Wernberg, T., Smale, D.A., Sunday, J.M., *et al.*, 2014. Defining and observing stages of climate-mediated range shifts in marine systems. Glob. Environ. Chang. 26, 27–38. doi:10.1016/j.gloenvcha.2014.03.009

Beatty, W.S., Jay, C.V., Fischbach, A.S., Grebmeier, J.M., Taylor, R.L., Blanchard, A.L., Jewett, S.C., 2016. Space use of a dominant Arctic vertebrate: Effects of prey, sea ice, and land on Pacific walrus resource selection. BIOC 203, 25–32. doi:10.1016/j.biocon.2016.08.035

Blanchard, A.L., Feder, H.M., 2014. Interactions of habitat complexity and environmental characteristics with macrobenthic community structure at multiple spatial scales in the northeastern Chukchi Sea. Deep-Sea Res. II 102, 132–143. doi:10.1016/j.dsr2.2013.09.022

Birchenough, S.N.R., Reiss, H., Degraer, S., Mieszkowska, N., Borja, A., Buhl-Mortensen, L., Braeckman, U., *et al.*, 2015. Climate change and marine benthos: a review of existing research and future directions in the North Atlantic. Wiley Interdiscip. Rev. Clim. Chang. 6, 203–223. doi:10.1002/wcc.330

Bracher, A., Taylor, M.H., Taylor, B., Dinter, T., Röttgers, R., Steinmetz, F., 2015. Using empirical orthogonal functions derived from remote-sensing reflectance for the prediction of phytoplankton pigment concentrations. Ocean Sci. 11, 139–158. doi:10.5194/os-11-139-2015

Brewin, R.J., Devred, E., Sathyendranath, S., Lavender, S.J., Hardman-Mountford, N.J., 2011. Model of phytoplankton absorption based on three size classes. Appl. Opt. 50, 4535–4549. doi:10.1364/AO.50.004535

Brewin, R.J.W., Hardman-Mountford, N.J., Lavender, S.J., Raitsos, D.E., Hirata, T., Uitz, J., Devred, E., *et al.*, 2011. An intercomparison of bio-optical techniques for detecting dominant phytoplankton size class from satellite remote sensing. Remote Sens. Environ. 115, 325–339. doi:10.1016/j.rse.2010.09.004

Brewin, R.J.W., Sathyendranath, S., Hirata, T., Lavender, S.J., Barciela, R.M., Hardman-Mountford, N.J., 2010. A three-component model of phytoplankton size class for the Atlantic Ocean. Ecol. Modell. 221, 1472–1483. doi:10.1016/j.ecolmodel.2010.02.014

Brewin, R.J.W., Sathyendranath, S., Lange, P.K., Tilstone, G., 2014. Comparison of two methods to derive the size-structure of natural populations of phytoplankton. Deep-Sea Res. I 85, 72–79. doi:10.1016/j.dsr.2013.11.007

Brey, T., Rumohr, H., Ankar, S., 1988. Energy content of macrobenthic invertebrates: general conversion factors from weight to energy. J. Exp. Mar. Biol. Ecol. 117, 271–278. doi:10.1016/0022-0981(88)90062-7

Bricaud, A., Morel, A., 1986. Light Attenuation and Scattering by Phytoplanktonic Cells - a Theoretical Modeling. Appl. Opt. 25, 571–580. doi:10.1364/AO.25.000571

Brugel, S., Nozais, C., Poulin, M., Tremblay, J.É., Miller, L.A., Simpson, K.G., Gratton, Y., *et al.*, 2009. Phytoplankton biomass and production in the southeastern Beaufort Sea in autumn 2002 and 2003. Mar. Ecol. Prog. Ser. 377, 63–77. doi:10.3354/meps07808

Butler, P.G., Scourse, J.D., Richardson, C.A., Wanamaker, A.D., Bryant, C.L., Bennell, J.D., 2009. Continuous marine radiocarbon reservoir calibration and the 13C Suess effect in the Irish Sea: Results from the first multi-centennial shell-based marine master chronology. Earth Planet. Sci. Lett. 279, 230–241. doi:10.1016/j.epsl.2008.12.043

Butler, P.G., Wanamaker, A.D., Jr., Scourse, J.D., Richardson, C.A., Reynolds, D.J., 2011. Long-term stability of δ13C with respect to biological age in the aragonite shell of mature specimens of the bivalve mollusk Arctica islandica. Palaeogeogr. Palaeoclimatol. Palaeoecol. 302, 21–30. doi:10.1016/j.palaeo.2010.03.038

Burrows, M.T., Schoeman, D.S., Buckley, L.B., Moore, P., Poloczanska, E.S., Brander, K.M., Brown, C., *et al.*, 2011. The Pace of Shifting Climate in Marine and Terrestrial Ecosystems. Science 334, 652–655. doi:10.1126/science.1210288

Byrnes, J.E., 2006. Species diversity, invasion success, and ecosystem functioning: disentangling the influence of resource competition, facilitation, and extrinsic factors. Mar. Ecol. Prog. Ser. 311, 251–262. doi:10.3354/meps311251

Byrén, L., Ejdung, G., Elmgren, R., 2006. Uptake of sedimentary organic matter by the deposit-feeding Baltic amphipods Monoporeia affinis and Pontoporeia femorata. Mar. Ecol. Prog. Ser. 313, 135–143. doi:10.3354/meps313135

Campbell, R.G., Sherr, E.B., Ashjian, C.J., Plourde, S., Sherr, B.F., Hill, V., Stockwell, D.A., 2009. Mesozooplankton prey preference and grazing impact in the western Arctic Ocean. Deep-Sea Res. II 56, 1274–1289. doi:10.1016/j.dsr2.2008.10.027

Carroll, M.L., Ambrose, W.G., Levin, B.S., Locke, W.L., V, Henkes, G.A., Hop, H., Renaud, P.E., 2011. Pan-Svalbard growth rate variability and environmental regulation in the Arctic bivalve Serripes groenlandicus. J. Mar. Syst. 88, 239–251. doi:10.1016/j.jmarsys.2011.04.010

Cavalieri, D.J., 2000. An enhancement of the NASA Team sea ice algorithm. IEEE Trans. Geosci. Remote Sensing 38, 1387–1398. doi:10.1109/36.843033

Chen, I.C., Hill, J.K., Ohlemuller, R., Roy, D.B., Thomas, C.D., 2011. Rapid Range Shifts of Species Associated with High Levels of Climate Warming. Science 333, 1024–1026. doi:10.1126/science.1206432

Chiswell, S.M., Bradford-Grieve, J., Hadfield, M.G., Kennan, S.C., 2013. Climatology of surface chlorophyll a, autumn-winter and spring blooms in the southwest Pacific Ocean. J. Geophys. Res. Oceans 118, 1003–1018. doi:10.1002/jgrc.20088

Ciotti, A.M., Bricaud, A., 2006. Retrievals of a size parameter for phytoplankton and spectral light absorption by colored detrital matter from water-leaving radiances at SeaWiFS channels in a continental shelf region off Brazil. Limnol. Oceanogr. Methods 4, 237–253. doi:10.4319/lom.2006.4.237.

Ciotti, A.M., Lewis, M.R., Cullen, J.J., 2002. Assessment of the relationships between dominant cell size in natural phytoplankton communities and the spectral shape of the absorption coefficient. Limnol. Oceangr. 47, 404–417. doi: 10.4319/lo.2002.47.2.0404

Coachman, L.K., Aagaard, K., 1966. On the water exchange through Bering Strait. Limnol. Oceangr. 11, 44–59. doi:10.4319/lo.1966.11.1.0044

Coachman, L.K., Aagaard, K., Tripp, R.B., 1975. Bering Strait: The Regional Physical Oceanography, Univ. of Washington Press, Seattle, 172 pp.

Comiso, J.C., Parkinson, C.L., Gersten, R., Stock, L., 2008. Accelerated decline in the Arctic sea ice cover. Geophys. Res. Lett. 35, 413. doi:10.1029/2007GL031972

Comiso, J.C., 2012. Large Decadal Decline of the Arctic Multiyear Ice Cover. J. Climate 25, 1176–1193. doi:10.1175/JCLI-D-11-00113.1Comiso, J.C., 2012. Large Decadal Decline of the Arctic Multiyear Ice Cover. J. Climate 25, 1176–1193. doi:10.1175/JCLI-D-11-00113.1

Cooper, L.W., Savvichev, A.S., Grebmeier, J.M., 2015. Abundance and Production Rates of Heterotrophic Bacterioplankton in the Context of Sediment and Water Column Processes in the Chukchi Sea. Oceanog. 28, 84–99. doi:10.5670/oceanog.2015.59

Cota, G., 2004. Transformation of global satellite chlorophyll retrievals with a regionally tuned algorithm. Remote Sens. Environ. 90, 373–377. doi:10.1016/j.rse.2004.01.005

Cota, G.F., Ruble, D.A., 2005. Absorption and backscattering in the Beaufort and Chukchi Seas. J. Geophys. Res. 110. doi:10.1029/2002JC001653

Craig, S.E., Jones, C.T., Li, W.K.W., Lazin, G., Horne, E., Caverhill, C., Cullen, J.J., 2012. Deriving optical metrics of coastal phytoplankton biomass from ocean colour. Remote Sens. Environ. 119, 72–83. doi:10.1016/j.rse.2011.12.007

Danielson, S.L., Eisner, L., Ladd, C., Mordy, C., Sousa, L., Weingartner, T.J., 2017. A comparison between late summer 2012 and 2013 water masses, macronutrients, and phytoplankton standing crops in the northern Bering and Chukchi Seas. Deep-Sea Res. II 135, 7–26. doi:10.1016/j.dsr2.2016.05.024

Danielson, S., Hedstrom, K., Aagaard, K., Weingartner, T., Curchitser, E., 2012. Wind-induced reorganization of the Bering shelf circulation. Geophys. Res. Lett. 39, L08601. doi:10.1029/2012GL051231

Danielson, S.L., Weingartner, T.J., Hedstrom, K.S., Aagaard, K., Woodgate, R., Curchitser, E., Stabeno, P.J., 2014. Coupled wind-forced controls of the Bering–Chukchi shelf circulation and the Bering Strait throughflow: Ekman transport, continental shelf waves, and variations of the Pacific–Arctic sea surface height gradient. Prog. Oceanogr. 125, 40–61. doi:10.1016/j.pocean.2014.04.006

Darecki, M., Stramski, D., 2004. An evaluation of MODIS and SeaWiFS bio-optical algorithms in the Baltic Sea. Remote Sens. Environ. 89, 326–350. doi:10.1016/j.rse.2003.10.012

Dawson, T.P., Jackson, S.T., House, J.I., Prentice, I.C., Mace, G.M., 2011. Beyond Predictions: Biodiversity Conservation in a Changing Climate. Science 332, 53–58. doi:10.1126/science.1200303

Dekker, R., Beukema, J.J., 1999. Relations of summer and winter temperatures with dynamics and growth of two bivalves, Tellina tenuis and Abra tenuis, on the northern edge of their intertidal distribution. J. Sea Res. 42, 207–220. doi:10.1016/S1385-1101(99)00026-X

Devred, E., Sathyendranath, S., Stuart, V., Platt, T., 2011. A three component classification of phytoplankton absorption spectra: Application to ocean-color data. Remote Sens. Environ. 115, 2255–2266. doi:10.1016/j.rse.2011.04.025

Deininger, M., Koellner, T., Brey, T., Teschke, K., 2016. Towards mapping and assessing antarctic marine ecosystem services – The weddell sea case study. Ecosyst. Serv. 22, 174–192. doi:10.1016/j.ecoser.2016.11.001

Devred, E., Sathyendranath, S., Stuart, V., Platt, T., 2011. A three component classification of phytoplankton absorption spectra: Application to ocean-color data. Remote Sens. Environ. 115, 2255–2266. doi:10.1016/j.rse.2011.04.025

Doney, S.C., Lima, I., Moore, J.K., Lindsay, K., Behrenfeld, M.J., Westberry, T.K., Mahowald, N., *et al.*, 2009. Skill metrics for confronting global upper ocean ecosystem-biogeochemistry models against field and remote sensing data. J. Mar. Syst. 76, 95–112. doi:10.1016/j.jmarsys.2008.05.015

Doney, S.C., Ruckelshaus, M., Emmett Duffy, J., Barry, J.P., Chan, F., English, C.A., Galindo, H.M., *et al.*, 2012. Climate Change Impacts on Marine Ecosystems. Annu. Rev. Marine. Sci. 4, 11–37. doi:10.1146/annurev-marine-041911-111611

Dore, J.E., Lukas, R., Sadler, D.W., Church, M.J., Karl, D.M., 2009. Physical and biogeochemical modulation of ocean acidification in the central North Pacific. PNAS 106, 12235–12240. doi:10.1073/pnas.0906044106

d'Ovidio, F., De Monte, S., Alvain, S., Dandonneau, Y., Lévy, M., 2010. Fluid dynamical niches of phytoplankton types. PNAS 107, 18366–18370. doi:10.1073/pnas.1004620107

Dussart, B.H., 1965. Les différentes catégories de plancton. Hydrobiologia 26, 72–74.

Eisner, L., Hillgruber, N., Martinson, E., Maselko, J., 2012. Pelagic fish and zooplankton species assemblages in relation to water mass characteristics in the northern Bering and southeast Chukchi seas. Polar Biol. 36, 87–113. doi:10.1007/s00300-012-1241-0

Eisner, L.B., Gann, J.C., Ladd, C., D Cieciel, K., Mordy, C.W., 2016. Late summer/early fall phytoplankton biomass (chlorophyll a) in the eastern Bering Sea: Spatial and temporal variations and factors affecting chlorophyll a concentrations. Deep-Sea Res. II 100–114. doi:10.1016/j.dsr2.2015.07.012

Eklöf, J., Austin, Å., Bergström, U., Donadi, S., Eriksson, B.D.H.K., Hansen, J., Sundblad, G., 2017. Size matters: relationships between body size and body mass of common coastal, aquatic invertebrates in the Baltic Sea. PeerJ 5, e2906. doi:10.7717/peerj.2906

Falk-Petersen, S., Sargent, J.R., Henderson, J., Hegseth, E.N., Hop, H., Okolodkov, Y.B., 1998. Lipids and fatty acids in ice algae and phytoplankton from the Marginal Ice Zone in the Barents Sea. Polar Biol. 20, 41–47.

Fetzer, I., Arntz, W.E., 2008. Reproductive strategies of benthic invertebrates in the Kara Sea (Russian Arctic): adaptation of reproduction modes to cold water. Mar. Ecol. Prog. Ser. 356, 189–202. doi:10.3354/meps07271

Field, C., Elphick, C., Correll, M., Huang, M., 2014. Sentinels of climate change: coastal indicators of wildlife and ecosystem change in Long Island Sound. Accessed at (http://longislandsoundstudy.net/wp-content/uploads/2015/08/Sentinels_final_report_summary.pdf) on 017-11-08.

Fisher, B., Turner, R.K., Morling, P., 2009. Defining and classifying ecosystem services for decision making. Ecol. Econ. 68, 643–653. doi:10.1016/j.ecolecon.2008.09.014

Frey, K.E., Moore, G.W.K., Cooper, L.W., Grebmeier, J.M., 2015. Divergent patterns of recent sea ice cover across the Bering, Chukchi, and Beaufort seas of the Pacific Arctic Region. Prog. Oceanogr. 136, 32–49. doi:10.1016/j.pocean.2015.05.009

Frey, K.E., Perovich, D.K., Light, B., 2011. The spatial distribution of solar radiation under a melting Arctic sea ice cover. Geophys. Res. Lett. 38, L22501. doi:10.1029/2011GL049421

Fujiwara, A., Hirawake, T., Suzuki, K., Eisner, L., Imai, I., Nishino, S., Kikuchi, T., *et al.*, 2016. Influence of timing of sea ice retreat on phytoplankton size during marginal ice zone bloom period on the Chukchi and Bering shelves. Biogeosciences 13, 115–131. doi:10.5194/bg-13-115-2016

Fujiwara, A., Hirawake, T., Suzuki, K., Imai, I., Saitoh, S.I., 2014. Timing of sea ice retreat can alter phytoplankton community structure in the western Arctic Ocean. Biogeosciences 11, 1705–1716. doi:10.5194/bg-11-1705-2014

Fujiwara, A., Hirawake, T., Suzuki, K., Saitoh, S.I., 2011. Remote sensing of size structure of phytoplankton communities using optical properties of the Chukchi and Bering Sea shelf region. Biogeosciences 8, 3567–3580. doi:10.5194/bg-8-3567-2011

Goethel, C.L., Grebmeier, J.M., Cooper, L.W., Miller, T.J., *in press*. Implications of ocean acidification in the Pacific Arctic: Experimental responses of three Arctic bivalves to decreased pH and food availability. Deep-Sea Res. II. doi:10.1016/j.dsr2.2017.08.013

Grebmeier, J.M., 2012. Shifting Patterns of Life in the Pacific Arctic and Sub-Arctic Seas. Annu. Rev. Mar. Sci. 4, 63–78. doi:10.1146/annurev-marine-120710-100926

Grebmeier, J.M., Bluhm, B.A., Cooper, L.W., Danielson, S.L., Arrigo, K.R., Blanchard, A.L., Clarke, J.T., *et al.*, 2015a. Ecosystem characteristics and processes facilitating persistent macrobenthic biomass hotspots and associated benthivory in the Pacific Arctic. Prog. Oceanogr. 136, 92–114. doi:10.1016/j.pocean.2015.05.006

Grebmeier, J.M., Bluhm, B.A., Cooper, L.W., Denisenko, S.G., Iken, K., Kędra, M., Serratos, C., 2015b. Time-Series Benthic Community Composition and Biomass and Associated Environmental Characteristics in the Chukchi Sea During the RUSALCA 2004-2012 Program. Oceanography 28, 116–133. doi:10.5670/oceanog.2015.61

Grebmeier, J., Cooper, L. 2014a. PacMARS Benthic Infaunal Parameters. Version 1.0. https://doi.org/10.5065/D6H70CVR; available at the PacMARS EOL data archive site <http://pacmars.eol.ucar.edu>.

Grebmeier, J., Cooper, L. 2014b. PacMARS Sediment Chlorophyll-a. Version 1.0. https://doi.org/10.5065/D6W9576K; available at the PacMARS EOL data archive site <http://pacmars.eol.ucar.edu>.

Grebmeier, J.M., Cooper, L.W. 2017. SWL13 Benthic Macrofaunal Parameters. Version 1.0 (doi in progress); available at the NSF Arctic Data Center.

Grebmeier, J., Cooper, L., Okkonen, S. 2015c. PacMARS Bottom water temperature and salinity (2000-2012)_CBL. Version 1.0. https://doi.org/10.5065/D6VM49BM; available at the PacMARS EOL data archive site <http://pacmars.eol.ucar.edu>.

Grebmeier, J.M., Moore, S.E., Overland, J.E., Frey, K.E., Gradinger, R., 2010. Biological Response to Recent Pacific Arctic Sea Ice Retreats. EOS 91, 161. doi:10.1029/2010EO180001

Grebmeier, J. M., Overland, J.E., Moore, S.E., Farley, E.V., Carmack, E.D., Cooper, L.W., Frey, K.E., *et al.*, 2006. A major ecosystem shift in the northern Bering Sea. Science 311, 1461–1464. doi:10.1890/13-0486.1

Grebmeier, J.M., Bluhm, B., Cooper, L.W., Denisenko, S.G., Iken, K., Kędra, M., Serratos, C., 2015a. Time-series benthic community composition and biomass and associated

environmental characteristics in the Chukchi Sea during the RUSALCA 2004–2012 program. Oceanog. 28, 116–133. doi:10.5670/oceanog.2015.61

Grebmeier, J.M., Bluhm, B.A., Cooper, L.W., Danielson, S.L., Arrigo, K.R., Blanchard, A.L., Clarke, J.T., *et al.*, 2015b. Ecosystem characteristics and processes facilitating persistent macrobenthic biomass hotspots and associated benthivory in the Pacific Arctic. Prog. Oceanogr. 136, 92–114. doi:10.1016/j.pocean.2015.05.006

Grebmeier, J.M., McRoy, C.P., 1989. Pelagic-benthic coupling on the shelf of the northern Bering and Chukchi Seas. Ill Benthic food supply and carbon cycling. Mar. Ecol. Prog. Ser. 53, 79–91. doi:10.3354/meps053079

Grebmeier, J.M., McRoy, C.P., Feder, H.M., 1988. Pelagic-Benthic Coupling on the Shelf of the Northern Bering and Chukchi Seas .1. Food-Supply Source and Benthic Biomass. Mar. Ecol. Prog. Ser. 48, 57–67. doi:10.3354/meps048057

Gregg, W.W., Rousseaux, C.S., 2014. Decadal trends in global pelagic ocean chlorophyll: A new assessment integrating multiple satellites, in situ data, and models. J. Geophys. Res. Oceans 119, 5921–5933. doi:10.1002/2014JC010158

Gutiérrez, D., Akester, M., Naranjo, L., 2016. Productivity and Sustainable Management of the Humboldt Current Large Marine Ecosystem under climate change. Environ. Dev. 17, 126–144. doi:10.1016/j.envdev.2015.11.004

Hadfield, M.G., Carpizo-Ituarte, E.J., del Carmen, K., Nedved, B.T., 2001. Metamorphic Competence, a Major Adaptive Convergence in Marine Invertebrate Larvae. Integr. Comp. Biol. 41, 1123–1131. doi:10.1093/icb/41.5.1123

Hansen, James, Sato, M., Ruedy, R., Lo, K., Lea, D.W., Medina-Elizade, M., 2006. Global temperature change. PNAS 103, 14288–14293. doi:10.1073/pnas.0606291103

Hansen, JLS, Josefson, A.B., 2003. Accumulation of algal pigments and live planktonic diatoms in aphotic sediments during the spring bloom in the transition zone of the North and Baltic Seas. Mar. Ecol. Prog. Ser. 248, 41–54. doi:10.3354/meps248041

Hansen, J., Sato, M., Ruedy, R., Lo, K., Lea, D.W., Medina-Elizade, M., 2006. Global temperature change. PNAS 103, 14288–14293. doi:10.1073/pnas.0606291103

Hayakawa, K., Handa, N., Kawanobe, K., Wong, C.S., 1996. Factors controlling the temporal variation of fatty acids in piculate matter during a phytoplankton bloom in a marine mesocosm. Mar. Chem. 52, 233–244. doi:10.1016/0304-4203(95)00087-9

Hernández-Delgado, E.A., 2015. The emerging threats of climate change on tropical coastal ecosystem services, public health, local economies and livelihood sustainability of small islands: Cumulative impacts and synergies. Mar. Poll. Bull. 101, 5–28. doi:10.1016/j.marpolbul.2015.09.018

Highsmith, R.C., Coyle, K.O., 1992. Productivity of Arctic Amphipods Relative to Gray Whale Energy-Requirements. Mar. Ecol. Prog. Ser. 83, 141–150.

Hirata, T., Hardman-Mountford, N.J., Brewin, R.J.W., Aiken, J., Barlow, R., Suzuki, K., Isada, T., *et al.*, 2011. Synoptic relationships between surface Chlorophyll-*a* and diagnostic pigments specific to phytoplankton functional types. Biogeosciences 8, 311–327. doi:10.5194/bg-8-311-2011

Hill, V., Cota, G., Stockwell, D., 2005. Spring and summer phytoplankton communities in the Chukchi and Eastern Beaufort Seas. Deep-Sea Res. II 52, 3369–3385. doi:10.1016/j.dsr2.2005.10.010

Hoegh-Guldberg, O., Bruno, J.F., 2010. The Impact of Climate Change on the World's Marine Ecosystems. Science 328, 1523–1528. doi:10.1126/science.1189930

Hoegh-Guldberg, O., Pearse, J.S., 1995, Temperature, Food Availability, and the Development of Marine Invertebrate Larvae. Integr. Comp. Biol., 35(4), 415–425. doi:10.1093/icb/35.4.415

Holmes, R.M., McClelland, J.W., Peterson, B.J., Shiklomanov, I.A., Shiklomanov, A.I., Zhulidov, A.V., Gordeev, V.V., *et al.*, 2002. A circumpolar perspective on fluvial sediment flux to the Arctic ocean. Glob. Biogeochem. Cycles 16, 1098. doi:10.1029/2001GB001849

Holm-Hansen, O., Lorenzen, C.J., Holmes, R.W., Strickland, J.D.H., 1965. Fluorometric Determination of Chlorophyll. ICES J. Mar. Sci. 30, 3–15. doi:10.1093/icesjms/30.1.3

Hueffer, K., O'Hara, T.M., Follmann, E.H., 2011. Adaptation of mammalian host-pathogen interactions in a changing arctic environment. Acta Vet. Scand. 53. doi:10.1186/1751-0147-53-17

Hunt, G.L., Coyle, K.O., Eisner, L.B., Farley, E.V., Heintz, R.A., Mueter, F., Napp, J.M., *et al.*, 2011. Climate impacts on eastern Bering Sea foodwebs: a synthesis of new data and an assessment of the Oscillating Control Hypothesis. ICES J. Mar. Sci. 68, 1230–1243. doi:10.1093/icesjms/fsr036

Hunt, G.L., Jr, Stabeno, P., Walters, G., Sinclair, E., Brodeur, R.D., Napp, J.M., Bond, N.A., 2002. Climate change and control of the southeastern Bering Sea pelagic ecosystem. Deep-Sea Res. II 49, 5821–5853. doi:10.1016/S0967-0645(02)00321-1

Huot, Y., Lee, Z., 2014. On the non-closure of particle backscattering coefficient in oligotrophic oceans. Opt. Express 22, 29223–29233. doi:10.1364/OE.22.029223

IPCC, 2014. Climate Change 2014: Mitigation of Climate Change. Contribution of Working Group III to the Fifth Assessment Report of the Intergovernmental Panel on Climate Change. Cambridge University Press, Cambridge, UK & New York, NY, USA.

Ishii, M., Kimoto, M., Sakamoto, K., Iwasaki, S.I., 2006. Steric sea level changes estimated from historical ocean subsurface temperature and salinity analyses. J. Oceanogr. 62, 155–170. doi:10.1007/s10872-006-0041-y

Jay, C.V., Fischbach, A.S., Kochnev, A.A., 2012. Walrus areas of use in the Chukchi Sea during sparse sea ice cover. Mar. Ecol. Prog. Ser. 468, 1–13. doi:10.3354/meps10057

Joint, I., Groom, S.B., 2000. Estimation of phytoplankton production from space: current status and future potential of satellite remote sensing. J. Exp. Mar. Biol. Ecol. 250, 233–255. doi:10.1016/S0022-0981(00)00199-4

Josefson, A.B., Forbes, T.L., Rosenberg, R., 2002. Fate of phytodetritus in marine sediments: functional importance of macrofaunal community. Mar. Ecol. Prog. Ser. 230, 71–85. doi:10.2307/24865095

Kędra, M., Moritz, C., Choy, E.S., David, C., Degen, R., Duerksen, S., Ellingsen, I., *et al.*, 2015. Status and trends in the structure of Arctic benthic food webs. Polar Res. 34. doi:10.3402/polar.v34.23775

Kishino, M., Takahashi, M., Okami, N., Ichimura, S., 1985. Estimation of the spectral absorption coefficients of phytoplankton in the sea. Bull. Mar. Sci. 37, 634–642.

Kostadinov, T.S., Siegel, D.A., Maritorena, S., 2007. Ocean color observations and modeling for an optically complex site: Santa Barbara Channel, California, USA. J. Geophys. Res. 112, C07011. doi:10.1029/2006JC003526

Kostadinov, T.S., Siegel, D.A., Maritorena, S., 2009. Retrieval of the particle size distribution from satellite ocean color observations. J. Geophys. Res. Oceans 114. doi:10.1029/2009JC005303

Kuklinski, P., Berge, J., McFadden, L., Dmoch, K., Zajączkowski, M., Nygård, H., Piwosz, K., Tatarek, A., 2013. Seasonality of occurrence and recruitment of Arctic marine benthic

invertebrate larvae in relation to environmental variables. Polar Biol. 36, 549–560. doi:10.1007/s00300-012-1283-3

Kutz, S.J., Checkley, S., Verocai, G.G., Dumond, M., Hoberg, E.P., Peacock, R., Wu, J.P., *et al.*, 2013. Invasion, establishment, and range expansion of two parasitic nematodes in the Canadian Arctic. Glob. Chang. Biol. 19, 3254–3262. doi:10.1111/gcb.12315

Lalande, C., Lepore, K., Cooper, L.W., Grebmeier, J.M., 2007. Export fluxes of particulate organic carbon in the Chukchi Sea: a comparative study using 234 Th/238 U disequilibria and drifting sediment traps. Mar. Chem 103, 185–196. doi:10.1016/j.marchem.2006.07.004

Lalli, C.M., Parsons, T.R., 1997. Biological Oceanography: An Introduction, 2nd ed. Elsevier, New York.

Laney, S.R., Sosik, H.M., 2014. Phytoplankton assemblage structure in and around a massive under-ice bloom in the Chukchi Sea. Deep Sea Research Part II: Topical Studies in Oceanography 105, 30–41. doi:10.1016/j.dsr2.2014.03.012

Le Quéré, C., Harrison, S.P., Prentice, I.C., Buitenhuis, E.T., Aumont, O., Bopp, L., Claustre, H., *et al.*, 2005. Ecosystem dynamics based on plankton functional types for global ocean biogeochemistry models. Glob. Chang. Biol. 11, 2016–2040. doi:10.1111/j.1365-2468.2005.01004.x

Lee, Z.P., Carder, K.L., Arnone, R.A., 2002. Deriving inherent optical properties from water color: a multiband quasi-analytical algorithm for optically deep waters. Appl. Opt. 41, 5755–5772. doi:10.1364/AO.41.005755

Lenoir, J., Svenning, J.C., 2015. Climate-related range shifts – a global multidimensional synthesis and new research directions. Ecography 38, 15–28. doi:10.1111/ecog.00967

Leu, E., Falk-Petersen, S., Kwaśniewski, S., Wulff, A., Edvardsen, K., Hessen, D.O., 2006. Fatty acid dynamics during the spring bloom in a High Arctic fjord: importance of abiotic factors versus community changes. Can. J. Fish. Aquat. Sci. 63, 2760–2779. doi:10.1139/f06-159

Levitus, S., Antonov, J.I., Boyer, T.P., Locarnini, R.A., Garcia, H.E., Mishonov, A.V., 2009. Global ocean heat content 1955-2008 in light of recently revealed instrumentation problems. Geophys. Res. Lett. 36, L07608. doi:10.1029/2008GL037155

Li, W.K.W., McLaughlin, F.A., Lovejoy, C., Carmack, E.C., 2009. Smallest Algae Thrive As the Arctic Ocean Freshens. Science 326, 539–539. doi:10.1126/science.1179798

Loarie, S.R., Duffy, P.B., Hamilton, H., Asner, G.P., Field, C.B., Ackerly, D.D., 2009. The velocity of climate change. Nature 462, 1052–1055. doi:10.1038/nature08649

Lovvorn, J.R., Anderson, E.M., Rocha, A.R., Larned, W.W., Grebmeier, J.M., Cooper, L.W., Kolts, J.M., *et al.*, 2014. Variable wind, pack ice, and prey dispersion affect the long-term adequacy of protected areas for an Arctic sea duck. Ecol. Appl. 24, 396–412. doi:10.1890/13-0411.1

Lovvorn, J.R., Cooper, L.W., Brooks, M.L., De Ruyck, C.C., Bump, J.K., Grebmeier, J.M., 2005. Organic matter pathways to zooplankton and benthos under pack ice in late winter and open water in late summer in the north-central Bering Sea. Mar. Ecol. Prog. Ser. 291, 135–150. doi:10.3354/meps291135

Lovvorn, J.R., Grebmeier, J.M., Cooper, L.W., 2009. Modeling marine protected areas for threatened eiders in a climatically changing Bering Sea. Ecol. Appl. 19, 1596–1613. doi:10.1890/08-1193.1

Lovvorn, J. R., North, C. A., Kolts, J. M., Grebmeier, J. M., Cooper, L. W., Cui, X., 2016. Projecting the effects of climate-driven changes in organic matter supply on benthic food webs in the northern Bering Sea. Mar. Ecol. Prog. Ser. 548, 11–30. doi:10.3354/meps11651

Lovvorn, J.R., Raisbeck, M.F., Cooper, L.W., Cutter, G.A., Miller, M.W., Brooks, M.L., Grebmeier, J.M., *et al.*, 2013. Wintering eiders acquire exceptional Se and Cd burdens in the Bering Sea: physiological and oceanographic factors. Mar. Ecol. Prog. Ser. 489, 245–261.

Lovvorn, J.R., Richman, S.E., Grebmeier, J.M., Cooper, L.W., 2003. Diet and body condition of spectacled elders wintering in pack ice of the Bering Sea. Polar Biol. 26, 259–267. doi:10.1007/s00300-003-0477-0

Lowry, K.E., van Dijken, G.L., Arrigo, K.R., 2014. Evidence of under-ice phytoplankton blooms in the Chukchi Sea from 1998 to 2012. Deep-Sea Res. II 105, 105–117. doi:10.1016/j.dsr2.2014.03.013

Marchese, C., Albouy, C., Tremblay, J.-É., Dumont, D., d'Ortenzio, F., Vissault, S., Bélanger, S., 2017. Changes in phytoplankton bloom phenology over the North Water (NOW) polynya: a response to changing environmental conditions. Polar Biol. 9, 1–17. doi:10.1007/s00300-017-2095-2

Maritorena, S., Siegel, D.A., Peterson, A.R., 2002. Optimization of a semianalytical ocean color model for global-scale applications. Appl. Opt. 41, 2705–2714.

Mathis, J.T., Grebmeier, J.M., Hansell, D.A., 2014. Carbon biogeochemistry of the western Arctic: primary production, carbon export and the controls on ocean acidification, in: Grebmeier, J.M., Maslowski, W. (Eds.), The Pacific Arctic Region, Springer, New York, pp. 223–368. doi:10.5194/bg-11-365-2014

Matsuoka, A., Huot, Y., Shimada, K., Saitoh, S.I., 2007. Bio-optical characteristics of the western Arctic Ocean: implications for ocean color algorithms. Can. J. Remote Sens. 33, 503–518. doi:10.5589/m07-059

Matsuoka, A., Hill, V., Huot, Y., Babin, M., Bricaud, A., 2011. Seasonal variability in the light absorption properties of western Arctic waters: Parameterization of the individual components of absorption for ocean color applications. J. Geophys. Res. 116, C02007. doi:10.1029/2009JC005594

MEA, M., 2005. Ecosystems and human well-being: synthesis. Island.

McClain, C.R., 2009. A Decade of Satellite Ocean Color Observations. Annu. Rev. Marine. Sci. 1, 19–42. doi:10.1146/annurev.marine.010908.163650

McMahon, K.W., Ambrose, W.G.J., Johnson, B.J., Sun, M.-Y., Lopez, G.R., Clough, L.M., Carroll, M.L., 2006. Benthic community response to ice algae and phytoplankton in Ny Alesund, Svalbard. Mar. Ecol. Prog. Ser. 310, 1–14. doi:10.1111/j.1365-2486.2006.01181.x

McTigue, N.D., Dunton, K.H., 2014. Trophodynamics and organic matter assimilation pathways in the northeast Chukchi Sea, Alaska. Deep-Sea Res. II 102, 84–96. doi:10.1016/j.dsr2.2013.07.016

Mincks, S.L., Smith, C.R., DeMaster, D.J., 2005. Persistence of labile organic matter and microbial biomass in Antarctic shelf sediments: evidence of a sediment “food bank.” Mar. Ecol. Prog. Ser. 300, 3–19.

Mitchell, B. G. 1990. Algorithms for determining the absorption coefficient of aquatic particulates using the quantitative filter technique (QFT). *In* Ocean Optics X, pp. 137–148. Ed. by R. W. Spinrad. Proceedings of the SPIE, 1302. doi:10.1117/12.21440

Moore, S.E., Grebmeier, J.M., 2017. The Distributed Biological Observatory: Linking Physics to Biology in the Pacific Arctic Region. Arctic.

Moore, S.E., Stabeno, P.J., 2015. Synthesis of Arctic Research (SOAR) in marine ecosystems of the Pacific Arctic. Progress in Oceanography 1–11. doi:10.1016/j.pocean.2015.05.017

Moore, S.E., Stabeno, P.J, Grebmeier, J.M., Okkonen, S.R., *in press*. The Arctic Marine Pulses Model: linking annual oceanographic processes to contiguous ecological domains in the Pacific Arctic. Deep-Sea Res. II. doi:10.1016/j.dsr2.2016.10.011

Mouw, C.B., Yoder, J.A., 2010. Optical determination of phytoplankton size composition from global SeaWiFS imagery. J. Geophys. Res. 115. doi:10.1029/2010JC006337

Moran, S.B., Lomas, M.W., Kelly, R.P., Gradinger, R., Iken, K., Mathis, J.T., 2012. Seasonal succession of net primary productivity, particulate organic carbon export, and autotrophic community composition in the eastern Bering Sea. Deep-Sea Res. II 65-70, 84–97. doi:10.1016/j.dsr2.2012.02.011

Morata, N., Michaud, E., Włodarska-Kowalczuk, M., 2015. Impact of early food input on the Arctic benthos activities during the polar night. Polar Biol. 38, 99–114. doi:10.1007/s00300-013-1414-5

Mueter, F.J., 2008. Sea ice retreat alters the biogeography of the Bering Sea continental shelf. Ecol. Appl. 18, 309–320. doi:10.1890/07-0564.1

Mullerlupp, T., Bauch, H., 2005. Linkage of Arctic atmospheric circulation and Siberian shelf hydrography: A proxy validation using O records of bivalve shells. Glob. Planet. Chang. 48, 175–186. doi:10.1016/j.gloplacha.2004.12.012

Munns, W.R., Poulsen, V., Gala, W.R., Marshall, S.J., Rea, A.W., Sorensen, M.T., Stackelberg, von, K., 2017. Ecosystem services in risk assessment and management. Integr. Environ. Assess. Manag. 13, 62–73. doi:10.1002/ieam.1835

Najdek, M., Puskaric, S., Bochdansky, A.B., 1994. Contribution of zooplankton lipids to the flux of organic matter in the northern Adriatic Sea. Mar. Ecol. Prog. Ser. 111, 241–249. doi:10.3354/meps111241

Nelson, R.J., Carmack, E.C., McLaughlin, F.A., Cooper, G.A., 2009. Penetration of Pacific zooplankton into the western Arctic Ocean tracked with molecular population genetics. Mar. Ecol. Prog. Ser. 381, 129–138. doi:10.3354/meps07940

Niebauer, H.J., 1981. Oceanography of the Eastern Bering Sea Ice-Edge Zone in Spring. Limnol. Oceangr. 26, 1111–1125.

Niebauer, H.J., Alexander, V., Henrichs, S.M., 1995. A time-series study of the spring bloom at the Bering Sea ice edge I. Physical processes, chlorophyll and nutrient chemistry. Cont. Shelf Res. 15, 1859–1877. doi:10.1016/0278-4343(94)00097-7

Nishino, S., Kikuchi, T., Fujiwara, A., Hirawake, T., Aoyama, M., 2016. Water mass characteristics and their temporal changes in a biological hotspot in the southern Chukchi Sea. Biogeosciences 13, 2563–2578. doi:10.5194/bg-13-2563-2016

North, C.A., Lovvorn, J.R., Kolts, J.M., Brooks, M.L., Cooper, L.W., Grebmeier, J.M., 2014. Deposit-feeder diets in the Bering Sea: potential effects of climatic loss of sea ice-related microalgal blooms. Ecol. Appl. 24, 1525–1542. doi:10.1890/13-0486.1

O'Reilly, J.E., Maritorena S., Siegel D., O'Brien M.O., Toole D., Mitchell B.G., Kahru M., *et al*., 2000. Ocean color chlorophyll a algorithms for SeaWiFS, OC2, and OC4: Version 4. In: SeaWiFS Postlaunch Technical Report Series, Greenbelt, Md., Goddard Space Flight Center.

Palmer, M., Bernhardt, E., Chornesky, E., Collins, S., Dobson, A., Duke, C., Gold, B. J., *et al.*, 2004. Ecology for a Crowded Planet. Science 304, 1251–1252. doi:10.1126/science.1095780

Palumbi, S.R., Sandifer, P.A., Allan, J.D., Beck, M.W., Fautin, D.G., Fogarty, M.J., Halpern, B.S., *et al.*, 2009. Managing for ocean biodiversity to sustain marine ecosystem services. Front. Ecol. Environ. 7, 204–211. doi:10.1890/070135

Parmesan, C., 2007. Influences of species, latitudes and methodologies on estimates of phenological response to global warming. Glob. Chang. Biol. 13, 1860–1872. doi:10.1111/j.1365-2486.2007.01404.x

Parmesan, C., Yohe, G., 2003. A globally coherent fingerprint of climate change impacts across natural systems. Nature 421, 37–42. doi:10.1038/nature01286

Pearse, J.S., Lockhart, S.J., 2004. Reproduction in cold water: paradigm changes in the 20th century and a role for cidaroid sea urchins. Deep-Sea Res. II 51, 1533–1549. doi:10.1016/j.dsr2.2004.06.023

Peck, L. S., Conway, L. Z., 2000. The myth of metabolic cold adaptation: oxygen consumption in stenothermal Antarctic bivalves. Geol. Soc. Spec. Publ. 177, 441–450, doi:10.1144/GSL.SP.2000.177.01.29.

Perovich, D.K., Richter-Menge, J.A., 2009. Loss of Sea Ice in the Arctic. Annu. Rev. Marine. Sci. 1, 417–441. doi:10.1146/annurev.marine.010908.163805

Perrette, M., Yool, A., Quartly, G.D., Popova, E.E., 2011. Near-ubiquity of ice-edge blooms in the Arctic. Biogeosciences 8, 515–524. doi:10.5194/bg-8-515-2011

Philippart, C.J.M., Anadón, R., Danovaro, R., Dippner, J.W., Drinkwater, K.F., Hawkins, S.J., Oguz, T., *et al.*, 2011. Impacts of climate change on European marine ecosystems: Observations, expectations and indicators. J. Exp. Mar. Biol. Ecol. 400, 52–69. doi:10.1016/j.jembe.2011.02.023

Pickart, R.S., Pratt, L.J., Torres, D.J., Whitledge, T.E., Proshutinsky, A.Y., Aagaard, K., Agnew, T.A., *et al.*, 2010. Evolution and dynamics of the flow through Herald Canyon in the western Chukchi Sea. Deep-Sea Res. II 57, 5–26. doi:10.1016/j.dsr2.2009.08.002

Pinsky, M.L., Worm, B., Fogarty, M.J., Sarmiento, J.L., Levin, S.A., 2013. Marine Taxa Track Local Climate Velocities. Science 341, 1239–1242. doi:10.1126/science.1239352

Pirtle-Levy, R., Grebmeier, J.M., Cooper, L.W., Larsen, I.L., 2009. Chlorophyll a in Arctic sediments implies long persistence of algal pigments. Deep-Sea Res. II 56, 1326–1338. doi:10.1016/j.dsr2.2008.10.022

Polashenski, C., Perovich, D., Courville, Z., 2012. The mechanisms of sea ice melt pond formation and evolution. J. Geophys. Res. 117, C01001. doi:10.1029/2011JC007231

Polyakov, I.V., Timokhov, L.A., Alexeev, V.A., Bacon, S., Dmitrenko, I.A., Fortier, L., Frolov, I.E., *et al.*, 2010. Arctic Ocean Warming Contributes to Reduced Polar Ice Cap. J. Phys. Oceanogr. 40, 2743–2756. doi:10.1175/2010jpo4339.1

Poloczanska, E.S., Brown, C.J., Sydeman, W.J., Kiessling, W., Schoeman, D.S., Moore, P.J., Brander, K., *et al.*, 2013. Global imprint of climate change on marine life. Nat. Clim. Chang. 3, 919–925. doi:10.1038/nclimate1958

Przeslawski, R., Falkner, I., Ashcroft, M.B., Hutchings, P., 2012. Using rigorous selection criteria to investigate marine range shifts. Estuar. Coast. Shelf Sci. 113, 205–212. doi:10.1016/j.ecss.2012.08.005

Poloczanska, E.S., Burrows, M.T., Brown, C.J., García Molinos, J., Halpern, B.S., Hoegh-Guldberg, O., Kappel, C.V., *et al.*, 2016. Responses of Marine Organisms to Climate Change across Oceans. Front. Mar. Sci. 3, 515–21. doi:10.3389/fmars.2016.00062

Qian, P.-Y., 1999. Larval settlement of polychaetes, in: Reproductive Strategies and Developmental Patterns in Annelids. Springer Netherlands, Dordrecht, pp. 239–253. doi:10.1007/978-94-017-2887-4_14

Rainville, L., Woodgate, R.A., 2009. Observations of internal wave generation in the seasonally ice–free Arctic. Geophys. Res. Lett. 36. doi:10.1029/2009GL041291

Renaud, P.E., Sejr, M.K., Bluhm, B.A., Sirenko, B., Ellingsen, I.H., 2015. The future of Arctic benthos: Expansion, invasion, and biodiversity. Prog. Oceanogr. 139, 244–257. doi:10.1016/j.pocean.2015.07.007

Ricciardi, A., Bourget, E., 1998. Weight-to-weight conversion factors for marine benthic macroinvertebrates. Mar. Ecol. Prog. Ser. 163, 245–251. doi:10.3354/meps163245

Roemmich, D., Davis, R., Sutton, P., Wijffels, S., 2007. Decadal spinup of the South Pacific subtropical gyre. J. Phys. Oceanogr. 37, 162–173. doi:10.1175/JPO3004.1

Roy, S., Sathyendranath, S., Bouman, H., Platt, T., 2013. The global distribution of phytoplankton size spectrum and size classes from their light-absorption spectra derived from satellite data. Remote Sens. Environ. 139, 185–197.

Sakshaug, E., 2004. Primary and secondary production in the Arctic Seas, in: Stein, R., Macdonald, R.W. (Eds.), The organic carbon cycle in the Arctic Ocean, Springer, Berlin, pp. 57–81.

Sathyendranath, S., Platt, T., Irwin, B., Horne, E., Borstad, G., Stuart, V., Payzant, L., *et al.*, 2004. A multispectral remote sensing study of coastal waters off Vancouver Island. Int. J. Remote Sens. 25, 893–919. doi:10.1080/0143116031000139836

Schonberg, S.V., Clarke, J.T., Dunton, K.H., 2014. Distribution, abundance, biomass and diversity of benthic infauna in the Northeast Chukchi Sea, Alaska: Relation to environmental variables and marine mammals. Deep-Sea Res. II 102, 144–163. doi:10.1016/j.dsr2.2013.11.004

Schöne, B.R., Fiebig, J., Pfeiffer, M., Gless, R., Hickson, J., Johnson, A., Dreyer, W., *et al.*, 2005. Climate records from a bivalved Methuselah (Arctica islandica, Mollusca; Iceland). Palaeogeogr. Palaeoclimatol. Palaeoecol. 228, 130–148. doi:10.1016/j.palaeo.2005.03.049

Schöne, B.R., Wanamaker, A.D., Fiebig, J., Thébault, J., Kreutz, K., 2011. Annually resolved δ13Cshell chronologies of long-lived bivalve mollusks (Arctica islandica) reveal oceanic carbon dynamics in the temperate North Atlantic during recent centuries. Palaeogeogr. Palaeoclimatol. Palaeoecol. 302, 31–42. doi:10.1016/j.palaeo.2010.02.002

Shiomoto, A., 2002. Distribution of biogenic particulate matter in the surface waters of the Bering Sea basin, winter 1993. Polar Biosci. 15, 1–10.

Sigler, M.F., Napp, J.M., Stabeno, P.J., Heintz, R.A., Lomas, M.W., Hunt, G.L., Jr, 2016. Variation in annual production of copepods, euphausiids, and juvenile walleye pollock in

the southeastern Bering Sea. Deep-Sea Res. II 134, 223–234. doi:10.1016/j.dsr2.2016.01.003

Sigler, M.F., Stabeno, P.J., Eisner, L.B., Napp, J.M., Mueter, F.J., 2014. Spring and fall phytoplankton blooms in a productive subarctic ecosystem, the eastern Bering Sea, during 1995–2011. Deep-Sea Res. II 109, 71–83. doi:10.1016/j.dsr2.2013.12.007

Sirenko, B.I., Gagaev, S.Y., 2007. Unusual abundance of macrobenthos and biological invasions in the Chukchi Sea. Russ. J. Mar. Biol. 33, 355–364. doi:10.1134/S1063074007060016

Sorte, C.J.B., Williams, S.L., Carlton, J.T., 2010. Marine range shifts and species introductions: comparative spread rates and community impacts. Glob. Ecol. Biogeogra. 19, 303–316. doi:10.1111/j.1466-8238.2009.00519.x

Springer, A.M., McRoy, C.P., Flint, M.V., 1996. The Bering Sea Green Belt: Shelf-edge processes and ecosystem production. Fish. Oceanogr. 5, 205–223. doi:10.1111/j.1365-2419.1996.tb00118.x

Springer, A.M., McRoy, C.P., Turco, K.R., 1989. The paradox of pelagic food webs in the northern Bering Sea—II. Zooplankton communities. Cont. Shelf Res. 9, 359–386. doi:10.1016/0278-4343(89)90039-3

Stabeno, P., Napp, J., Mordy, C., Whitledge, T., 2010. Factors influencing physical structure and lower trophic levels of the eastern Bering Sea shelf in 2005: Sea ice, tides and winds. Prog. Oceanogr. 85, 180–196. doi:10.1016/j.pocean.2010.02.010

Steele, M., Ermold, W., Zhang, J., 2008. Arctic Ocean surface warming trends over the past 100 years. Geophys. Res. Lett. 35, L02614. doi:10.1029/2007GL031651

Stramski, D., Boss, E., Bogucki, D., Voss, K.J., 2004. The role of seawater constituents in light backscattering in the ocean. Prog. Oceanogr. 61, 27–56. doi:10.1016/j.pocean.2004.07.001

Stroeve, J.C., Markus, T., Boisvert, L., Miller, J., Barrett, A., 2014. Changes in Arctic melt season and implications for sea ice loss. Geophys. Res. Lett. 41, 1216–1225. doi:10.1002/2013GL058951

Sun, M.-Y., Carroll, M.L., Ambrose, W.G.J., Clough, L.M., Zou, L., Lopez, G.R., 2007. Rapid consumption of phytoplankton and ice algae by Arctic soft-sediment benthic communities: Evidence using natural and C-13-labeled food materials. J. Mar. Res. 65, 561–588. doi:10.1357/002224007782689094

Sun, M.-Y., Clough, L.M., Carroll, M.L., Dai, J., Ambrose, W.G., Lopez, G.R., 2009. Different responses of two common Arctic macrobenthic species (Macoma balthica and Monoporeia affinis) to phytoplankton and ice algae: Will climate change impacts be species specific? J. Exp. Mar. Biol. Ecol. 376, 110–121. doi:10.1016/j.jembe.2009.06.018

Sun, M.-Y., Lee, C., Aller, R.C., 1993. Laboratory studies of oxic and anoxic degradation of chlorophyll-a in Long Island Sound sediments. Geochim. Cosmochim. Acta 57, 147–157. doi:10.1016/0016-7037(93)90475-C

Sunday, J.M., Bates, A.E., Dulvy, N.K., 2012. Thermal tolerance and the global redistribution of animals. Nat. Clim. Chang. 54, 14–19. doi:10.2486/indhealth.2015-0069

Sunday, J.M., Pecl, G.T., Frusher, S., Hobday, A.J., Hill, N., Holbrook, N.J., Edgar, G.J., *et al.*, 2015. Species traits and climate velocity explain geographic range shifts in an ocean-warming hotspot. Ecol. Lett. 18, 944–953. doi:10.1111/ele.12474

Sukhanova, I.N., Flint, M.V., Pautova, L.A., Stockwell, D.A., Grebmeier, J.M., Sergeeva, V.M., 2009. Phytoplankton of the western Arctic in the spring and summer of 2002: Structure and seasonal changes. Deep-Sea Res. II 56, 1223–1236. doi:10.1016/j.dsr2.2008.12.030

Suzuki, R., Ishimaru, T., 1990. An improved method for the determination of phytoplankton chlorophyll using N, N-dimethylformamide. J. Oceanogr. Soc. Japan 46, 190–194. doi:10.1007/BF02125580

Tassan, S., Ferrari, G.M., 1995. An alternative approach to absorption measurements of aquatic particles retained on filters. Limnol. Oceangr. 40, 1358–1368. doi:10.4319/lo.1995.40.8.1358

Thackeray, S.J., Sparks, T.H., Frederiksen, M., 2010. Trophic level asynchrony in rates of phenological change for marine, freshwater and terrestrial environments. Glob. Chang. Biol. 16, 3304–3313. doi:10.1111/j.1365-2486.2010.02165.x

Thorson, G., 1950. Reproductive and Larval Ecology of marine bottom invertebrates. Biol. Rev. 25, 1–45. doi:10.1111/j.1469-185X.1950.tb00585.x

Turner, J.T., 2002. Zooplankton fecal pellets, marine snow and sinking phytoplankton blooms. Aquat. Microb. Ecol. 27, 57–102. doi:10.3354/ame027057

Van der Putten, W.H., Macel, M., Visser, M.E., 2010. Predicting species distribution and abundance responses to climate change: why it is essential to include biotic interactions across trophic levels. Phil. Trans. R. Soc. B 365, 2025–2034. doi:10.1098/rstb.2010.0037

VanDerWal, J., Murphy, H.T., Kutt, A.S., Perkins, G.C., Bateman, B.L., Perry, J.J., Reside, A.E., 2012. Focus on poleward shifts in species' distribution underestimates the fingerprint of climate change. Nat. Clim. Chang. 3, 239–243. doi:10.1038/nclimate1688

Vidussi, F., Claustre, H., Manca, B.B., Luchetta, A., Marty, J.C., 2001. Phytoplankton pigment distribution in relation to upper thermocline circulation in the eastern Mediterranean Sea during winter. J. Geophys. Res. 106, 19939–19956. doi:10.1029/1999JC000308

Waga, H., Hirawake, T., Fujiwara, A., Kikuchi, T., Nishino, S., Suzuki, K., Takao, S., *et al.*, 2017. Differences in rate and direction of shifts between phytoplankton size structure and sea surface temperature. Remote Sens. 9, 222. doi:10.3390/rs9030222

Wallace, K.J., 2007. Classification of ecosystem services: Problems and solutions. Biol. Cons. 139, 235–246. doi:10.1016/j.biocon.2007.07.015

Wang, J., Cota, G.F., 2003. Remote-sensing reflectance in the Beaufort and Chukchi seas: observations and models. Appl. Opt. 42, 2754–2765. doi:10.1364/AO.42.002754

Wang, M., Overland, J.E., 2015. Projected future duration of the sea-ice-free season in the Alaskan Arctic. Prog. Oceanogr. 136, 50–59. doi:10.1016/j.pocean.2015.01.001

Wang, M., Overland, J.E., 2009. A sea ice free summer Arctic within 30 years? Geophys. Res. Lett. 36, L07502. doi:10.1029/2009GL037820

Walsh, J.J., McRoy, C.P., Coachman, L.K., Goering, J.J., Nihoul, J.J., Whitledge, T.E., Blackburn, T.H., *et al.*, 1989. Carbon and nitrogen cycling within the Bering/Chukchi Seas: Source regions for organic matter effecting AOU demands of the Arctic Ocean. Prog. Oceanogr. 22, 277–359. doi:10.1016/0079-6611(89)90006-2

Wanamaker, A.D., Heinemeier, J., Scourse, J.D., Richardson, C.A., Butler, P.G., Eiríksson, J., Knudsen, K.L., 2008. Very Long-Lived Mollusks Confirm 17th Century AD Tephra-Based Radiocarbon Reservoir Ages for North Icelandic Shelf Waters. Radiocarbon 50, 399–412. doi:10.1017/S0033822200053510

Wang, S., Ishizaka, J., Hirawake, T., Watanabe, Y., Zhu, Y., Hayashi, M., Yoo, S., 2015. Remote estimation of phytoplankton size fractions using the spectral shape of light absorption. Opt. Express 23, 10301–19. doi:10.1364/OE.23.010301

Wassmann, P., Duarte, C.M., Agustí, S., Sejr, M.K., 2011. Footprints of climate change in the Arctic marine ecosystem. Glob. Chang. Biol. 17, 1235–1249. doi:10.1111/j.1365-2486.2010.02311.x

Welshmeyer, N.A., 1994. Fluorometric analysis of chlorophyll budgets: Zooplankton grazing and phytoplankton growth in a temperate fjord and the central Pacific gyres. Limnol. Oceangr. 39, 1985–1992.

Wood, K.R., Bond, N.A., Danielson, S.L., Overland, J.E., Salo, S.A., Stabeno, P.J., Whitefield, J., 2015. A decade of environmental change in the Pacific Arctic region. Prog. Oceanogr. 136, 12–31. doi:10.1016/j.pocean.2015.05.005

Woodgate, R.A., Aagaard, K., 2005. Monthly temperature, salinity, and transport variability of the Bering Strait through flow. Geophys. Res. Lett. 32, L04601. doi:10.1029/2004GL021880

Woodgate, R.A., Aagaard, K., Weingartner, T.J., 2006. Interannual changes in the Bering Strait fluxes of volume, heat and freshwater between 1991 and 2004. Geophys. Res. Lett. 33, L15609. doi:10.1029/2006GL026931

Woodgate, R.A., Stafford, K.M., Prahl, F.G., 2015. A Synthesis of Year-Round Interdisciplinary Mooring Measurements in the Bering Strait (1990-2014) and the RUSALCA Years (2004-2011). Oceanog. 28, 46–67. doi:10.5670/oceanog.2015.57

Woodgate, R.A., Weingartner, T., Lindsay, R., 2010. The 2007 Bering Strait oceanic heat flux and anomalous Arctic sea-ice retreat. Geophys. Res. Lett. 37, L01602. doi:10.1029/2009GL041621

Woodgate, R.A., Weingartner, T.J., 2012. Observed increases in Bering Strait oceanic fluxes from the Pacific to the Arctic from 2001 to 2011 and their impacts on the Arctic Ocean water column. Geophys. Res. Lett. 39, L24603. doi:10.1029/2012GL054092

Wyllie-Echeverria, T., Wooster, W.S., 1998. Year–to–year variations in Bering Sea ice cover and some consequences for fish distributions. Fish. Oceanogr. 7, 159–170. doi:10.1046/j.1365-2419.1998.00058.x

Young, J.K., Black, B.A., Clarke, J.T., Schonberg, S.V., Dunton, K.H., 2017. Abundance, biomass and caloric content of Chukchi Sea bivalves and association with Pacific walrus (Odobenus rosmarus divergens) relative density and distribution in the northeastern Chukchi Sea. Deep-Sea Res. II 144, 125–141. doi:10.1016/j.dsr2.2017.04.017